AIAA 2022-2023 Undergraduate Team Aircraft Design

Final Design Report

Team Jackalope - Bounden

Stephanie Dutra, Noor Ansari, Evher Benjamin Aponte, Hsien-Kuei Chang, Sarah Erne,

Anish Joshi, & Krishna Modi

AE 443 - Aircraft Systems Design II
Department of Aerospace Engineering
University of Illinois, Urbana-Champaign
May 12, 2023

Stephanie Dutra   **Noor Ansari**   **Evher Benjamin Aponte**
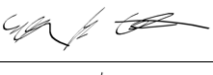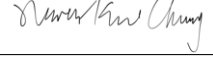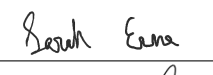
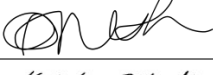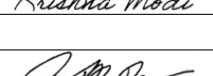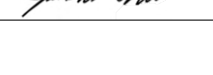**Hsien-Kuei Chang**   **Sarah Erne**   **Anish Joshi**   **Krishna Modi**

Fig. 1   Team Jackalope Members

Table 1   Team Member Contributions

Team Member	Primary Discipline(s)	Secondary Discipline(s)	AIAA Number	Signature
Stephanie Dutra	Team Lead	Interior Design & Avionics	1422590	
Noor Ansari	Performance	Acoustics & Emissions	1404731	
Evher Benjamin Aponte	Aerodynamics and Stability & Control	Landing Gear	1422067	
Hsien-Kuei Chang	Structures and Loads & Dynamics	Maintenance	1339475	
Sarah Erne	Propulsion	Certification	1086217	
Anish Joshi	Systems	Configuration	1389819	
Krishna Modi	Mass Properties	Cost	1421663	

Dr. Jason Merret	Faculty Advisor	-	155270	

Contents

List of Figures

List of Tables

Nomenclature

α	=	Angle of Attack
b	=	Wingspan
β	=	Sideslip
c	=	Chord
$\overline{c}$	=	Mean Aerodynamic Chord
c'	=	Flapped Chord
c_f	=	Flap Chord
C_D	=	Drag Coefficient
C_{D_i}	=	Induced Drag Coefficient
C_{D_0}	=	Parasite Drag Coefficient
$C_{D_{leak}}$	=	Drag Contribution from Leakage and Protuberance
$C_{D_{trim}}$	=	Drag Contribution from Trim State
C_f	=	Flat-Plate Skin-Friction Coefficient
C_H	=	Horizontal Tail Volume Coefficient
c_l	=	2 Dimensional Lift Coefficient
C_L	=	3 Dimensional Lift Coefficient
C_{L_α}	=	Lift Curve Slope
C_{L_p}	=	Lift Coefficient Response to a Change of Pitch
$C_{L_{TOT}}$	=	Total Lift Coefficient
C_{l_β}	=	Coefficient of Wing Dihedral Effect
$C_{l_{\delta r}}$	=	Rolling Moment Response to Elevator Deflection
C_{l_p}	=	Rolling Moment Response to a Change in Roll Rate
C_{l_r}	=	Rolling Moment Response to a Change in Yaw
C_M	=	Pitching Moment Coefficient
$C_{M_{cg}}$	=	Moment Coefficient about the Center of Gravity
C_{m_α}	=	Pitching Moment Response to a Change in Angle of Attack
$C_{m_{\delta e}}$	=	Pitching Moment Response to Elevator Deflection
C_{n_β}	=	Coefficient of Lateral Stability
C_{n_p}	=	Yawing Moment Response to a Change in Roll
C_{n_r}	=	Yawing Moment Response to a Change in Yaw
$C_{n_{\delta r}}$	=	Yawing Moment Coefficient of Rudder Control Power
C_r	=	Root Chord
C_t	=	Tip Chord
C_v	=	Vertical Tail Volume Coefficient
C_{y_β}	=	Side Force Response to a Change in Sideslip
C_{y_p}	=	Side Force Response to a Change in Roll
δ	=	Deflection Angle
λ	=	Taper Ratio
Λ	=	Sweep
$\Lambda_{c/4}$	=	Quarter-Chord Sweep
L/D	=	Lift to Drag Ratio
Q	=	Interference Factor
Re	=	Reynolds Number
$S_{flapped}$	=	Wing Flapped Area
S_h	=	Horizontal Tail Area
S_{ref}	=	Planform Wing Area
S_v	=	Vertical Tail Area
t/c	=	Thickness to Chord Ratio
W_{TO}	=	Takeoff Weight

Acronyms

$2H2E$	=	2 Hydraulic 2 Electric Circuits Architecture
$AFCS$	=	Automatic Flight Control System
$AIAA$	=	American Institute of Aeronautics and Astronautics
AoA	=	Angle of Attack
APU	=	Auxiliary Power Unit
AR	=	Aspect Ratio
AVL	=	Athena Vortex Lattice
CAD	=	Computer-Aided Design
CFD	=	Computational Fluid Dynamics
CFR	=	Code of Federal Regulations
CG	=	Center of Gravity
CPI	=	Consumer Price Index
$DAPCA$	=	Development and Procurement Cost of Aircraft
$DATCOM$	=	Data Compendium
$EASA$	=	European Union Aviation Safety Agency
EIS	=	Entry Into Service
FAA	=	Federal Aviation Administration
$FADEC$	=	Full Authority Digital Engine Control
GPS	=	Global Positioning System
HP	=	High Pressure
HUD	=	Heads Up Display
$ICAO$	=	International Civil Aviation Organization
IFR	=	Instrument Flight Rules
$IPPS$	=	Integrated Power Plant System
ISA	=	International Standard Atmosphere
$KTAS$	=	Knots, True Airspeed
$KEAS$	=	Knots, Equivalent Airspeed
LCD	=	Liquid Crystal Display
LFL	=	Landing Field Length
LP	=	Low Pressure
MLW	=	Maximum Landing Weight
MRW	=	Maximum Ramp Weight
$MTOW$	=	Maximum Takeoff Weight
$MZFW$	=	Maximum Zero Fuel Weight
MAC	=	Mean Aerodynamic Chord
$NACA$	=	National Advisory Committee for Aeronautics
NLF	=	Natural Laminar Flow
OEI	=	One Engine Inoperative
OEW	=	Operating Empty Weight
$OpenVSP$	=	Open Vehicle Sketch Pad
$PMDS$	=	Power Management and Distribution System
$PSFC$	=	Power Specific Fuel Consumption
$RDT\&E$	=	Research, Development, Test, and Evaluation
RFP	=	Request for Proposal
ROC	=	Rate of Climb
SL	=	Sea Level
$STOL$	=	Short Takeoff and Landing
SVS	=	Synthetic Vision System
TOC	=	Top of Climb
$TOFL$	=	Takeoff Field Length
VFR	=	Visual Flight Rules
VTO	=	Takeoff Velocity

Compliance Chart

The AIAA 2022-2023 RFP outlines mandatory and tradable requirements, in addition to design objectives. The compliance checklists outlined in Table 2 and Table 3 include the aircraft characteristics and compliance of Bounden relevant to these major requirements, and the sections in which these requirements are addressed. In addition to these requirements, the aircraft was designed in compliance with the FAA 14 CFR Part 25, and the compliance for these various design qualities are listed throughout the report in relevant sections.

Table 2   Bounden Requirements Compliance Checklist

Type	Description	RFP Requirement	Bounden	Met	Section
R	Aircraft EIS	2035	2035	✓	II
R	Propulsion EIS	2034	2034	✓	V
R	Passenger Capacity	50 +0/-4	50	✓	IV.B
R	Design Range with full passengers	1,000 nmi	1,000 nmi	✓	XI
R	Cruise Speed	≥ 275 KTAS, Target: 350 KTAS	300 KTAS	✓	XI
R	Seat Width	≥ 17.2", Target: 18"	18"	✓	IV.B
R	Aisle Width	≥ 18"	18"	✓	IV.B
R	Wing Span	Maximum of ICAO Code C (< 36) m	114 ft (34.7 m)	✓	VI.C
R	Approach Speed	Approach Speed Category C (< 141 kts)	132 kts	✓	XI.D
R	Design Range TOFL (ISA + 18 deg F)	≤ 4500' over a 50' obstacle to a runway with dry pavement at sea level	2,555 ft	✓	XI.B
		≤ 4500' over a 50' obstacle to a runway with dry pavement at 5,000' above mean sea level	2,552 ft	✓	XI.B
R	Climb Distance	≤ 200 nmi	143 nmi	✓	XI.C
R	Initial Cruising Altitude	≥ FL280	FL280	✓	II
R	Crew	2 pilots and 1 cabin crew member	2 pilots and 1 cabin crew member	✓	IX
R	Climb Gradient	Meet 14 CFR 25.121 Climb Gradient Requirements	Met	✓	III
R	Autopilot	Capable of VFR and IFR flight with an autopilot	Met	✓	X.B
R	Icing	Capable of flight in known icing conditions	Met	✓	X

Table 3   Bounden Objectives Compliance

O	Autonomy	Systems and avionics architecture to enable autonomous operations	Trade discussed		X.B
O	Block Fuel	20% Reduction in block fuel on a 500 nmi mission vs. current turboprops	21.2 %		XII.A
O	Emissions	Reduction in emissions (CO2, NOX, soot, etc) vs. current turboprops	Met		XII.B

I. Introduction

With the projected growth of the regional aircraft market over the next 20 years and the focus on sustainable aviation, the 50-seater incumbent products — turboprops and turbojets originally designed in the 1980s — need to be re-imagined to meet the US Domestic Scope Clause advocating for better fuel burn, emissions, and economics than that of the current aircraft in-service [1]. Bounden, a 50-seat turboprop that reduces emissions and block fuel compared to the aircraft in its class, perfectly taps into the unsaturated portion of the market, providing a clear market case [2]. The truss-braced design minimizes battery and fuel weight to bring down block fuel and overall cost. Through a parallel hybridization structure that utilizes batteries to hybridize the climb and cruise portions of the flight, Bounden reduces block fuel, emissions, and fuel costs with an EIS of 2035. The major design metrics are summarized in Table 4.

Table 4   Bounden Design Metrics Summary

General Metrics	Value	Performance Metrics	Value
MTOW	63,526 lb	BFL (Sea Level)	2,383 ft
Span	114 ft	LFL (Sea Level)	3,955 ft
S_{ref}	760 sq. ft	Cruise Speed	300 kts
Block Fuel Reduction	21.2 %	Cruise Altitude	28,000 ft
Cost with 15 % Profit (2023 Dollars)	$37.4 million	Electric Throttle	35 %

II. Concept of Operations

A. Market Analysis

As the aviation market grows and aims to build a net-zero sustainable aviation system by 2050 [3], regional turboprops provide a more sustainable and realistic alternative for achieving these objectives compared to the current fleet of regional jets. The U.S. Aviation Climate Action Plan identifies methods to decrease emissions, including through the development of more efficient aircraft and engines and the electrification of short-haul aviation [3]. In addition, turboprop engines are more efficient at producing thrust at lower speeds in comparison to turbofans [4]. For short-haul flights, where the majority of the mission profile is spent in climb and descent as opposed to cruise, turboprops are the more efficient choice.

Although turboprops are common for commuter and business aircraft, customers tend to prefer jets for numerous factors in spite of their inefficiency [4]. The regional turboprop market is currently based upon older designs with their roots in the 1980s [5] that have older interior configurations and out-of-date avionics suites. Turboprops also fly at lower altitudes than jets, where the effects of weather make the passenger experience less enjoyable. For turboprops to break into the short-haul market, they must not only align with the efficiency goals outlined by the government and FAA, but also provide a passenger experience comparable to those offered by regional jets.

The age and lack of innovation in the 50-seat class of both turboprops and jets is clearly illustrated by their evolutionary chart shown in Figure 2 [6] [7]. A 50-seat hybrid-electric regional turboprop like Bounden that can exceed the performance and economics of traditional regional jets while improving upon the designs of incumbent turboprops provides solutions to multiple unaddressed problems driving the market space.
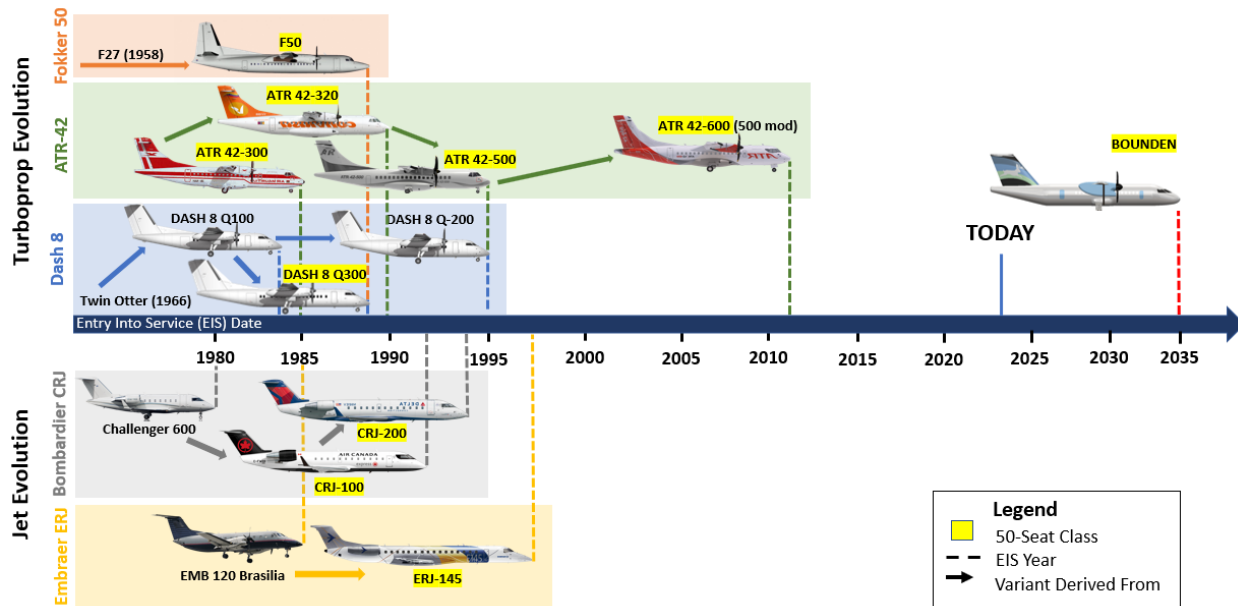
Fig. 2   Turboprop and Jet Evolution and EIS Timeline

B. Market Analysis Driving Design

The US domestic "Scope Clause" requires significantly better fuel burn and economics in comparison to the existing options, including the old lines of turboprops in service across the world. The COVID-19 pandemic also revealed a stable demand for regional flights compared to long-haul flights, and with large aircraft not at full capacity, turboprops provide a more economic solution compared to jets [8]. To satisfy this market, the team proposes Bounden, a regional parallel hybrid-electric turboprop design that reduces emissions and overall block fuel through hybridization, cutting operating costs for airlines while satisfying the sustainability requirements guiding the future of aviation with an EIS of 2035. The high-wing 50-seater with tricycle landing gear is configured similarly to turboprops such as the ATR-42 and Dash 8-Q300. Bounden is based on these configurations but redesigned to leverage newer technology such as composites, batteries, and new avionics suites while reducing maintenance, cost, and fuel burn. Additionally, its high cruising altitude of 28,000 ft and its modern interior and avionics suite improves passenger and crew experience, making it a comparable experience to that of regional jets.

While designed to the US Scope Clause goals, a large portion of the market for the aircraft and regional turboprops is outside of North America, with new routes and growing demand forecast in Asia Pacific, Europe, Africa, the Middle East, Latin America, and the Caribbean [9]. For example, the aviation industry in Asia is expected to have significant growth. China's "second-tier" cities are often situated in more rural surroundings, which promotes the need for short-range flight. Another factor that might contribute to the favorability of turboprops in China is that aviation fuel is more expensive in China due to government regulation [10]. These problems, in addition to the pollution problem China is facing, would make the proposed hybrid-electric turboprop a favorable design internationally.

C. Design Requirements

In addition to meeting the outlined RFP requirements, additional requirements were derived and allocated by the team. When creating the initial design of the aircraft, TOFL, LFL, cruise requirements, range, passengers, weight, and entry into service drove the design decisions. A summary of the derived and allocated requirements is shown in Table 5.

Table 5   Aircraft Design Requirements

Requirement	Derived Requirements	Allocated Requirements
EIS 2035, IPPS by 2034	Use systems that can be certified by 2030-2032	Battery technology by 2032, certified by 2034 Motor technology by 2032, certified by 2034 Use current avionics/systems packages Ability to retrofit for future technologies
20% Block Fuel Reduction on 500 nmi mission	2,165 lb block fuel maximum	Electric throttle constant at 35% for 500 nmi mission
4,500 ft TOFL/LFL	8,500 hp takeoff power Takeoff $C_{L_{max}}$ = 2.37 Landing $C_{L_{max}}$ = 2.53	11,000 hp engine power
1,000 nmi design range	Minimum constant power from gas engine to climb Descent power Idle power Cruise C_L = 0.665 L/D = 18 AOA = -2.5 to 11.3 degrees	Required Power at Cruise
Autonomy trade	Additional sensors to support autonomy	Extra wiring and space for retrofitting autonomous technology (if pursuing)

D. Operations

1. Mission Profile

Bounden's mission profile is broken into five sections (taxi & takeoff, climb, cruise, descent, landing & taxi) and reserves. The mission parameters are defined in Table 6 and shown visually in Figure 3. The mission was designed for a 1,000 nmi flight at 28,000 ft cruise altitude at a speed of 300 kts. With the current design, climb and cruise will be utilizing the hybrid-electric features while other portions of the mission will remain all gas.

Table 6   Mission Profile

Mission Section	Description	Additional Information
1-2	Taxi & Takeoff	15 min taxi
2-3	Climb	145 KCAS
3-4	Cruise	300 KTAS
4-6	Descent	Idle throttle
5	Loiter	150 KTAS at 10,000 ft
6-7	Landing & Taxi	10 min taxi
8-9	Reserve Climb	Gas engine
9-10	Reserve Cruise	Gas engine
10-11	Reserve Descent	Gas engine
9-10	Reserve Landing & Taxi	Gas engine
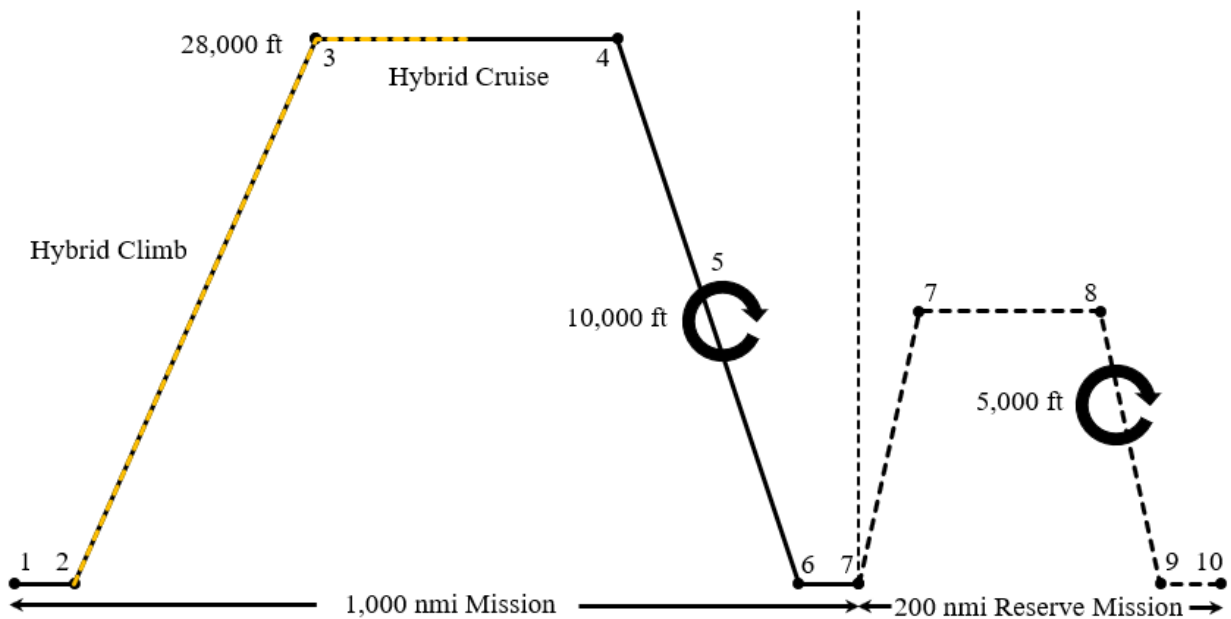
Fig. 3   Mission Profile

2. Battery Removal and Charging

In order to stay competitive in the regional turboprop market, the team worked to optimize turnaround time as much as possible. The turnaround time for an aircraft includes the time to disembark passengers, refuel, perform pre-flight checks, and board the next flight's passengers. In the case of a hybrid-electric aircraft, this turnaround time must also include time to replace the energy depleted from the batteries during the flight. Bounden requires 1,200 kWh of battery energy to hybridize at the optimal level, and with current battery and charging technology, charging batteries in between flights would significantly increase the turnaround time. Even with a very powerful 100 kW DC-DC charger, charging each battery pack would still take 2 hours. Considering the team's goal of keeping turnaround time under 30 minutes as turboprops are more profitable than jets for short turnaround times, the charging option was deemed not viable. The alternative to charging the batteries on the plane is replacing the drained batteries with charged batteries between flights. While this method would require more labor, this process is estimated to take about 10 minutes, which would align with the turnaround time goal. This battery charging process, coupled with the typical loading and unloading process, is shown in Figure 4.
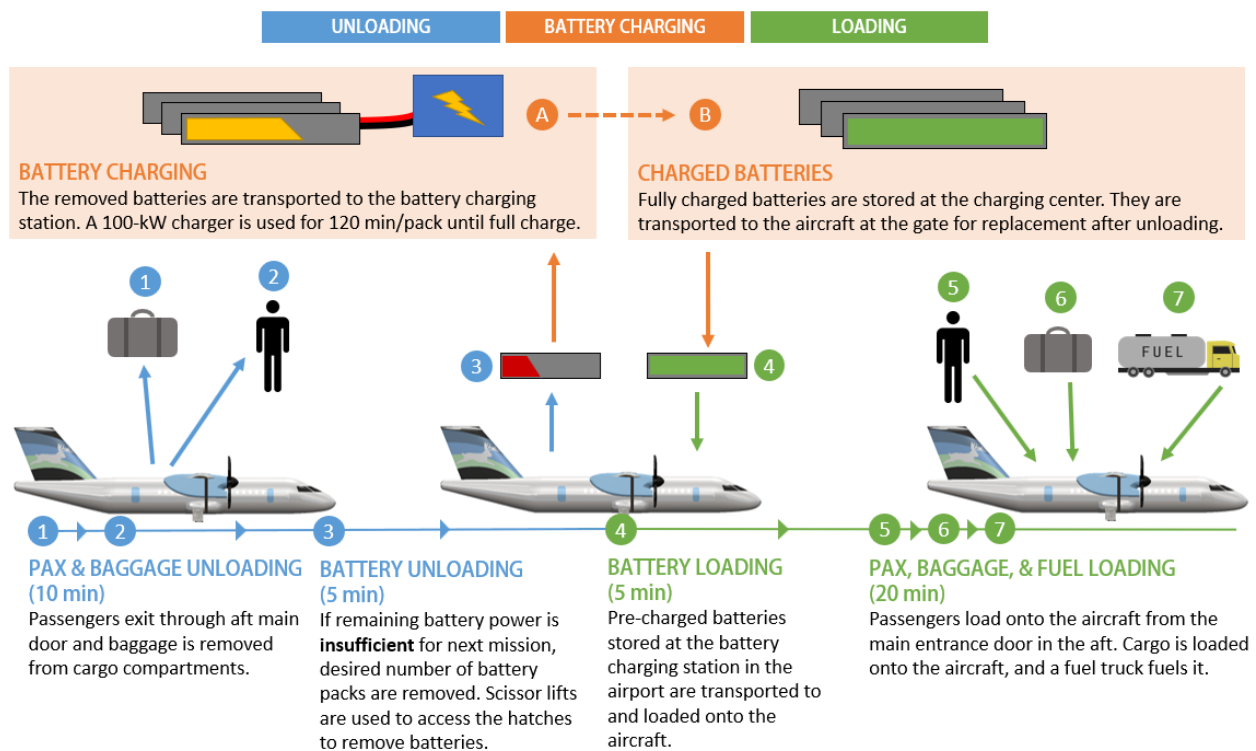
Fig. 4   Loading, Unloading, and Battery Charging Process

Upon Bounden's landing and taxi to an airport gate, ground crew members will approach the aircraft with a mechanical dolly system that will be used to remove the battery packs from the aircraft. Since the battery packs are stored at the bottom of the fuselage, there is a hatch installed on the side of the aircraft that will give access to each battery pack. There are 3 packs stacked on top of each other, with 3 packs in front of the aircraft's center of gravity

and 3 packs behind. There are 2 hatches to access the packs for removal. The crew members will detach any cables that attach the battery packs to the motors and then adjust the dolly such that the device is grabbing one of the packs. The packs will be pulled out with the dolly and taken to a separate area to charge. Then, fully charged packs will be replaced with the dolly and locked and plugged in by crew members. The packs taken to charge will be charged with 100 kW chargers, once again to help with turnaround time. To accommodate these operations, each airline that services Bounden will have additional batteries as part of their fleet for the charging rotation.

III. Sizing Analysis

A. Similarity Analysis

To initialize the sizing process, similar aircraft within the regional turboprop class were considered, and the parameters of the aircraft with the best potential to achieve the design requirements were chosen for initial sizing estimates. The three aircraft chosen were the Bombardier Dash 8-Q300, Fokker 50, and ATR 42-600 since they each had key parameters that were close to the requirements set by the RFP. The aircraft were researched and the parameters for each are shown in Table 7. All the data for the Bombardier Dash 8-Q300 was obtained from the Dash 8-Q300 Airport Planning Manual [11], EASA [12], Air-Tec Global [13], and CemAir [14]. Information for the Fokker 50 was found from a Fokker 50 information booklet [15]. Information for the ATR 42-600 was obtained from the ATR 42-600 brochure [16], SKYbrary [17], and Airfoil Tools [18].

Ultimately, the Fokker 50 was selected as the "seed" aircraft since its performance is much closer to that of the RFP requirements than the Dash 8-Q300 and the ATR 42-600. The "seed" aircraft is an aircraft that initializes the sizing process in which the chosen aircraft's parameters are used to conduct a first pass analysis. As more analysis is conducted, the dependency of this aircraft on the sizing process decreases until the team has developed new parameters for a design that meets the requirements. The Fokker 50 was chosen since the aircraft has a capacity of 50 passengers compared to 56 for the Dash 8-Q300 and 48 for the ATR 42-600. The Fokker 50 also has a range that is larger than the RFP requirement by 80 nmi. This would ensure that an unchanged configuration from the "seed" would achieve the requirement of reaching 1,000 nmi unlike the ranges for the Dash 8-Q300 and the ATR 42-600, which are already lower than the RFP requirement by 76 and 297 nmi, respectively. Additionally, this aircraft weighs more than the Dash 8-Q300 and the ATR 42-600 due to the larger maximum fuel weight and the lower PSFC. This will help to balance the weight increase when implementing and accounting for the hybrid components since the amount of fuel needed should decrease as electric power is used to power the aircraft during certain segments of flight. Another similarity analysis for tail configuration of current regional turboprop aircraft and future concepts from Embraer and ATR is shown in Table 8 and was used to justify tail decisions in Section IV.

6

Table 7   Key Aircraft Parameters from Similarity Analysis

Parameters	Bombardier Dash 8-Q300	Fokker 50	ATR 42-600
Max Ramp Weight [lb]	43,200	45,900	41,005
Empty Weight [lb]	26,065	29,542	25,794
Max Zero Fuel Weight [lb]	39,500	41,665	37,148
Max Payload Weight [lb]	13,435	12,125	11,684
Max Fuel Weight [lb]	3,700	9,090	3,527
Max Landing Weight [lb]	42,000	44,160	40,344
Wing Area [ft^2]	604	750	586
Wing Span [ft]	90	95.14	80.58
Taper Ratio	0.47	0.39	0.50
Sweep [deg]	0	0	0
W/S [lb/ft^2]	71.52	61.20	69.97
Horizontal Tail Span [ft]	26	32	30
Horizontal Tail Area [ft^2]	196.1	171.9	109.7
Vertical Tail Area [ft^2]	201.7	150.7	180.7
Fuselage Length [in]	953	992	893
Fuselage Diameter [in]	106	107.9	106.3
Max Operating Altitude [ft]	25,000	25,000	26,000
Cruise Mach	0.451	0.469	0.500
Range [nmi]	924	1,080	703
Approximate PSFC at Cruise [lb/hp-hr]	0.500	0.459	0.500
Number of Engines	2	2	2
P/W IPPS [hp/lb]	1.599	1.996	1.356
Takeoff $C_{L,max}$	2.07	1.88	2.19
TOFL [ft]	3,768	3,632	3,632
Landing $C_{L,max}$	2.55	2.16	2.53
Landing Distance [ft]	2,610	3,169	2,972

Table 8   Configuration Trade Study

Aircraft	Wing	Tail	Engine	Landing Gear
Fokker 50	High	Conventional	2x under wing	Tricycle; 1 under nose, 2 on wing
ATR 42-600	High	T	2x under wing	Tricycle; 1 under nose, 2 under fuselage
Dash 8-Q300	High	T	2x under wing	Tricycle; 1 under nose, 2 under wing
Saab 340B	Low	Conventional	2x on wing	Tricycle; 1 under nose, 2 under wing
Saab 2000	Low	Conventional	2x on wing	Tricycle; 1 under nose, 2 under wing
ATR EVO	High	T	2x under wing	Tricycle; 1 under nose, 2 under fuselage
Embraer Concept Aircraft	Low	T	2x at tail	Tricycle; 1 under nose, 2 under fuselage

B. Design Space

The initial sizing process follows the methods described by Roskam for propeller-driven aircraft [19]. Using historical data and mission requirements to drive the initial sizing, constraints for takeoff, climb, cruise, and landing were generated as shown in Figure 5. These requirements include stall speed and the 14 CFR §25.121 OEI climb conditions, in addition to the takeoff, cruise, and landing requirements.
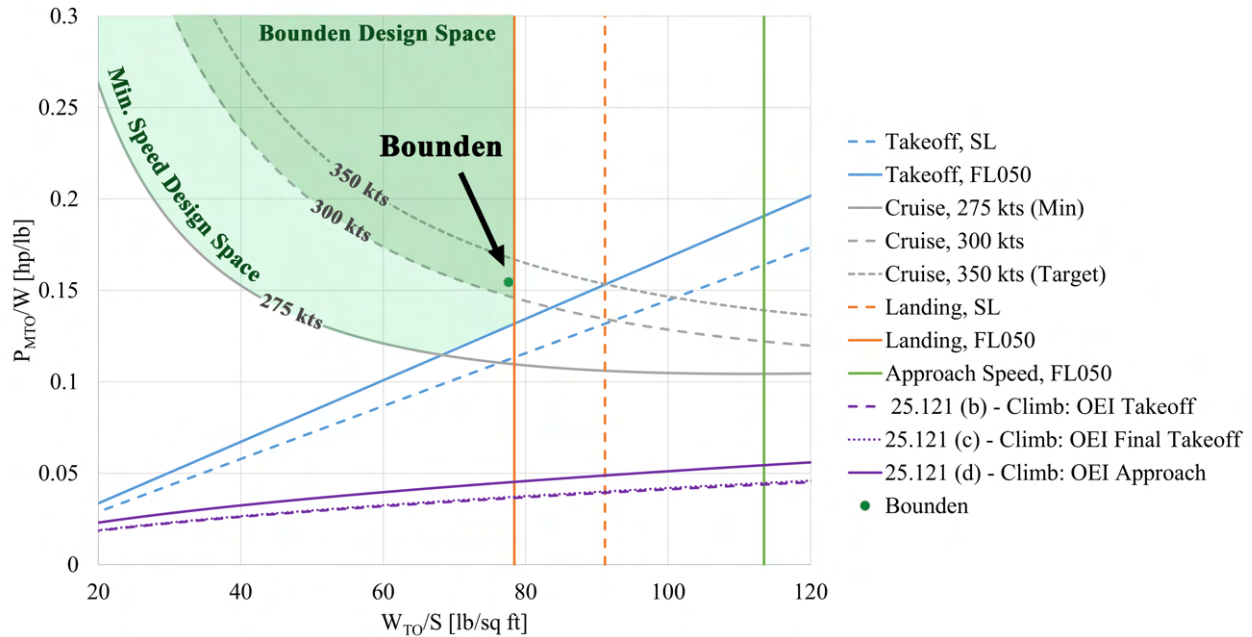
Fig. 5   Design Space Constraint Diagram

The assumptions and requirements driving the constraint diagram are shown in Table 9. The constraint diagram assumptions for the mission were driven by the outlined requirements and historical analysis. Minimum requirements from the AIAA RFP were allocated to drive the constraints in Figure 5, and additional parameters and requirements were derived by using averages from the similarity analysis shown in Table 7 and other historical values for turboprop aircraft. The flap performance of the Fokker 50 is inconsistent with the ATR-42 and Q300 due to its age, so it was not used when deriving the C_{Lmax} values. The power ratio was adjusted to include an approximate hybridization factor of 0.15, as the power produced by batteries is not impacted by altitude like the power of the turboprop engine.

The design space is driven almost entirely by the cruise and landing requirements. This is due to the high cruising altitude requirement as it increases the required power at cruise, and due to the weight of the aircraft at landing since battery weight remains constant throughout the flight. Constraints are more challenging for a hot day of $\Delta ISA = +18°F$, so the aircraft is driven by the cruise, takeoff, and landing for that case. The design point of Bounden, illustrated in Figure 5, is the minimum weight solution given a cruise speed of 300 kts. A cruise speed of 350 kts would require a higher power-to-weight ratio, and when sizing estimates were analyzed for this speed, the overall weight of the aircraft

increased significantly. While the cruise speed of 275 kts provided an even lower weight solution, approaching the target cruise speed requirement was prioritized to provide a competitive cruise speed within the market. The trade between cruise speeds is further discussed in Section III.C. This initial design space provided an estimate for initial sizing given the power-to-weight ratio and wing loading. The cruise constraint can be used as an initial estimate to size the takeoff power and thus, the engine required using weights of similar aircraft, and the wing loading can be used to determine the AR and S_{ref} from trade study plots.

Table 9   Key Parameters Driving Constraint Diagram

Parameter	Value	Justification
Rate of Climb	5 fps	Average rate of climb for turboprops at top of climb
Takeoff Parameter	13.4	Parameter for Raymer takeoff equation derived from similarity analysis [4]
Landing Parameter	20.6	Parameter for Raymer landing equation derived from similarity analysis [4]
Propeller Efficiency	0.85	Average propeller efficiency
Hybridization Factor	0.15	Average in the optimal hybridization range
S_{air}	1,100 ft	Historical average for similar aircraft using Raymer [4]
μ	0.47	Braking coefficient of rubber on tarmac
Cruising Altitude	28,000 ft	AIAA RFP minimum requirement
Cruising Speed	275 KTAS	AIAA RFP minimum requirement
$C_{L,max,TO}$	2.10	Derived from similarity analysis with Q300/ATR 42
$C_{L,max,L}$	2.54	Derived from similarity analysis with Q300/ATR 42
W_{CRS}/W_{TO}	0.97	Derived from similarity analysis
W_{LDG}/W_{TO}	0.98	Derived from similarity analysis
P_{TO}/P_{CRS}	0.46	Scales hybrid power at FL280 cruising altitude given hybridization factor

C. Initial Sizing

1. Trade Studies

A sizing loop was conducted for cruise speeds ranging from the RFP minimum to the target requirement to justify the speed to use for sizing the aircraft. The results for the impact on MRW are shown in Figure 6.
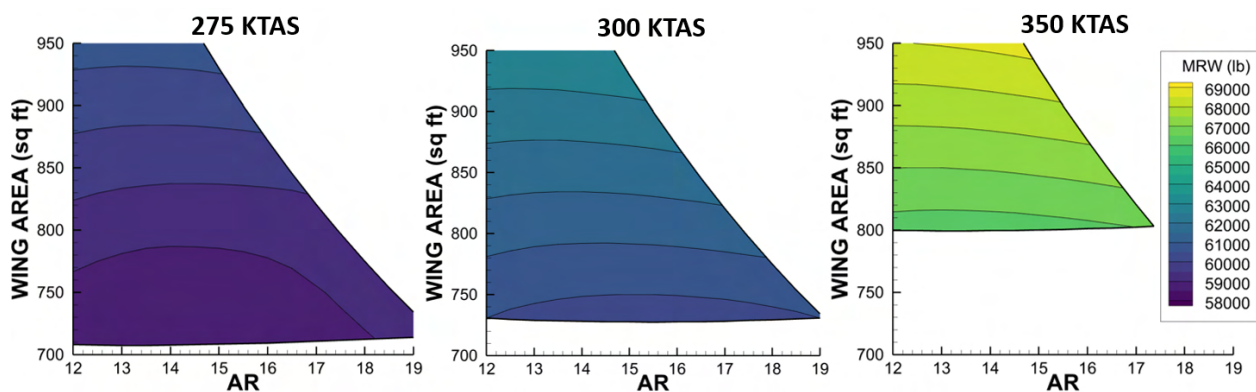
Fig. 6   Maximum Ramp Weight Trade Study for Varying Cruise Speeds

From these results, it can be seen that MRW increases significantly at the full speed of 350 KTAS, and a significant portion of the lower S_{ref} design space is invalid due to not meeting LFL requirements. The high AR and low S_{ref} design space is where the other weights, such as battery and fuel weights, are at their lowest. In this regime, a truss-brace is necessary to support the load on the high AR wing and reduce adverse effects such as flutter. This regime which minimizes battery weight, fuel weight, empty weight, and MRW is fully available in the 275 KTAS design space and mostly available for 300 KTAS. At 350 KTAS, a majority of the design space is constrained. Between these speeds at 300 KTAS, the MRW is slightly heavier than at the minimum 275 KTAS but still thousands of pounds lighter than the design space for 350 KTAS. At this speed, most of the design space is still valid unlike at 350 KTAS. As a result, a speed of 300 KTAS is used for sizing. The faster design cruise speed will also keep Bounden competitive with its class and with jets in the market space.

This analysis is validated by the design spaces for each cruise speed illustrated in the constraint diagram in Figure 5. The cruise speed of 350 kts requires a greater power-to-weight ratio than the other speeds. With a hybridization factor of 15%, this resulted in a higher battery and fuel weight, which also drove up the empty weight to account for the additional hybridization factor. To still meet the required wing loading at landing, greater wing areas are required, also driving up weight. Although minimum weight solutions exist within this design space, the team found that the additional weight of the aircraft from these factors caused block fuel to fall below a 20% reduction. As a result, the design cruise speed was chosen as 300 kts as validated by multiple models.

2. Design Point

An initial sizing pass was analyzed using the parameters of the Fokker 50 and an allocated battery weight of 10,000 lbs, but these initial calculations did not account for some factors such as hybridization infrastructure. The "seed" parameters were then scaled up appropriately to account for the additional weight and infrastructure to support hybridization, and the overall weight increased. The significant increase in weight signified that the engine power required was higher than the power provided by the engines of the Fokker 50. The engines were up-sized to the PW150A to increase takeoff power such that it was possible to meet the power-to-weight requirement driven by cruise shown in Figure 5. The required propulsion power is further analyzed in Section XI and the engine performance is detailed in Section V. A trade study was performed analyzing how a range of S_{ref} and AR values impacted the various weights required to achieve range and balanced field length. The results of these iterations are shown in Figure 7, with the constraints on the design space outlined in Table 10.

The design point was chosen such that it minimized all of the weights shown in Figure 7. The point was picked with enough margin from the constraints such that it would still meet them with slight shifts in the weight throughout the refinement process, as shown by the location of the star representing the point in Figure 7. Additionally, this sizing process was a starting place for the design. Higher fidelity methods would be used to determine more accurate design and

performance parameters, so a point not directly on the edge was chosen. After determining this design point, an iterative empty weight process was used to calculate the increase in empty weight to support the hybridization infrastructure for the battery sized in this process. This weight was then used as the starting point and basis for the analysis of Bounden.

(a) Maximum Ramp Weight Trends (lb)

(b) Empty Weight Trends (lb)

(c) Fuel Weight Trends (lb)

(d) Battery Weight Trends(lb)
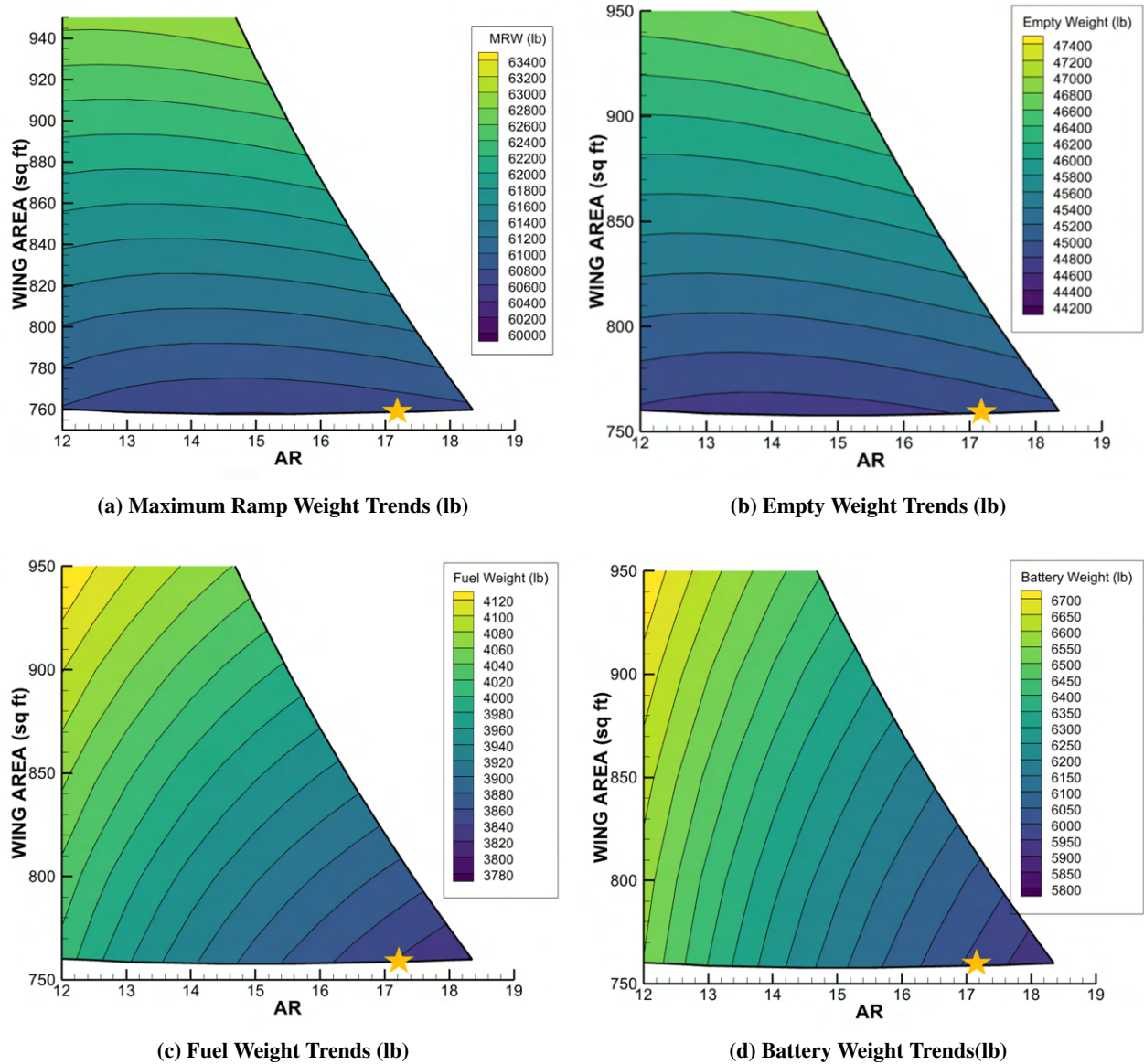
Fig. 7   Weights for Wing Area and Aspect Ratio Combinations

Table 10   Allocated and Derived Requirements for Initial Sizing

Parameter	Value	Source	Requirement Type
Span	118.1 ft	Maximum of ICAO Code C	Allocated
LFL	4,500 ft	RFP Requirement	Allocated
TO W/S	80 psf	Similarity Analysis	Derived
Landing W/S	78.4 psf	Constraint Diagram	Derived

D. Comparison to Class

When comparing Bounden to the rest of the class, Bounden can serve the same passenger count as the ATR-42 with 50 passengers, but is closer to the weight of the ATR-72. This can be observed in Table 11 as Bounden is heavier in weight due to the added infrastructure used to support the hybrid propulsion system. The addition of the hybrid system will make Bounden attractive to the market due to its newer technology, lower emissions, and lower fuel costs when compared to other aircraft within the class. Additionally, Table 11 highlights the fuselage length and diameter of the aircraft within the class. It can be observed that Bounden offers a larger diameter than comparable aircraft to provide increased comfort for passengers.

Table 11   Competitive Aircraft Comparison

Parameter	ATR-42	ATR-72	Bounden
MTOW [lb]	41,005	50,705	**63,526**
OEW [lb]	25,794	29,983	**47,245**
MZFW [lb]	37,148	46,296	**58,028**
Maximum Payload Weight [lb]	11,684	16,313	**12,125**
Maximum Fuel Weight [lb]	3,527	11,024	**9,180**
Maximum Landing Weight [lb]	40,344	49,272	**62,314**
Fuselage Length [in]	893	1,070	**992**
Fuselage Diameter [in]	106	101	**111**

IV. Configuration

A. Aircraft Morphology

Many different factors were considered for the configuration of Bounden. High wing and low wing were the two main options for wing placement. After analyzing both configurations, the benefits and drawbacks of each are presented in Table 12. Ultimately, the high wing was chosen as the low wing configuration introduces additional challenges surrounding propeller clearance, which must be at least 7 inches off the ground in accordance with 14 CFR §25.925. In addition, aft-mounted and wing-mounted engine configurations were considered. The wing-mounted configuration was found to be superior through the analysis shown in Table 13 given the market and operations of Bounden.

Table 12   Wing Configuration Trade Study

Wing Configuration	Pros	Cons
High	Shorter takeoff distance Naturally stable Less ground effect	Landing gear must go in fuselage or nacelle
Low	Lower drag Landing gear can go in wing box	More difficult to load passengers

Table 13   Engine Location Trade Study

Engine Location	Pros	Cons
Wing-Mounted	Center of gravity is closer to the center of aircraft Easier to maintain	Simpler structural design Harder to control aircraft in the case of one engine inoperative
Aft-Mounted	Less cabin noise Cleaner wing	Structural issues when mounting engines Larger wire weight for hybrid engine

A twin-engine configuration was chosen for Bounden. Since the chosen power unit produces enough thrust for the aircraft with just two engines, having more than 2 engines on Bounden would add significantly to the aircraft's weight without major benefits. The extra two engines, which would be located on the wing, would also add drag to the aircraft. Since two engines produce enough thrust for operation, adding two additional engines could not be justified.

Once the final wing and engine configurations were chosen, the tail was chosen to be a T-tail. The main benefit of a T-tail over other configurations, such as a conventional tail, is that a T-tail's high horizontal stabilizer will allow it to avoid the propeller airflow. This would be optimal for both engine placements. The two initial configurations considered for Bounden are shown in Figure 8. Between the two, Configuration A was chosen. The primary drivers of Configuration A include the high wing, lower wire weight, shorter takeoff distance, and a center of gravity closer to the center of the aircraft.
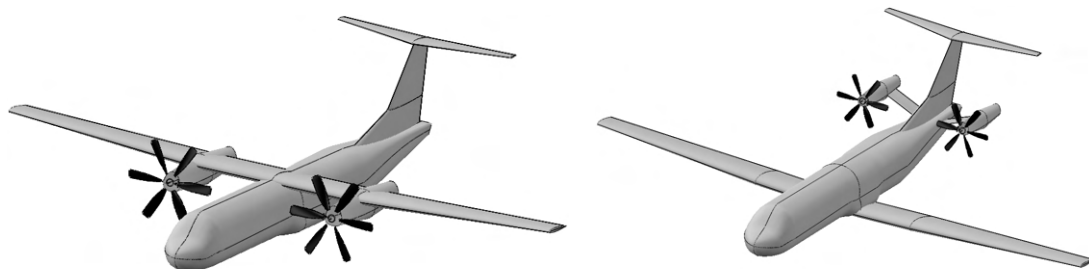
(a) A High-Wing, Wing-Mounted Engines Configuration With a T-tail.

(b) A Low-Wing, Aft-Mounted Engines Configuration With a T-tail

Fig. 8   Candidate Configurations

In addition to the two configurations shown above, truss-bracing the wing was also considered. This configuration would have two engines that were mounted on the wing and a truss that would travel below the nacelle. The benefits of a truss-braced wing include a reduced structural load on the wing, a lighter wing, increased lift, and aeroelastic benefits [20], all of which would improve the performance of Bounden. As a result, the team decided to add a truss-braced wing to Bounden. This final configuration is shown in the 3-view of the aircraft in Figure 9, with the render shown in Figure 10.
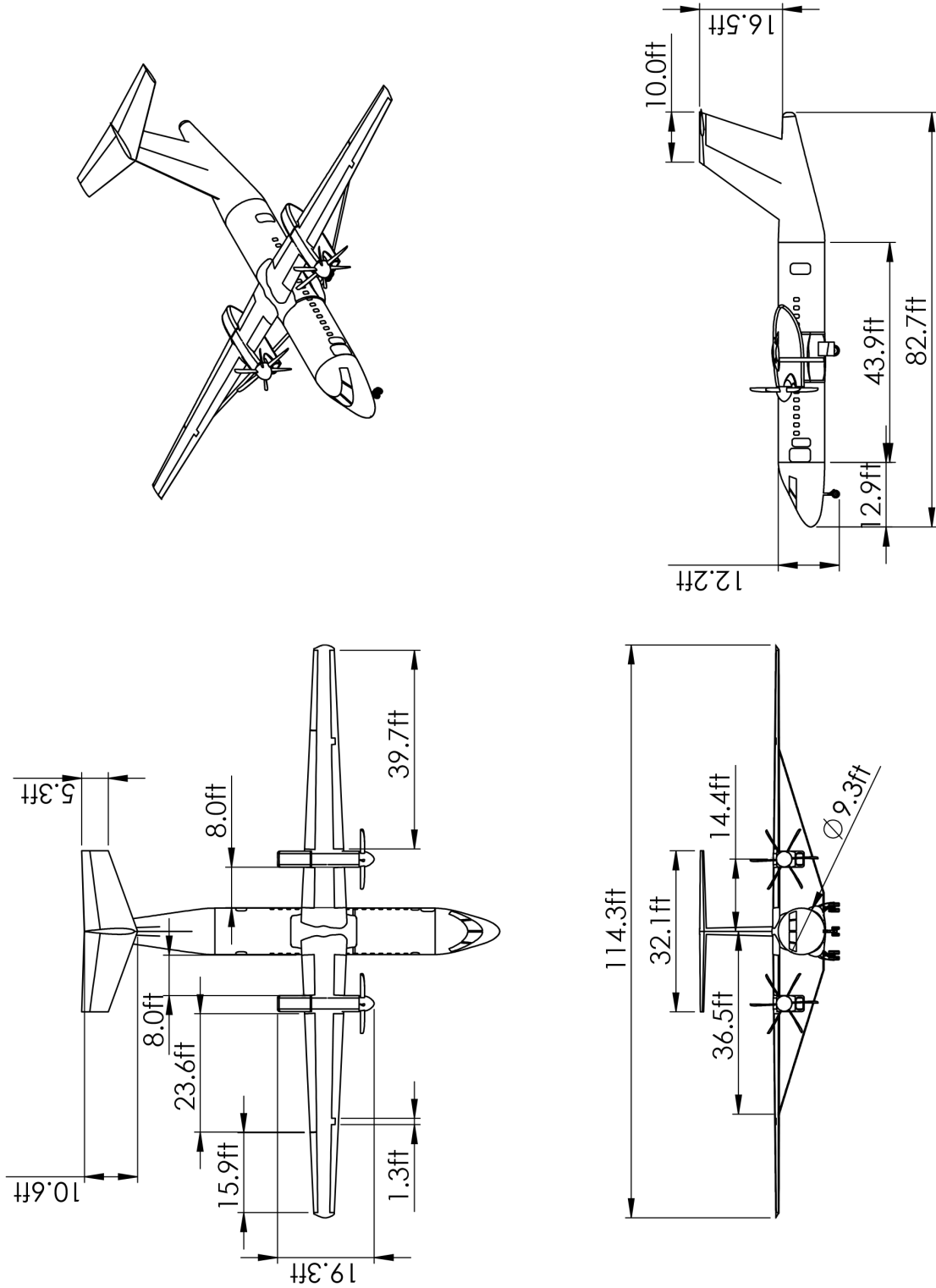
Fig. 9   Dimensioned 3-view of Bounden with an Isometric View

Fig. 10   Final Configuration with Truss-Braced Wing

B. Main Cabin Design

The design philosophy for the interior of Bounden was driven by balancing three major objectives: meeting the target requirements for a positive customer experience, maximizing cargo space above the floor to drive revenue, and maximizing space below the floor for the battery and other systems requirements.

A passenger configuration of 12 rows of seats arranged at a 30 inch pitch with an additional row of 2 in the aft of the main cabin was chosen to achieve a PAX count of 50 passengers. This decision to maximize the PAX in the required single-class arrangement drives down the cost per passenger for the customer. The aft of the cabin features a galley and crew wardrobe, with cargo space distributed between two compartments in both ends of the cabin as shown in Figure 11. A foldable crew jumpseat is also located in the aft of the cabin. The overall dimensions of the cabin are detailed in Table 14 and 15.
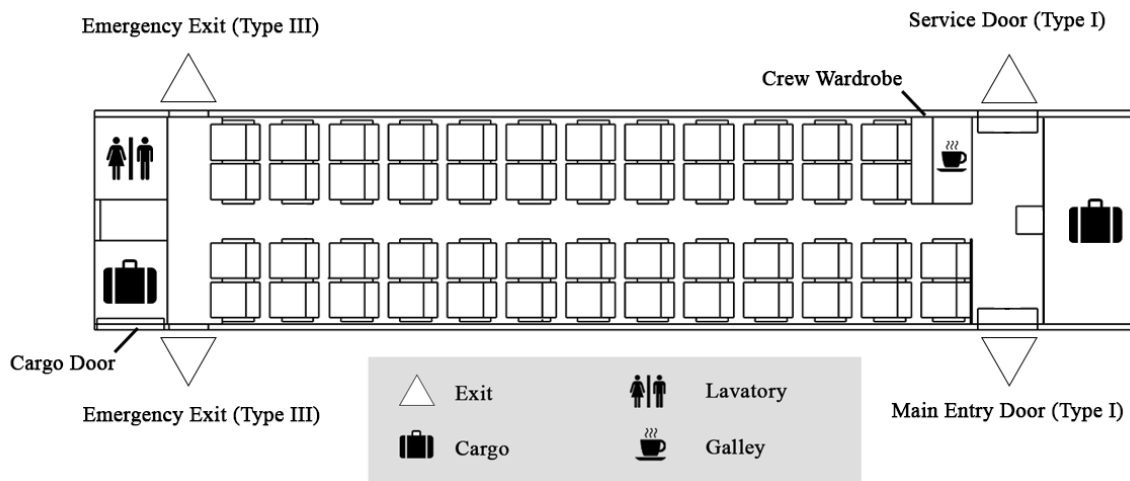
Fig. 11   Cabin Layout

For a passenger seat configuration of 50, CFR §25.807 requires that there must be at least two exits on each side of the fuselage, one of which must be Type I or larger. As shown in Figure 11, the aircraft has a Type I and Type III exit on each side of the fuselage, with the former in the aft of the cabin and the latter in the forward. CFR §25.815 also requires a minimum aisle width of 20 inches when measured 25 inches or more from the floor, driving the armrest height. Table 15 summarizes spacing allocations for all of the features in the main cabin.

Table 14   Interior Configuration

Parameter	Value
PAX Count	50
Rows	13
Seat Pitch	30 in.
Cabin Length	526 in.
Cabin Width	105 in.
Aisle Height	74 in.
Aisle Width below 25 in.	18 in.
Aisle Width above 25 in.	20 in.

Table 15   Interior Configuration Features

Type	Quantity	Size
Main Entrance Door (Type I)	1	26 in. x 48 in.
Service Door (Type I)	1	26 in. x 48 in.
Type III Emergency Exit	2	20 in. x 44 in.
Cargo Door	1	33 in. x 50 in.
Galley	1	20 in. x 42 in.
Lavatory	1	37 in. x 42 in.
Forward Cargo Compartment	1	37 in. x 42 in.
Aft Cargo Compartment	1	51 in. x 104 in.

With the 18 inch seat width target requirement driving the seat sizing, similarly sized example airplane seats from Roskam Part III were used to determine the other dimensions [21]. Using historical sizing values for economy seats described by Roskam and the required seat width, armrest width, and aisle requirements, the seats were designed to fit in a 2x2 configuration given a cabin height of 74 inches, an average height for similar aircraft. A cross-section of the seating configuration and the overhead baggage in the main cabin is shown in Figure 12.
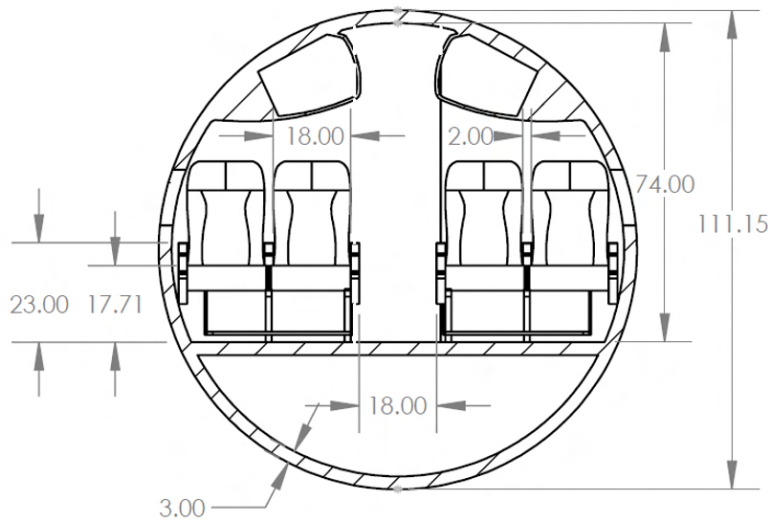
Fig. 12   Cross Section, in inches

The cargo requirements of 262 ft^3 as given by the RFP for 50 passengers and 3 crew members drove the sizing of the cargo compartments located in the main cabin. As shown in Figure 11, there is one cargo compartment in the forward of the main cabin, and one larger compartment in the aft. The available cargo storage is described in Table 16. All of the cargo is stored above the floor level as shown in Figure 12. The forward cargo can be accessed through a cargo door on the left side of the aircraft, while the aft cargo can be loaded in through the service door, similar to the cargo operations of the ATR-72.

The volume of each cargo hold was calculated to ensure volume passenger and crew requirements were met. The cargo requirements are satisfied by the main holds such that full-size luggage can be stored for all passengers and crew, and the overhead baggage compartments provide additional passenger cargo space to be competitive with other aircraft in its class and the market. The approximate bags for each cargo hold were calculated using the RFP requirements of 4 ft^3 of baggage per crew and 5 ft^3 per passenger. The weights of all the projected cargo are accounted for in Section IX.

Table 16   Cargo Available

Hold	Volume [ft^3]	Approximate Bags
Forward Cargo Hold 1	56	12
Aft Cargo Hold	193	41
Crew Wardrobe	16	Additional Crew Storage
Overhead Baggage	131	5lb Additional Baggage/PAX
Cargo Hold/Wardrobe Volumes	**265**	53 (50 PAX + 3 Crew)
Total Cargo Volume	**396**	53 + 1250 lb Overhead Baggage

C. Flight Deck Design

The following considerations drove the flight deck layout: the ability for the crew to see flight essential instruments and reach all controls comfortably, communicate by voice or touch easily, and maintain the cockpit viewing angles outlined by 14 CFR §25.773 [21]. The flight deck layout is illustrated in Figure 13. Design decisions were made with the philosophy of enhancing historical layouts to improve the current best-in-class configurations while easing pilot training with familiar layouts and systems. To minimize training costs for pilots, the decision was made to use a traditional yoke rather than a side stick to control the aircraft. The flight deck was designed in accordance with 14 CFR §25.1303 and includes all necessary flight controls and interfaces. The autonomy trade and specifications of the avionics and controls are discussed in Section X.B.
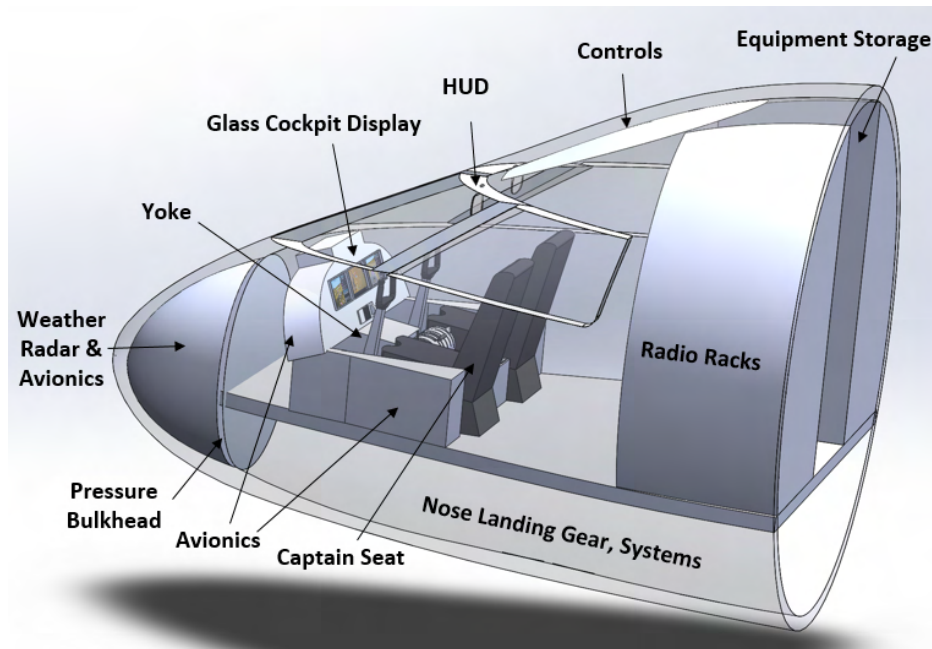
Fig. 13   Flight Deck Layout

A reference point of a male in the 95th percentile is used in the flight deck sizing, but several aspects of the flight deck are made adjustable including seat height to achieve the listed objectives for a range of human body sizes [21]. The pilot viewing angles are also determined given the approximate eye level of a male crew member in the 95th percentile but can be obtained with seat adjustments for different percentile pilots. Recommended pilot viewing angles are outlined in Advisory Circular (AC) 25.773-1. Bounden's pilot viewing angles are shown in Figure 14, and meet the horizontal recommendations, but not the vertical. However, Bounden's vertical viewing angles are in-line with the class per historical analysis in Roskam Part III and meet the requirements of 14 CFR §25.773 for visibility [21].
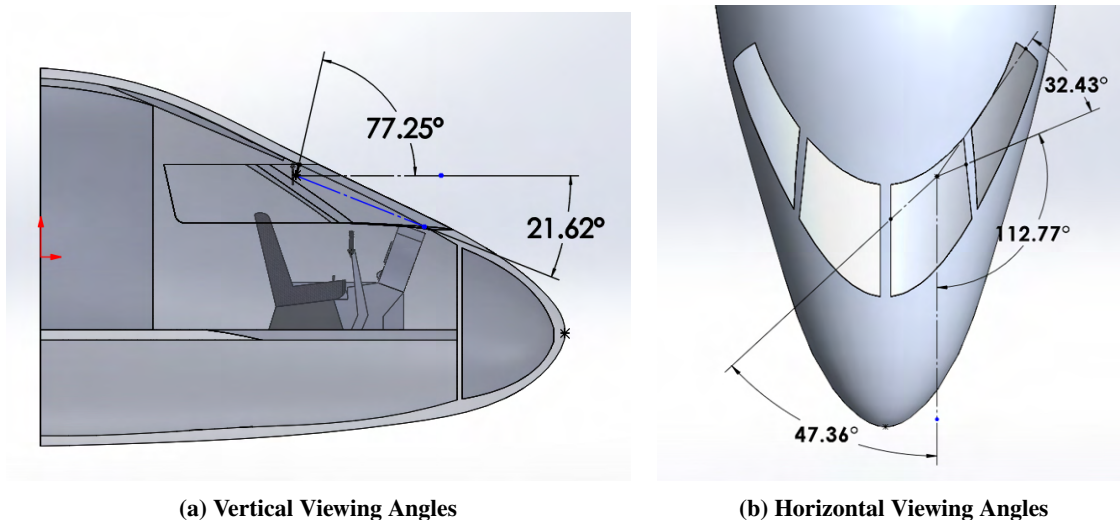
(a) Vertical Viewing Angles

(b) Horizontal Viewing Angles

Fig. 14   Pilot Viewing Angles

D. Landing Gear

The initial configuration of the landing gear was determined using maximum takeoff weight and class similarity per historical trends in Raymer, resulting in a tricycle configuration with two wheels per strut [4]. The main landing gear is stored in the fuselage as opposed to the nacelles. This choice was made to both reduce the overall length of the nacelles and to allow the space within the nacelle to be used for the hybrid architecture. From these initial conditions, further analysis was used to choose and size an absorber, the wheel-rim systems, and requirements for clearance to determine the overall length and position of the landing gear.

The calculated wheel loads of the landing gear had a 7% margin for the nominal load per FAR 25 provisions as outlined by Raymer, with an additional 3% added for initial design margin [4]. The main landing gear struts were sized by nominal static load while the nose landing gear strut was sized with the maximum braking force as shown in Table 17. Using the aft and forward CG limits as well as a preliminary landing gear position based on the extreme aft CG limit, a moment balance was performed, resulting in the calculated loads in Table 17 [22].

Table 17 Landing Gear Loads

Strut Load	Main Landing Gear	Nose Landing Gear
Nominal Static [lbf]	28,560	2,048
Max Static [lbf]	-	5,088
Max Braking [lbf]	-	10,010

Bounden will use an Oleo shock absorber system, the most common type of shock-absorbing landing gear [4]. The dimensions of the stroke and Oleo length are shown in Table 18. These dimensions take into consideration the requirement of at least 7 inches of propeller ground clearance as stated in CFR §25.925. Traditional braking technology will be used as well as the Oleo system operating with compressed air. The main landing gear will be stored in blisters as shown in Figure 15a while the nose landing gear is stored in the fuselage directly underneath the flight deck [22].
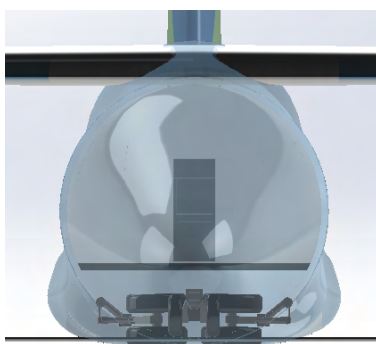
(a) Stowed Landing Gear

(b) Fully Extended Landing Gear

Fig. 15 Landing Gear Configuration

(a) Tipover Clerance

(b) Tailstrike angle in degrees
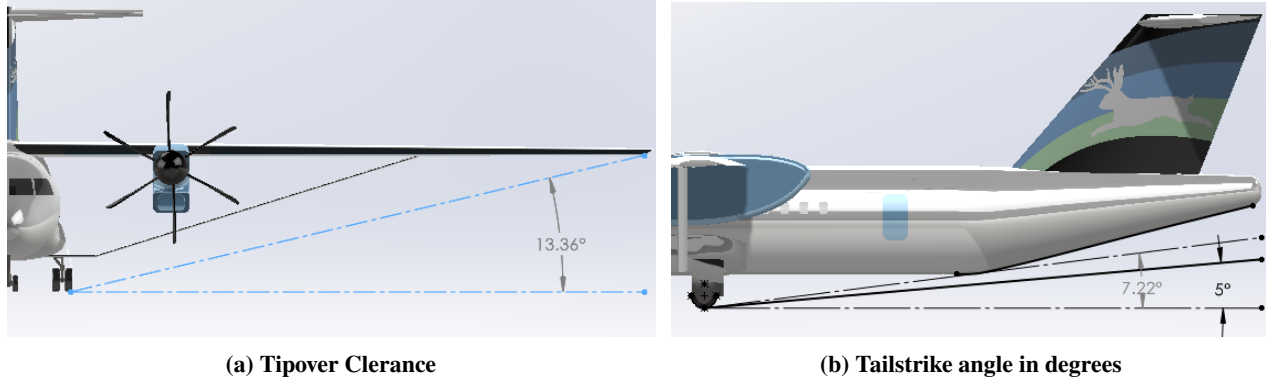
Fig. 16   Landing Gear Ground Lines

The minimum wheel size was found in the Michelin catalog by searching through the maximum loading and the speed index. The resulting maximum load was found by dividing the maximum loads from Table 17 by the number of wheels per strut. The selected tires are the 18"x5.5" and 25.5"x8.0"-14 for the nose and main landing gears, respectively. Table 18 details the selected tires, Oleo stroke, and the total required length for certification. As shown in Figure 15b, the 7-inch clearance is met, and the ground lines are shown in Figures 16a and 16b as they are above the 5° minimum detailed by the FAA with a tipover angle of 13° and a tailstrike angle at 7°. In takeoff and landing, the aircraft will be at angles of attack of 2.75° and 2.55° which is ahead of the tip angle of 7° as shown in Figure 32a in Section VI.

Table 18   Landing Gear Dimensions

Parameter	Main Landing Gear	Nose Landing Gear
Wheel Max Width [in]	8.0	5.75
Wheel Diameter [in]	25.5	17.9
Rolling Radius [in]	10.1	7.9
Piston Area [sq. ft]	19.04	6.67
Stroke [in]	9.33	9.33
Stroke with Safety [in]	10.33	10.33
Total Length with Propeller Clearance [in]	45	50

V. Propulsion

A. Engine Selection

1. Propulsion Requirements

Based on the RFP requirements to design a hybrid-electric turboprop aircraft, existing turboprop engines were considered to reduce the complexity of the propulsion system. From the sizing analysis, Bounden required 9,000 hp for takeoff. This value is much larger than turboprop aircraft with similar passenger capacities due to the increased weight due to the batteries. A low power-specific fuel consumption (PSFC) for the engine is also required to reduce block fuel.

2. Candidate Engines

In the civil turboprop category, engine options that provided the large amount of power Bounden needed for takeoff were limited. In order to decide on the best possible candidate, similarity analysis was completed on engines that could provide the required power. The parameters for each engine were compared in Table 19 [23].

Table 19   Engine Specification Similarity Analysis

Engine	Aircraft Utilized On	Max. Takeoff Power [shp]	Dry Weight [lb]	PSFC [lb hp/hr]	Year First Variant Certified
PW 150A	Dash Q400	5,492	1,580	0.433	1995
Rolls Royce AE 2100	Saab 2000	4,637	1,727	0.460	1993
PW 127	ATR 42 & ATR 72	2,750	1,060	0.459	1992
PW 123	Dash Q300	2,380	992	0.470	1987

The PSFC of each considered engine was plotted against its certification date as shown in Figure 17 [23]. Although the engine options other than the 150A have more modern variants, they all have higher PSFCs and older original designs. As seen from the figure, the PW150A engine has the lowest PSFC by far out of all the engines compared, even though it only has one variant ever released. The AE2100, PW127, and PW123 all have had multiple variants released and certified, but still cannot reach the PSFC of the PW150A. Based on this analysis, the PW150A engine was selected for Bounden as the engine could easily provide the required power based on the sizing analysis and has the lowest PSFC in its class. In addition, the engine has been certified and satisfies all the necessary certification requirements as stated in 14 CFR §33.3 [24].
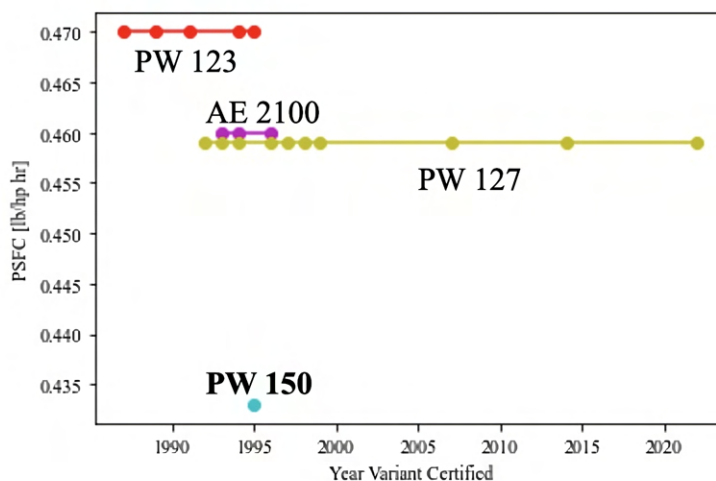
Fig. 17   PSFC Vs. Time

3. Engine Performance

Power available and PSFC data for the PW150A engine are shown in Figures 18 and 19. This data was calculated using the GasTurb software [25].
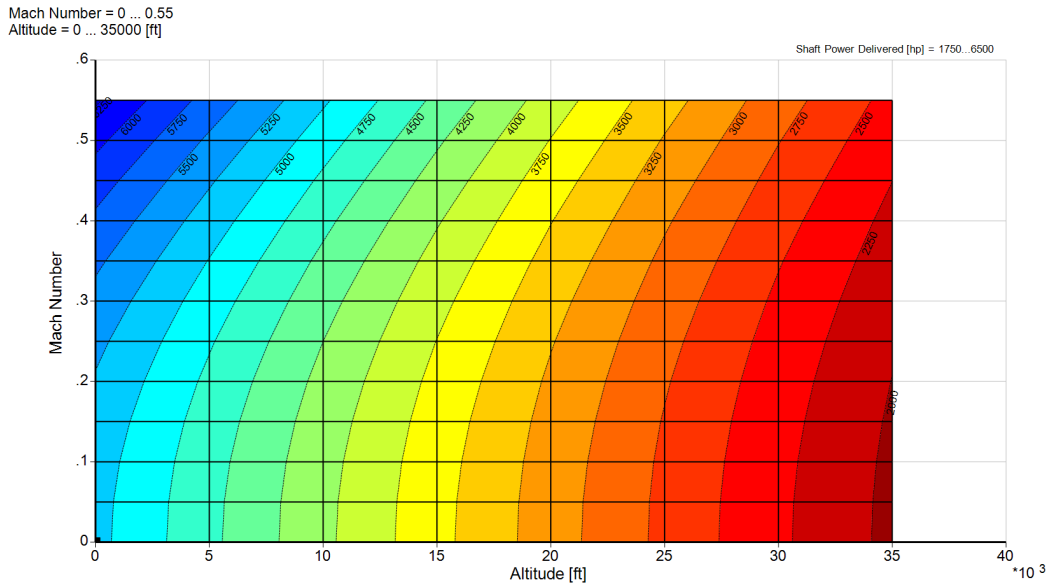
Fig. 18   Shaft Power Delivered Vs. Altitude Vs. Mach
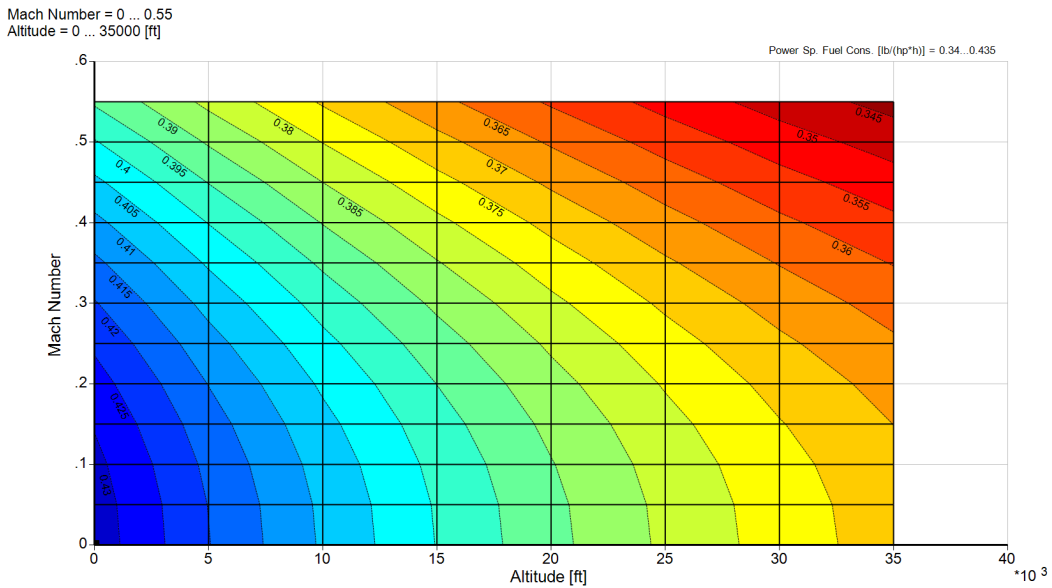
Fig. 19   PSFC Vs. Altitude Vs. Mach

This data was used to validate scaled data from Raymer based on historical turboprop engine performance. Ultimately, the Gasturb data was not used in performance analysis as the throttle could not be adjusted. Given the throttling schedule described in Section XI, the Raymer data was chosen for analysis purposes.

4. Propeller Selection

A statistical method for propeller sizing described by Raymer was used to size the required propeller diameter [4]. A six-blade design was chosen for Bounden. The decision was made to use existing propellers on the market that would fit the diameter requirement of at least 12.6 feet. This led to the selection of the Dowty R408 propellers, with the specifications shown in Table 20 [26]. These propellers are used on the Dash Q400 aircraft, an aircraft that uses the PW 150A. Therefore, the propellors will be compatible with the PW 150A engine selected for Bounden.

Table 20   Propeller Specifications

Parameter	Value
Diameter	13.5 ft
Max Power	5,071 shp
Max RPM	1,020
Cruise RPM	850
Tip Sweep	18 degrees

B. Electric Propulsion

Bounden features a complex hybrid-electric propulsion system that aims to reduce block fuel up to 20% compared to current regional turboprop aircraft. The electric propulsion architecture and components are described in the following sections.

1. Hybrid Architecture

Determining the architecture of the hybrid system is the first step in designing it. After extensive research, potential architectures were narrowed down to two types: a parallel architecture and a series architecture. The parallel architecture consists of a fuel tank and internal combustion engine connected in parallel with a battery system and electric motor. Both of these systems are connected through a mechanical coupling system, which is then connected to the propeller. In the series architecture, the fuel tank, internal combustion engine, battery, generator, electric motor, and propeller are all connected in series. Schematics for both are these architectures are included below in Figure 20 and Figure 21 [27].
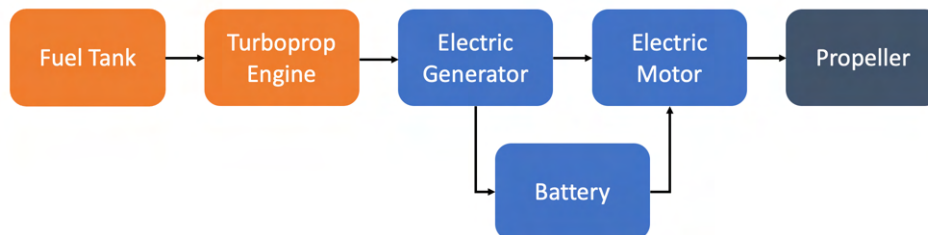
Fig. 20   Series Hybrid Architecture
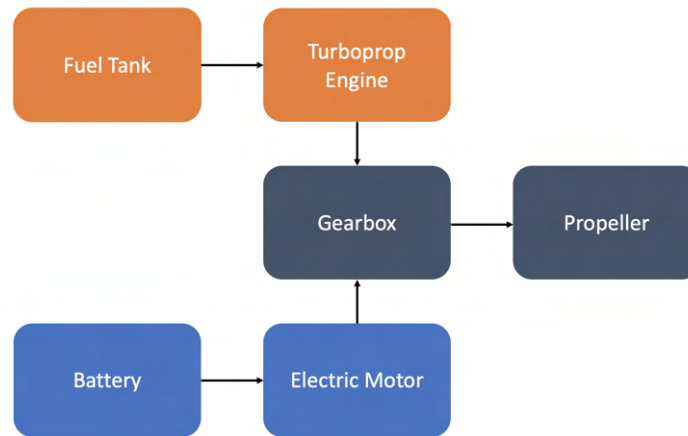
Fig. 21   Parallel Hybrid Architecture

In order to decide which architecture was best for Bounden's goals, a qualitative trade study was conducted. In this trade study, several metrics were taken into consideration and ranked in terms of importance to the design goals (most important is ranked a 3, least important is ranked a 1). In addition to the parallel and series configurations, an all-electric architecture was also considered in the trade study as a point of comparison. The numerical rankings and results for the trade study are shown in Table 21.

Table 21   Hybrid Architecture Trade Study

Feature	Weight	Parallel	Series	All-Electric
Battery and System Weight	3	3	2	1
Complexity	2	1	2	3
Hybridization Flexibility	1	3	2	1
Raw Score	-	7	6	5
Weighted Score	-	**14**	12	10

As for the system and battery weight rankings, the parallel architecture has the lowest overall weight. Since the amount of electric power can be adjusted in this architecture, the battery weight can be reduced to as little as needed. In addition, the extra weight of an electric generator is not necessary. In the series architecture, the electric power must be running at all times that the propulsion system is running, which drives up battery weight. Also, a generator is required in this architecture, which adds weight. In the all-electric configuration, the battery weight required to match the power output for the whole duration of the flight would be extremely high with the current battery technology, surpassing the weight of the aircraft itself.

For the complexity category, the all-electric architecture is proven to be the least complex. This is because this architecture is straightforward and only needs a few components: batteries, an electric motor, and possibly a simple reduction gearbox. The series architecture comes in second in this category, as both electric and gas-powered components are needed. The parallel architecture is the most complex, due to the need for a complex gearbox system to combine the two different modes of power.

The parallel architecture is the most flexible in its hybridization with the ability to adjust the hybridization factor throughout the mission profile to whatever the team desires. In the series architecture, the electric motor drives the turbine, so the hybridization can only be adjusted slightly. In the all-electric architecture, only one mode of propulsion source is available, so there is no hybridization factor as the system is 100% electric.

After this assessment, final scores were calculated. These scores were calculated by multiplying the scores in each category by the weights assigned in Table 21. The final scores are shown in the last row of Table 21. Based on this analysis, the parallel architecture was chosen for Bounden's propulsion system. This decision was made based on the flexibility the parallel architecture provides in terms of hybridization ratio, as well as the reduced battery weight the architecture can provide based on this flexibility.

2. Battery Technology

Studies on the battery technology currently available were conducted to ensure that the required EIS dates for certification could be met with the technology utilized in the design. Three different lithium batteries were considered during this study: lithium-ion, lithium-sulfur, and lithium-air. Research from [28] found cell-level specific energies for each of the battery types which are tabulated in Table 22.

Table 22 Lithium Battery Study

Battery Type	Specific Energy [W-hr/kg]
Current Traditional Li-ion	250
Current Li-S	500
2030 market ready Li-air non-aqueous	1,700

Lithium-ion batteries have higher energy densities than all the other rechargeable batteries and are currently the basis for all other future batteries. Lithium-sulfur batteries, although highly dense compared to lithium-ion, are under development still for a long lifetime to properly be considered. Lithium-air is a highly experimental field at the moment, but it is the most desirable for design given its high density and reversibility abilities. With current experimental developments, the capabilities of the battery the team would require for the aircraft to meet performance requirements are larger than what would be expected by 2034. For these reasons, lithium-ion batteries were chosen for Bounden.

The team predicted an improvement in Li-ion battery technology by 2034. Although the current specific energy is about 250 Wh/kg on the cell level, this only equates to about 175 Wh/kg on the pack level. This difference is due to the additional casing needed in between each cell to contain any potential fires. However, with the trend of battery improvement in the years until 2035, a pack level energy of 275 Wh/kg battery pack was estimated. This specific energy value was used to calculate the mass of the battery pack based on the energy required.

The battery pack volume was sized using volumetric specific energy, which describes how much energy can be contained in the battery per unit volume. The team decided on a volumetric specific volume of 800 Wh/L, which is on trend with advances in technology, as seen in Figure 22 [29].
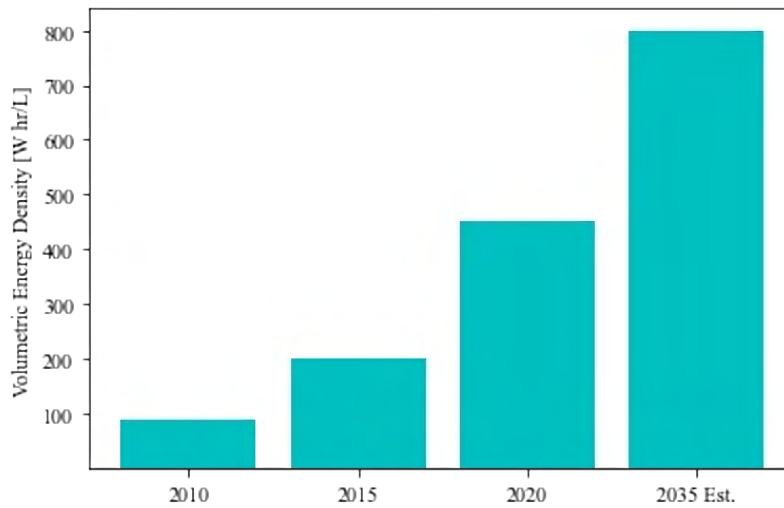
Fig. 22   Lithium-Ion Volumetric Specific Energy Trends

3. Battery Pack

The battery pack was sized using the volumetric specific energy chosen. Since the total battery energy used for propulsion throughout the mission profile was 1,200 kWh, a large volume of battery is required. In order to reduce the size of each battery pack for ease of operation, the battery was divided into 6 battery packs, each with an energy capacity of 200 kWh. Each pack has a volume of 11 cubic feet. Three packs are stacked on top of each other to create a module in order to conserve space under the fuselage, where the batteries are stored. There are 2 modules, each placed on either side of the center of gravity of Bounden under the cabin floor. The dimensions of each module are shown in Table 23.

Table 23   Battery Module Dimensions

Dimension	Value
Length	9.8 ft
Width	6.1 ft
Height	0.83 ft

4. Electric Motor

In order to utilize the energy from the battery pack, an electric motor must be integrated into the propulsion system. With more and more hybrid-electric aircraft being developed, more high-power electric motors are being introduced into the market. For example, the Collins Aerospace 1 Megawatt electric motor will be used in the joint hybrid-electric turboprop between Collins and sister company Pratt & Whitney that will begin flight testing in 2024 [30]. However, little information has been released regarding this motor, besides its maximum power ratings. There is a less publicized project, though, that is being conducted at The Ohio State University to create a 10 MW electric motor. While the technology is still quite far out for the 10 MW motor, a more appropriately sized 1 MW motor was designed and tested successfully [31]. This motor is not for sale, but the team would contract Ohio State and NASA to build the motor for them. This electric motor was chosen for Bounden, and the specifications are listed in Table 24.

Table 24   Electric Motor Specifications

Parameter	Value
Diameter	24 in
Weight	176 lb
Max. Design Power	1 MW (1341 hp)
Max RPM	4000
Normalized Power Density	5 kW/kg

C. Integration

In order to fully integrate the hybrid architecture into the propulsion system, mechanical coupling devices, cables, and safety features were necessary. Each of Bounden's engines requires one electric motor, one gearbox, and sufficient cables to reach from the battery to the nacelle, in addition to the turbine engine.

1. Nacelle and Inlet

The electric motor, cables, and gearbox are stored inside the nacelle along with the PW150A turboprop. The Bombardier Dash 8-Q400 utilizes a long and slender nacelle to house the PW150A engine, as well as the landing gear. Therefore, for initial sizing, the Dash 8-Q400 nacelle was downsized slightly to ensure all the extra electric components could fit in the nacelle while still keeping an aerodynamic profile. The final nacelle is designed to be 17 ft long, 5.5 ft tall, and 3.2 ft wide. The nacelle layout can be seen in Figure 23. In order to save space, the electric motor will be mounted sideways on top of the engine. The inlet used was the same size inlet as the Dash 8-Q400: 1.5 inches tall and 2.5 inches wide. In order to account for losses due to bleed and pressure losses, a differential of 60 hp is discounted from the designed engine performance.
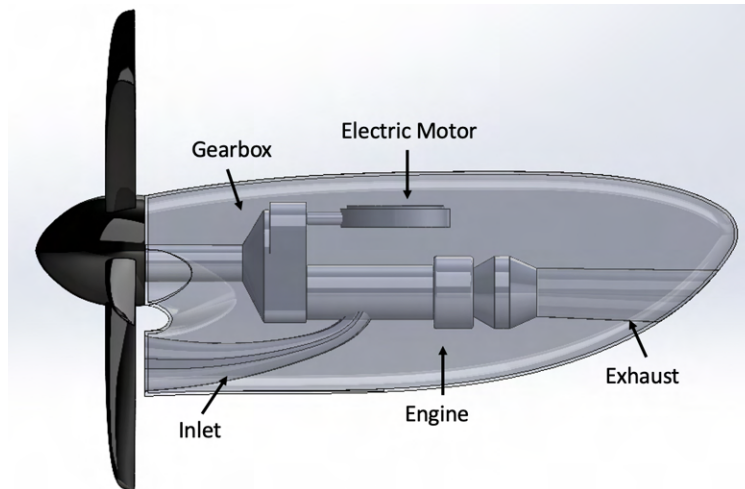
Fig. 23   Nacelle Design

2. Gearbox

Since the parallel-hybrid architecture requires a coupling system to combine the 2 power sources into one output, a reduction planetary gearbox system was designed specifically for Bounden's propulsion system. This gearbox was based on the hybridization factors throughout the mission profile. It was determined that the electric motor would be running at 40% throttle during the climb and cruise phases of the flight. The engine will be running at varying throttles. The gearbox system is set up in 4 stages of planetary gearboxes: 2 reduction stages to reduce the turboprop rotation, one combination stage to combine the rotations from the electric motor and the turboprop engine, and one final reduction stage to match the combined rotation rate to the maximum rate of rotation the propellers are rated for (1,020 RPM). A planetary gearbox consists of 3 different types of gears: the sun gear, the ring gear, and a number of smaller planetary gears which are connected by a carrier. An example drawing of a planetary gearbox is shown in Figure 24, with the ring gear shown in red, sun gear in yellow, planet gears in blue, and the carrier shown in green [32].
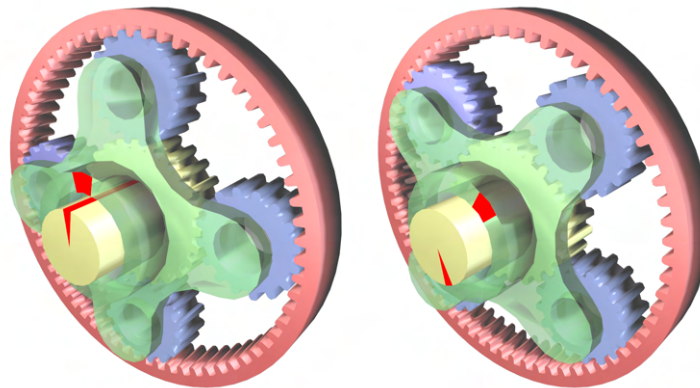
Fig. 24   Example Planetary Gearbox Schematic, From [32]

In Bounden's gearbox, the first stage will take the output directly from the turboprop to drive the sun gear, and the reduced output is transferred to the carrier mechanism connecting the 4 planet gears. This output will be used as the input in the second gear system, attached to the sun gear and with the second gearbox output driving the carrier. This completes the initial reduction phases. Next, the rotation from the electric motor is used to drive the sun gear in the third planetary system, and the reduced engine output drives the outside ring gear, producing a combined output rotation from the carrier. Lastly, the output from the third gearbox drives the sun gear, and the rotation is reduced to 1,020 rpm, carried from the final carrier to the propeller shaft. For each gear system, the number of teeth was calculated using the following relationship [33]:

$$(R + S)T_c = ST_s + RT_r \tag{1}$$

In this relationship, R and S are the number of teeth in the ring and sun gears respectively, and T_c, T_s, and T_r are the speeds of the carrier, sun, and ring gears. The speeds are the gear and the teeth number on each gear were calculated and shown in Table 25.

Table 25   Gear Speeds and Teeth Number

Stage	Gear Speeds			Gear Teeth Number		
	Sun Gear	Ring Gear	Planet Gears	Sun Gear	Ring Gear	Planet Gears
1	27,000 rpm	0 rpm	9,000 rpm	30	60	15
2	9,000 rpm	0 rpm	3,000 rpm	30	60	15
3	1,600 rpm	3,000 rpm	4,000 rpm	25	55	15
4	4,000 rpm	0 rpm	1,020 rpm	10	29	9

3. Safety Systems

The PW150A turboprop engine Bounden is using complies with all engine certification requirements as stated in 14 CFR §33 [24] in addition to OEI requirements as stated in 14 CFR §25.121. The gas turbine and electric propulsion combination provides plenty of additional power to ensure a successful climb, even with one engine inoperative. Another safety consideration is the integration of the electric motor into the nacelle. This is a flammable element and should be protected from the rest of the engine. Therefore, a firewall will be installed around the motor in compliance with 14 CFR §25.1191 [34].

4. Overall Efficiency

The efficiencies for each component of the propulsion system were tabulated based on historical values. These values are shown in Table 26. After multiplying all these efficiencies, the total overall propulsive efficiency is 80%. This efficiency makes Bounden very competitive with other turboprop aircraft on the market, even with the added complexity of hybridization.

Table 26   Component Efficiencies

Component	Efficiency [%]
Engine & Propeller	85
Battery [35]	99
Motor [31]	98
Gearbox [36]	97

VI. Aerodynamics

A. Methodology of Design

The wing loading constraints and minimization of weight drove the overall planform sizing of the wing as discussed in Section III. The other characteristics of the wing are driven by the objectives described in Table 27. Given the large AR, a truss brace was chosen over a simple cantilever beam connection for structural and aeroelastic reasons.

Table 27   Key Wing Requirements

Parameters	Proposed Design
Cruise C_L	0.665
Wing Weight	Minimize
α Linear Range (°)	-3 to 12
$C_{L_{TO}}$	2.37
$C_{L_{LDG}}$	2.53

To analyze the aerodynamic performance of the wing and truss system, analysis was broken into three parts: the wing, truss, and wing-truss system. Early implementation and testing of the truss with inviscid solvers including AVL [37] and OpenVSP [38]resulted in an interference of vortices of the solvers overlaying each other and producing an invalid solution. To circumvent this issue, superposition was used to analyze the truss, wing, empennage, and fuselage body with nacelles separately. Once the desired truss and wing geometries were designed, the configuration was analyzed and verified together as one system [39].

When comparing AVL and OpenVSP results, AVL calculates a smaller C_{L_α} than OpenVSP but AVL did not have a method of predicting C_{D_o} as OpenVSP does, as shown in Figure 25a. AVL also tends to under-calculate C_{D_i} as shown in Figures 25 and 25c while not having capabilities to calculate C_L in the non-linear regime. Even with differences, both programs converged on the required C_L for cruise conditions at an angle of attack of 0.3 degrees. Due to OpenVSP's capability of modeling the nonlinear regime, the basis for aerodynamics will be using OpenVSP's data.
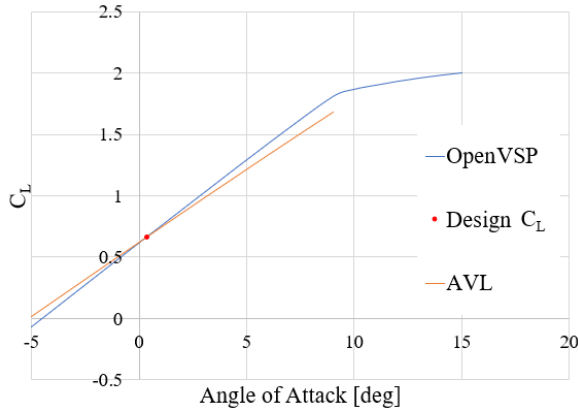
(a) Bounden C_L vs. α Curves at Cruise
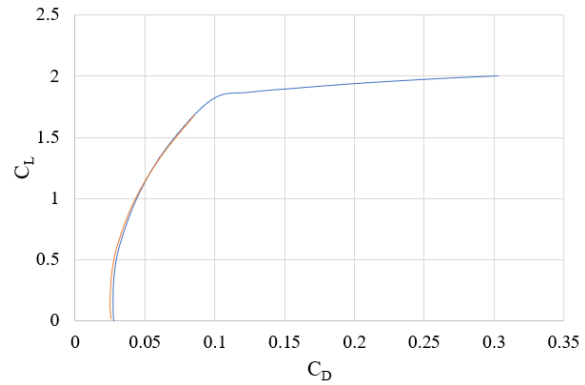
(b) Bounden Drag Polar Curves at Cruise
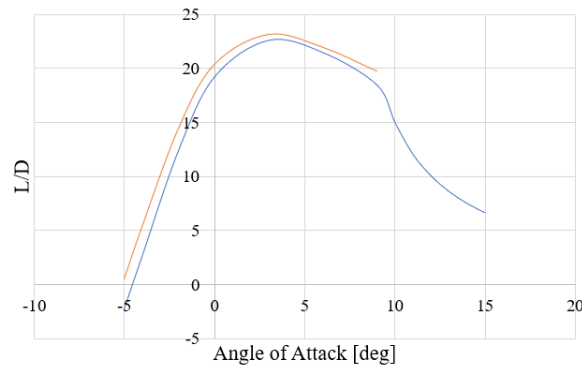
(c) Bounden L/D vs. α Curves at Cruise

Fig. 25   Bounden's Aerodynamic Performance with AVL and OpenVSP

B. Wing Airfoil Selection

In addition to the major requirements outlined in Table 27, drag reduction during the cruise was a major consideration when selecting the airfoil used for Bounden, as reducing drag would improve performance and reduce block fuel. Based on the design lift coefficient requirements, several NACA 6-series airfoils were chosen for analysis in addition to airfoils from the Eppler series, NASA experimental airfoils, and Goettingen series that had values of C_{L_0} above 0.5. Since the cruise speed is 0.505 Mach which is in the subsonic regime, NLF airfoils were considered. NLF airfoils are designed to have laminar flow attachment throughout most of the upper surface, allowing for better lift values as well as decreasing drag from the lack of turbulent flow upstream on the airfoil. With these additions to the airfoil performance, the necessary power required for Bounden decreases. The minimum camber required was calculated by using a method by Raymer for NLF airfoils in which the cruise C_L was multiplied by a factor of 5.5, resulting in a minimum camber of 3.5% for the airfoils. This constraint was used to further narrow down the selection pool, as well as an additional constraint of a C_{L_0} of at least 0.6 to reduce the angle of incidence of the wing. In doing so, the manufacturability of the wing would be driven down, saving costs in addition to extending the linear regime.

Analysis was run on the selected airfoils using XFLR, a 2-D solver for both viscid and inviscid flow conditions [40] [41]. A Reynolds number of 11 million was used to simulate analysis at cruise conditions. Using the viscous solver for the airfoils, the lift, drag, and L/D curves of the Eppler 397, Eppler 421, NASA NLF(1) 1015, NASA NLF(1) 0215F, NACA 64(3)-418, and NACA 64(4)-421 airfoils were compared in Figure 26. From this analysis, it can be seen that the Eppler 397 and NASA NLF(1)-1015 airfoils have the best c_{l_0} values compared to the rest of the airfoils as shown in Figure 26a. In Figure 26b, both the Eppler 397 and NASA NLF(1)-1015 perform the best in minimizing the amount of drag at higher c_l values while still maintaining a c_{l_0} value that would have minimal incidence.

(a) Candidate Airfoil c_l vs. α Curves

(b) Candidate Airfoil Drag Polar Curves

—Eppler 397   —Eppler 421   —NACA 64(3)-418
—NACA 64(4)-421   —NASA NLF(1) 1015 —NLF(1)-0215

(c) Candidate Airfoil L/D vs. α Curves
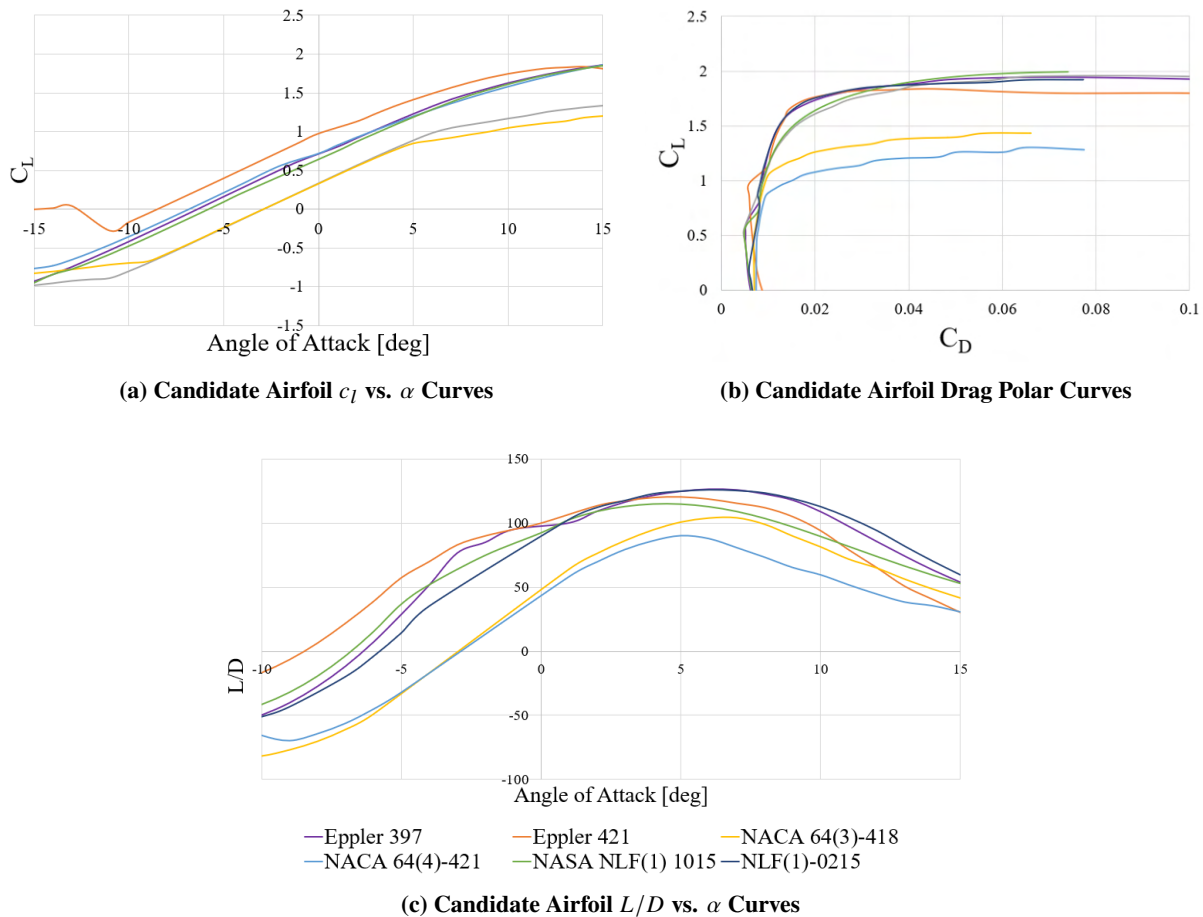
Fig. 26   Candidate Airfoil Performance

Due to the similar performance of the airfoils, further analysis was required to select an airfoil. Using the Wing Weight Equation detailed in Section IX, the wing structural weight was calculated for both the Eppler 397 and the NASA NLF(1)-1015 airfoils. As shown in Table 28, the NASA NLF(1)-1015 reduces weight by over 100 lb compared to the Eppler 397. Reducing weight in the design reduces the power required in various conditions, reducing the overall block fuel. In addition, the NASA NLF(1)-1015 airfoil has a larger maximum thickness which both provides more space for the hybrid architecture and a thicker leading edge radius allowing for better performance at subsonic speeds [4].

Table 28   Wing Weight for Airfoil Contenders

Airfoil	Wing Structural Weight [lb]
Eppler 397	4,733
NASA NLF(1)-1015	4,587

C. Wing Design

One of the main drivers for the planform design is minimizing C_{D_i}, which can be accomplished by tapering or twisting the wing. Tapering the wing also reduces weight which benefits performance. Twisting is only effective at minimizing C_{D_i} at certain C_L while tapering is effective in all flight conditions. A trade study was performed to find a taper ratio that would reduce induced drag, reduce weight, and improve span loading efficiency. Based on Prandtl wing theory, a set of taper ratios ranging from 0.28 to 0.45 were iterated through and analyzed for their performance in the trade study criteria. The taper ratios ranging from 0.39 to 0.45 had span efficiencies that were within 1% of the best span efficiency loading. Figure 27 shows the percent difference from a chosen taper ratio of 0.41 compared to the other taper ratios within the stated range. A taper ratio of 0.41 provides the best aerodynamic characteristics in regard to span loading efficiency and κ while also minimizing structural weight. At this taper ratio, the wing planform has a span efficiency factor of 0.98 and an inviscid C_{D_i} of 0.0105 at 11 million Re. Figure 27 was normalized at a taper of 0.41 as this point had the best span loading efficiency.[4][42]
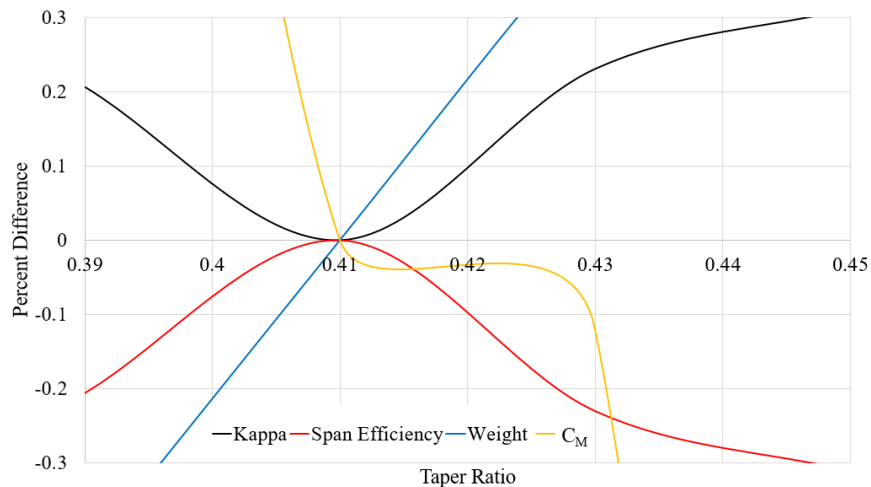
Fig. 27   Taper Study

Since the taper ratio was chosen to minimize C_{D_i}, wing twist was added to the design to delay stalling at the wing tip. Using the available inviscid solver and extrapolating two-dimensional data, a geometric twist of -1.5 degrees is applied at the wing tip from the root chord. Due to the relatively low cruising speed of Bounden, sweep would

result in unfavorable stalling characteristics from overloading the wing tip [43]. Furthermore, sweep on a high-wing configuration can result in an increased dihedral effect due to the air pushing upward on the forward wing while the fuselage is in sideslip [4]. Based on historical analysis, unswept high-wings have minimal or no dihedral, typically ranging from 0 to 2 degrees due to C_{l_β} being negative [4]. Due to these factors, the wing design has no quarter-chord sweep or dihedral as Bounden's C_{l_β} is already negative and of an adequate magnitude as shown in Section VII. As further discussed in Section VI.G, based on the trim C_L conditions for cruise, an angle of incidence of 0.25 degrees is needed to maintain the required cruise conditions. The thickness of the wing is a byproduct of the airfoil selection process. The NASA NLF(1)-1015 airfoil has a thickness of 15%, matching the historical trends for airfoil thickness in general aviation design described by Raymer [4]. The overall dimensions of the wing planform are provided in Table 29.

Table 29   Wing Planform Dimensions

Parameter	Bounden
Wing Area [ft^2]	760
Span [ft]	114
AR	17.2
Cruise Wing Loading [lb/ft^2]	81.6
Root Chord [ft]	9.4
Tip Chord [ft]	3.9
MAC [ft]	7.0
Taper Ratio	0.41
Dihedral Angle [deg]	0
Root Incidence Angle [deg]	0.25
Tip Incidence Angle [deg]	-0.8

To reduce weight and drag, Hoerner wing tips are implemented in the design. This wing tip shape provides both an increase in lift and a decrease in drag from the effective span. As about two-thirds of lift is produced on the upper surface of the wing, a reduction in parasite drag in the lower surface of the wing results in minimal reduction in lift while decreasing drag, resulting in less power required.

D. High-Lift System

To meet the necessary field lengths requirements, the required $C_{L_{max}}$ calculated for takeoff and landing conditions are 2.37 and 2.53 respectively. In order to minimize the cost, weight, and maintenance of the high lift devices, single-slotted Fowler flaps were selected as they offer the least amount of weight and complexity for the amount of ΔC_L that is provided.[44]

In addition to the Fowler flap, a rigid Krueger leading edge flap will be used with its primary reason as an insect mitigation screen. Using a Krueger flap as an insect mitigation screen is necessary as any insect residue that is collected during low altitude conditions will have an impact on the NASA NLF(1)-1015 airfoil. NLF airfoils are sensitive to any type of deformation of the upper surface, which can lead to separation of the laminar flow, which the airfoil is designed for. A Krueger flap extends the camber of the wing section while simultaneously lower the leading edge when deployed. With these effects, the Krueger flap will also lead to an increase in ΔC_L, allowing the Fowler flap to be undersized for more weight savings. Figure 28 depicts a top view of Bounden's high lift devices, with the major dimensions detailed in Table 30. The high-lift devices layout can be seen in the airfoil cross-section shown in Figure 29.
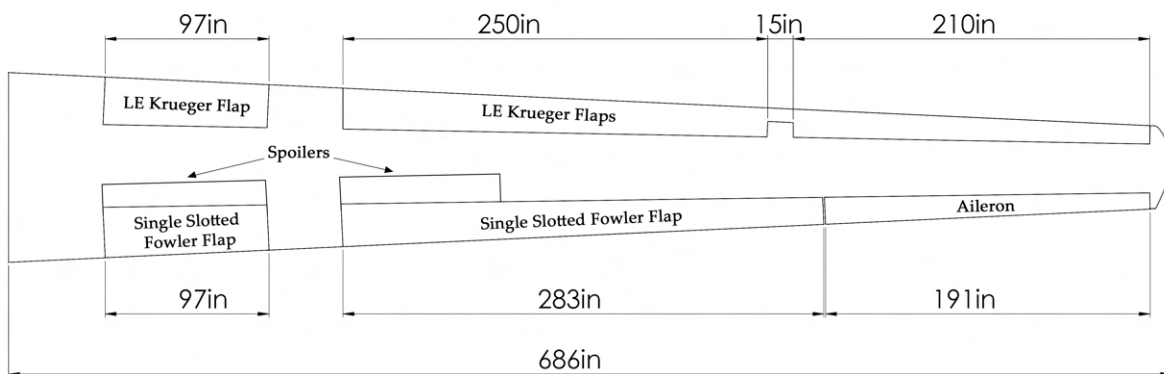
Fig. 28   High Lift Devices layout

Table 30   High Lift Devices Sizing

Device	Span %	c'/c
Fowler Single Flap	42.1	1.19
Krueger Leading Edge Flap	72.9	0.15
Spoilers	12	0.30
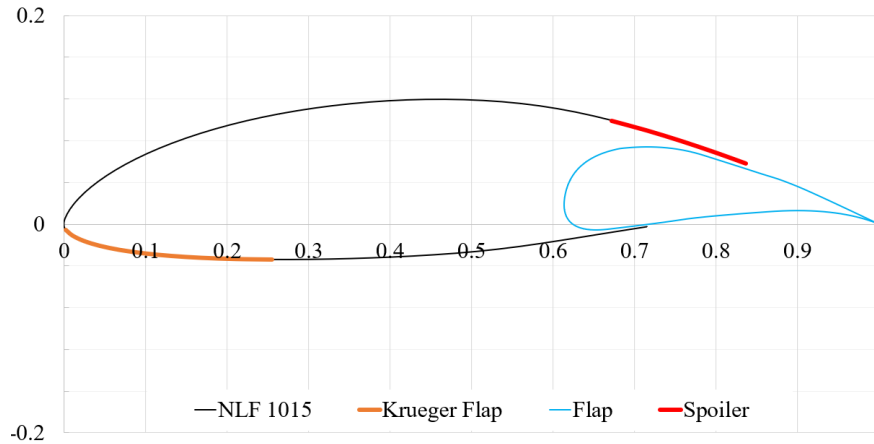
Fig. 29   Airfoil cross section

E. Truss

The truss on Bounden acts mainly as a structural unit and is not designed to be a major lifting body as the wing planform produces sufficient lift. As a result, the main goals driving the selection of the airfoil and aerodynamic characteristics were to reduce drag, weight, and loading. Symmetric airfoils were considered to make the required beam as aerodynamic as possible. The NACA 00XX family was chosen and analyzed, starting from the NACA 0008 airfoil to the NACA 0024 airfoil. As Figure 30 shows, a parabolic trend became apparent when calculating the truss through OpenVSP. The NACA 0021 proved to be the vertex of the trend, and as such, was selected for the truss. The process of for the analysis in Figure 30 was by maintaining the thickness of the truss while varying the chord length. NACA 0021 truss has the least amount of wetted surface, which in turn leads to a minimum for C_{D_o}.
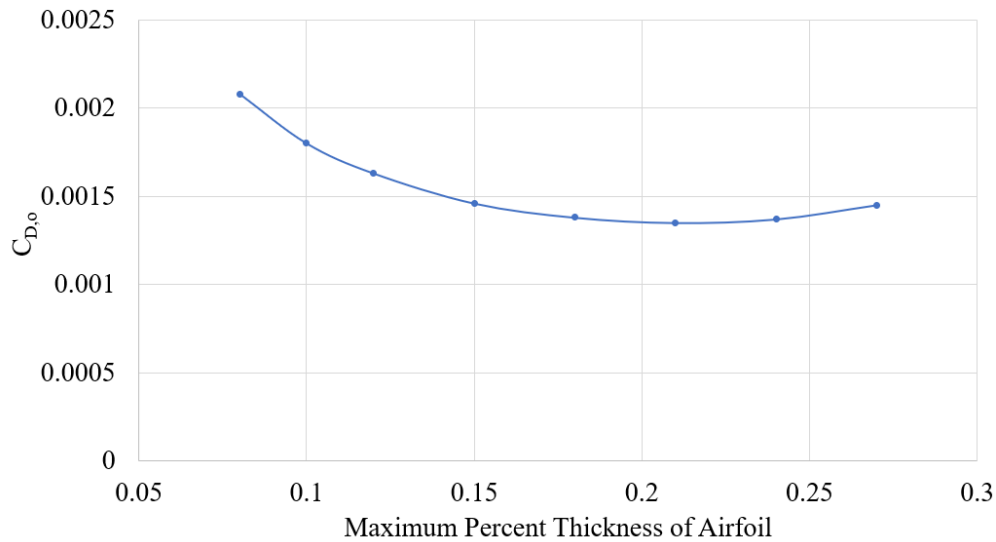
Fig. 30 C_{D_0} of varying thickness percentage

The dimensions of the truss are dependent on the structural needs required for the wing's beam. Once an airfoil was chosen, the percent of maximum thickness was used to find the chord. A conservative factor of 1.5 was applied to calculate the local Mach speed that the truss would have behind the propeller wash. With a calculated Mach speed of 0.7575, the Mach drag divergence may cause issues [4]. As such, the geometry of the truss was manipulated to reduce the amount of surface that would be in the prop wash while maintaining the structural needs. The final design of the truss has a truss kink that has no dihedral and a half-span of 92 inches. At the junction, a dihedral angle of 17.2 ° starts until the juncture with the wing's front spar, as shown in Figure 31. Table 31 summarizes the truss characteristics as well as the internal beam required.

Table 31   Truss Characteristics

Parameters	Proposed Design
Airfoil	NACA 0021
Required Span	875"
Internal Beam	2"x1"
Chord	9.52"
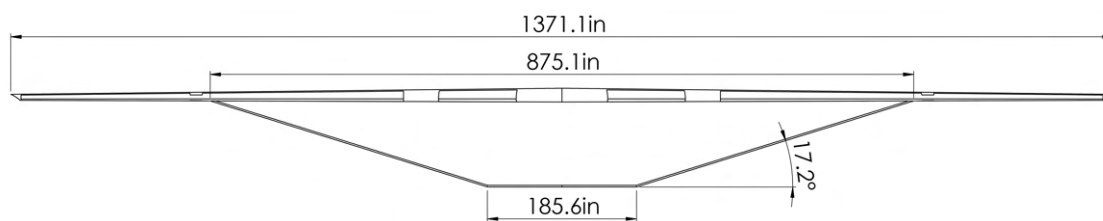
Fig. 31   Layout of Truss

F. Drag Build-up

Bounden has a wetted area-to-reference area ratio of 6.66. Compared to the class, this is larger than most but this is attributed to the addition of a truss. The drag build-up of the aircraft is calculated using OpenVSP Parasite Drag function as shown in Table 32. Three main configurations will be utilized: cruise, landing, and take-off, with landing and take off both at 50 ft above sea level to emulate the end and start of flare with the corresponding flap deflection of 55° and 38°. Spoilers are computed for ground roll, shown in Table 33. When combining the C_{D_o}, C_{D_i}, $C_{D_{trim}}$, $C_{D_{leak}}$, the total C_D for Bounden is 0.039, which is shown in Table 34. Similarly, Table 33 gives the C_{D_o} build-up for takeoff and landing with flaps deploys and Table 35 provides the total C_D values.

Table 32   Parasite Drag Building of Bounden

Condition	Cruise			Landing/Takeoff		
Component	Re [1e7]	C_f	C_{D_O}	Re [1e6]	C_f	C_{D_O}
Wing	1.1	2.97	0.0072	8.4	3.09	0.0075
Truss	0.1	4.31	0.0011	1	4.51	0.0011
Fuselage	12.7	2.06	0.0057	100	2.13	0.0059
Nacelle	2.5	2.60	0.0027	20	2.70	0.0028
Horizontal Tail	1.3	2.89	0.0024	10	3.01	0.0025
Vertical Tail	2.1	2.68	0.0022	16	2.78	0.0022
Total	-	-	0.0213	-	-	0.022

Table 33   Additional Drag Contributions for Takeoff and Landing

Surface	$\Delta C_{D,TO}$	$\Delta C_{D,L}$
TE Flaps	0.0190	0.032
LE Flaps	0.001	0.001
Spoilers	0.0	0.025
C_{D_o}	0.042	0.055

Table 34   Drag Totals for Cruise

C_{D_0}	C_{D_i}	$C_{D_{trim}}$	$C_{D_{leak}}$	$C_{D_{tot}}$
0.022	0.011	0.002	0.0012	0.036

G. Aircraft Aerodynamic Performance

Table 35 summarizes the aerodynamic conditions that Bounden will encounter in a typical mission. Figure 32a shows the required ΔC_L for landing and takeoff at 5,000 ft altitude and a ΔISA of +18°F. Krueger leading edge flaps will be fully deployed to act as an insect mitigation screen to prevent insect residue build up on the wing. The required flap deflections of 55 °and 38 °for landing and takeoff respectively are for a 5,000 ft altitude and a ΔISA of +18°F. At sea level with a ΔISA of 0°F, the necessary ΔC_L for take-off and landing is 1.2 and 1.0 respectively.

Figure 32c shows the L/D curve of Bounden excluding all forms of drag outside of C_{D_i} and C_{D_o}. Analysis was run under the assumption that all flow over Bounden would be turbulent. Instead of assuming a percentage of laminar flow to reduce drag, aerodynamic analysis was conducted for the worst-case scenario, as the aerodynamic solvers were not of high fidelity. Initially assuming and designing with this worst-case scenario allows for better performance in flight testing, which would allow for margin once Bounden is constructed and undergoes flight testing.

Table 35   Major Aerodynamic Characteristics Summary Throughout Flight

Parameter	Takeoff	Cruise	Landing
α [deg]	2.75	0.33	2.55
C_L	2.37	0.665	2.53
$C_{D_{tot}}$	0.35	0.033	0.64
L/D	6.77	20.15	5.67
Re	8.5×10^6	11×10^6	8.5×10^6
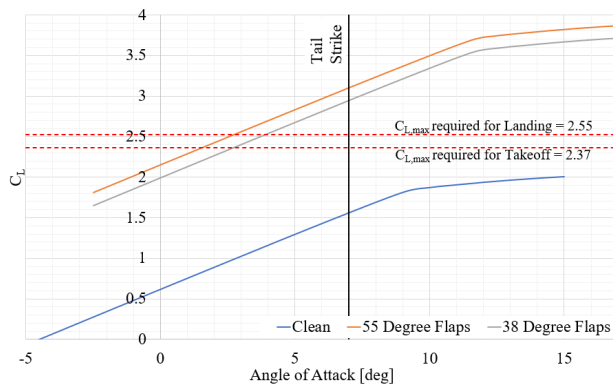
(a) $C_L - \alpha$ curves at Cruise, Landing and Take-Off
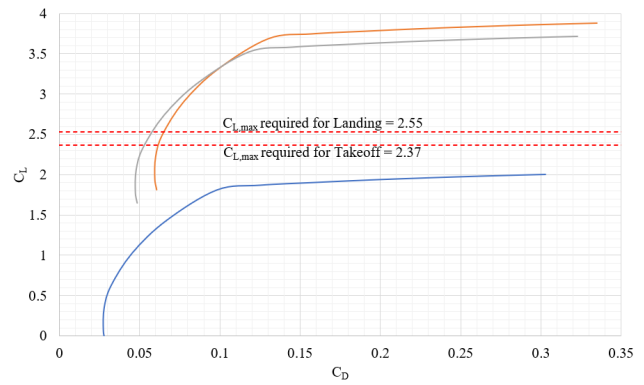
(b) Drag Polar curves at Cruise, Landing and Take-Off
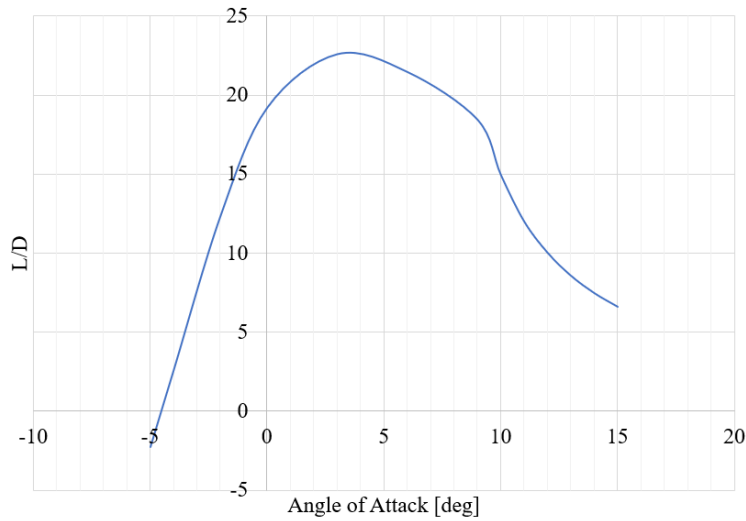
(c) Cruise L/D of Bounden

Fig. 32   Bounden's Aerodynamic Performance

VII. Stability and Control

A. Empennage

Initial sizing of the empennage was found through a similarity study of the class of aircraft based on configuration and weight class. These findings were verified with a notch diagram and other analytical methods. As discussed in Section IV, a T-tail configuration will be used to maximized the elevator's authority. The addition of an untrimmable aerodynamic body in the truss led to analysis of the stability and control of Bounden in having to use a superposition method as discussed in Section VI, with each component analyzed separately in AVL before summing together the results for an inviscid approximation of Bounden. The horizontal and vertical components on the empennage were sized separately before being added together for analysis of stability and control. In order to minimize weight, a NACA 0012 airfoil was selected for both stabilizers as this airfoil tends to have excellent performance [43]. A symmetric airfoil with the usage of a plain flap enables the elevator and rudder to have the same authority in either negative or positive deflection.

1. Vertical Tail

The initial sizing of the vertical stabilizer was done using the similarity of the $\frac{S_v}{S_{ref}}$ ratios with the similarity class and then compared with the needed rudder deflection through OEI and sideslip conditions. Table 36 details the required surface area for, at most, ± 20° rudder deflection angle. This limit for rudder deflection was based on industry standards as well as allowing pilots to have an additional 5% margin of safety should the need arise for it in emergency conditions. Figure 33 shows the side view of the vertical tail with the rudder dimensions. Table 37 gives a more detailed view of the overall vertical stabilizer planform. All of the planform values were selected from a database of aircraft of similar weight class and tail configuration [43].

The rudder initial sizing used the tail configuration class data. Through directional stability analysis, the $\frac{c'}{c}$ was increased in order to decrease the overall surface area of the vertical tail. The main limiting condition for sizing was OEI with no aileron deflection as shown in Table 36 but with the addition of aileron deflection as described in CFR §25.149 in maintaining bank angle through OEI.

Table 36   Vertical Tail Study

	Raymer Tail Coefficient Method	Similarity Analysis	OEI (Rudder Only)	Sideslip	OEI (5°Ailerons)
Vertical Tail Area [ft^2]	130.4	200.8	243.2	143.6	218.6
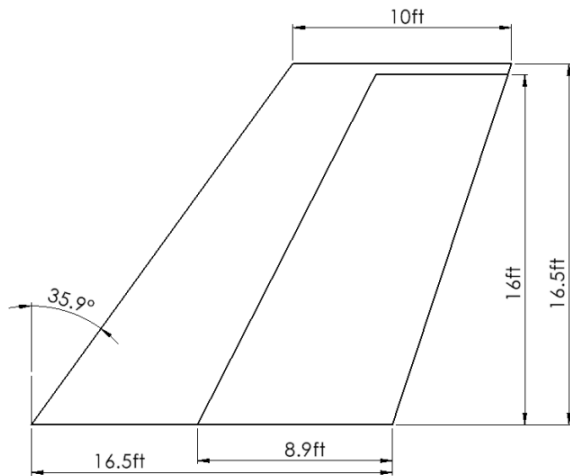
Table 37   Vertical Tail Planform Dimensions

Parameter	Value
Span [ft]	16.5
AR	1.25
Taper Ratio	0.61
$\Lambda_{c/4}$ [deg]	20.6
S_v $[ft^2]$	218.6
C_v	0.10

Fig. 33   Sideview of Vertical Tail

2. Horizontal Tail

As the horizontal tail is integral to the overall stability of the aircraft and Bounden does not have a class with which to compare itself, similarity analysis was not used to find the surface area and instead, a notch diagram was derived to relate $\dfrac{S_h}{S_{ref}}$. Figure 34 shows the limits of Bounden which were based on the Roskam rotation balance equation and the neutral point was calculated through moment analysis of Bounden lifting surfaces. Table 38 details the derived values of longitudinal stability of Bounden. The static margin was evaluated using the operating neutral point and the aft CG limit for maximum ramp weight conditions during flight. Figure 35 shows a top view of the aircraft with Table 39 tabulating the planform values. As with the vertical tail planform, all of these values were selected from a database of similar weight class and tail configuration. After initial sizing for the elevators, the horizontal tail area needed to increase to a $\dfrac{S_h}{S_{ref}}$ of 0.34. The larger S_h was needed in order to increase $C_{m_{\delta e}}$ for longitudinal stability [43].
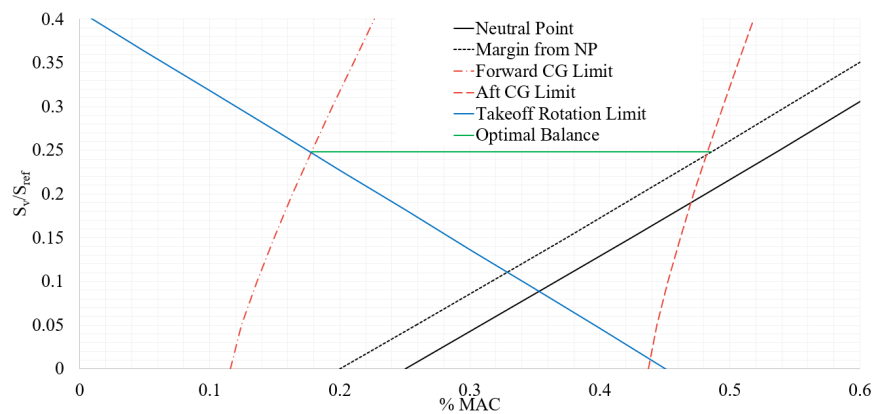
Fig. 34   Notch Diagram

Table 38   Longitudinal Stability Values

Neutral point [%$\overline{c}$]	Forward Aero Limit [%$\overline{c}$]	Operational Range [%$\overline{c}$]	Static Margin [%$\overline{c}$]	$\dfrac{S_h}{S_{ref}}$	Neutral Point Margin [%$\overline{c}$]
48	17.5	31	14.18	0.25	5

Fig. 35   Top view of Horizontal Tail

Table 39   Horizontal Tail Planform

Parameter	Value
Span [ft]	32.1
AR	4.0
Taper Ratio	0.5
$\Lambda_{c/4}$ [deg]	25.7
S_H [ft^2]	255.2
C_H	1.4

B. Control Surfaces

The control surfaces were initially sized with a balance between the similarity class and using values from databases [4]. Table 40 shows the comparison between Bounden's control surfaces to Raymer and similarity. The elevator was verified under longitudinal trim analysis which from landing conditions resulted in Figure 36. From historical deflection values, all deflection angles for control surfaces were bound to ± 20° in order to have at least a 5° margin of safety. From an aerodynamic standpoint, deflection past 30° tends to lead to a detrimental increase in drag when compared to the minimal lift gains. The rudder was sized and verified in the design of the vertical tail and for OEI conditions with aileron deflection of 4.5°. Ailerons thus were also sized with the rudder and the rudder through trim analysis. Stability derivatives also show that there is enough aileron authority for rolling recovery from perturbations.

Table 40   Control Surfaces Dimensions

Control Surface	c'/c	Span %	Raymer		Similarity Analysis	
			c'/c	Span %	c'/c	Span %
Aileron	0.30	27.9	30	40	30	30
Elevator	0.30	82	20	85	85	85
Rudder	0.54	82	50	80	35	96
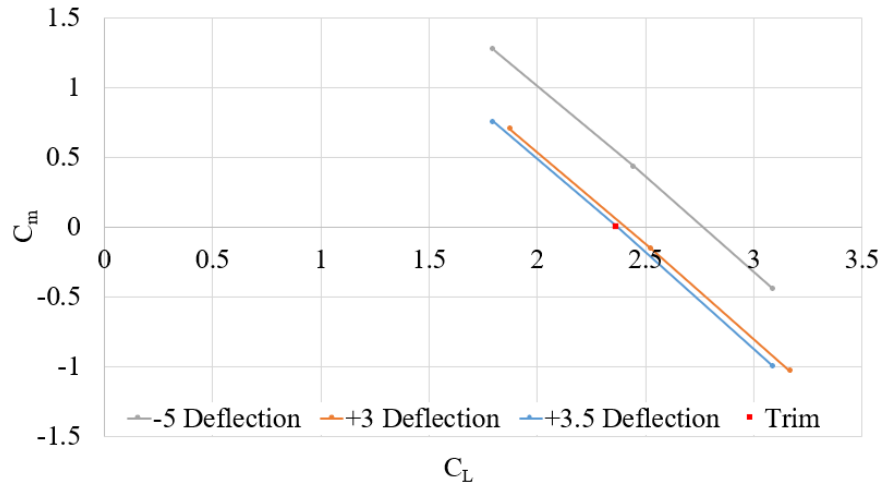
Fig. 36   Elevator Deflections During Landing

C. Static Longitudinal Analysis

Through superposition, the pitching and lift derivatives and coefficients were added together to each component of Bounden. As only the elevator controls the pitch, different elevator deflections were iterated through to find the trim deflection for the required trim state. The method of superposition with the use of an inviscid solver will need to be verified with a higher fidelity method due to the nature of the truss pitch and yaw derivatives. Figure 37 shows that Bounden is trimmable at all 3 flight conditions of cruise, landing, and takeoff, with these conditions having elevator deflections of +4, +3.5, and -4.5 degrees respectively.
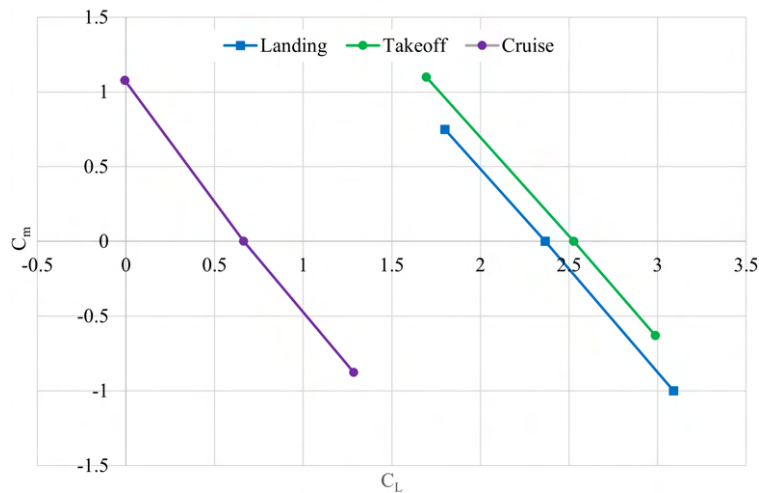
Fig. 37   Trim Diagram of Cruise, Takeoff and Landing

D. Stability Derivatives

AVL was used to solve for the stability derivatives of Bounden, with results shown in Table 41. An angle of attack of 0 was chosen to evaluate the stability of the aircraft as it will be operating at or near this condition for the majority of cruise. C_{L_a} is larger than 2π, which can be attributed to the nature of superposition, in which there is no interaction between the various surfaces of Bounden. Without accounting for the interactions between the surfaces, C_{L_a} will be overcalculated. From stability theory, the vast majority of the collected values from AVL show that Bounden is statically stable. All derivatives but C_{l_r} have a positive derivative at an angle of attack of 0. C_{l_r} should be positive as it is the rolling moment coefficient due to yaw rate that results from the effective velocity flowing over lifting surfaces. C_{n_β}, the dihedral effect, shows that no geometric dihedral is necessary as it is of negative value.

Table 41   Stability Derivatives of Bounden at Cruise Conditions

Derivative	C_{L_a}	C_{y_β}	C_{l_β}	C_{m_α}	C_{n_β}	C_{n_r}	C_{y_p}	C_{l_p}	C_{l_r}	$C_{m_{\delta e}}$	$C_{l_{\delta r}}$	$C_{n_{\delta r}}$
Value [1/°]	6.5	-0.39	-0.066	-6.32	-0.01	-0.095	-0.034	-0.65	0.17	-0.1	-0.001	0.0024

VIII. Structures and Loads

A. Material Selection

Traditionally, passenger aircraft were made out of different types of aluminum and other metal alloys, such as steel and titanium. Some more modern aircraft, such as Boeing 787 and Airbus A350, have significant portions of the aircraft made out of composites such as carbon fiber. Aluminum has a decent yield strength while also having a higher specific strength than steel. Meanwhile, composites are both light and strong but they are more expensive. The cost of aerospace-grade carbon fiber would be four times the cost of aerospace-grade aluminum given the same weight [45]. Table 42 documents the specifications of these different material options [46] [47] [48].

Table 42   Material Specifications

Material	Density [g/cm^3]	Yield strength [MPa]	Ultimate tensile strength [MPa]	Ultimate shear strength [MPa]	Young's modulus [GPa]	Poisson's ratio
Aluminium 2024-T4	2.78	325	470	285	73	0.33
Aluminium 6061-T6	2.70	275	310	205	69	0.33
Aluminium 7075-T6	2.80	505	570	330	72	0.33
Carbon fiber	1.6–2.20	N/A	1,700 - 7,000	N/A	228 - 724	0.26 - 0.28
Hexcel M21	1.56	N/A	885	97	67.6	0.2

From Table 42, Hexcel M21, a type of composite with carbon fiber and epoxy matrix, has a specific tensile strength 2.7 times that of aluminum 7075 T6. Due to the requirement stated by the RFP regarding 20 percent block fuel reduction for a 500 nmi mission, composite materials were designed to be incorporated within the structural design of Bounden to reduce weight and make block fuel reduction more attainable. Composite materials, however, are complicated to manufacture. There are many parameters that could affect the strength of a composite during manufacturing, such as layer structure, orientation, material, and temperature. Due to the extensive factors that could affect the characteristics of composites, the carbon fiber composite described in Table 42 is a generalization that gives a range of values instead of one.

The main advantages of composites are their strength and light weight. Some of the newer passenger aircraft, such as the Boeing 787 and Airbus A350, have adopted composite materials in a significant portion of their structures, such as the fuselage, the non-leading edge portion of the wing, and the tail. The main disadvantages of composites are their cost and their more complex behavior under load. This could make the aircraft cost more due to the material cost and difficulties to design and manufacture. Nonetheless, composites will still yield significant weight reduction which was why Hexcel M21 was adopted for the major load-bearing structures.

B. Load Factor

The maneuver envelope consists of two curves determined by the maximum and minimum C_L at stall condition. The positive and negative loading factors were set to be 2.5 and -1 respectively. The dive speed was set to be 1.4 times the cruise speed per the convention described in Raymer [4].
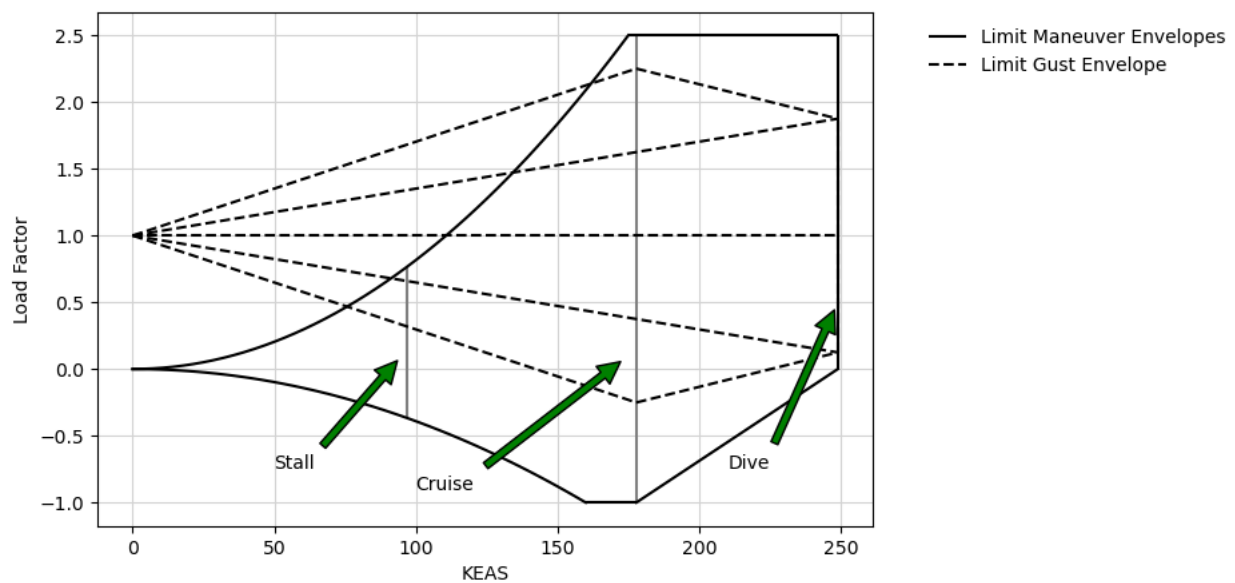
Fig. 38   V-N Diagram

With the equivalent cruise speed of 178 knots, the load contributed by the gust did not exceed the load factors stated by CFR §25.301 [34]. Therefore, both the maximum and minimum load factors were set according to CFR §25.301. The load factor range displayed by Figure 38 is within the norm for transport aircraft.

C. Structural Arrangement

In order to test the effectiveness of a truss-braced wing, the wing without a truss was analyzed as well. The wing of Bounden consists of a main spar and an aft spar. The main spar will be located at 17% of the chord while the aft spar will be at 57% of the chord. The span-wise lift distribution along the wing was approximated using the AVL inviscid lift coefficient data and was plotted using Python [49][50].

With the lift distribution, the shear and moment diagrams can be analyzed. The shear diagram in Figure 39 has displayed a reasonable trend as the shear at the center of the aircraft is 2.5 times the weight of the aircraft with a safety factor of 1.5. The shear distribution of the wing can be used to calculate the moment distribution as shown in Figure 40.
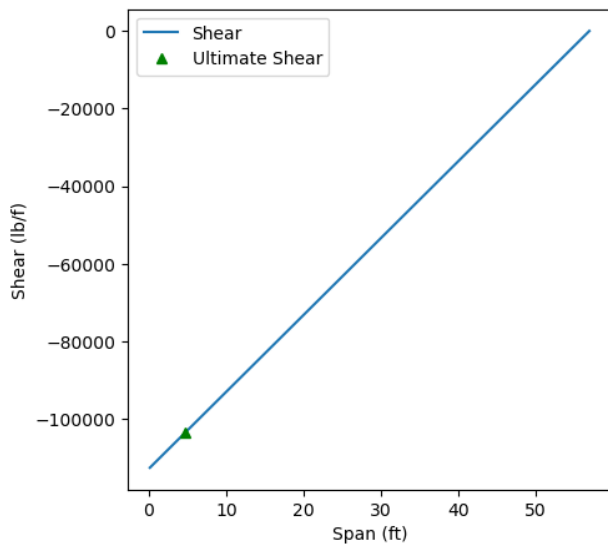
Fig. 39   Half-Span Shear Distribution
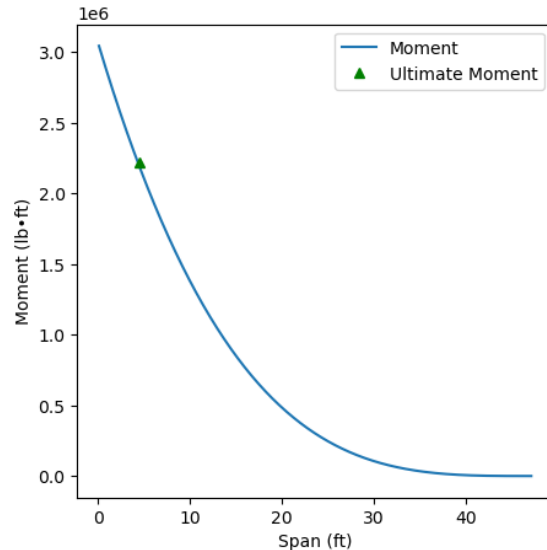
Fig. 40   Half-Span Moment Distribution

Knowing the ultimate moment, the required moment of inertia was calculated such that the stress experienced by the spar would not exceed the ultimate tensile strength of the material used for the spar.

Table 43   Main Structural Components Dimensions at Wing Root

Component	Length [in]	Width [in]	Cross-section area [in^2]
Cantilever spar cap	5.77	3	17.31
Cantilever spar web	7.54	1.39	10.48
TBW spar cap	4.06	0.5	2.03
TBW spar web	12.54	0.28	3.51
Truss spar	2	1	2

Without the truss, the main spar would be required to be much larger to support the wing. In the preliminary design phase, only the spar caps' moment of inertia were accounted for as they provide the vast majority of the moment of inertia that resists bending. Knowing the needed moment of inertia, the dimension of the caps was determined by using the parallel axis theorem which yielded a ratio between the thickness and width of the caps. Then, the web thickness of the spar was determined through the maximum shear force. Once the thickness of the web was calculated, the spar caps were trimmed down according to the moment of inertia provided by the web. The spar sizing for the empennage was determined using the same method.

With the addition of a truss to support the main wing, the ultimate moment the main wing experienced decreased by more than 80 %. This analysis was performed with the assumption that the moment experienced by the wing root remains constant with the moment experienced by the connection of the main wing and truss according to the study done by Virginia Polytechnic Institute and State University [51]. The approximate loading condition of a truss-braced wing can be described using static equilibrium equations. The setup of the static problem is setting the sum of forces and moments in all directions to zero while also constraining the moment experienced by the wing root to be the same as the moment present at the connection of the wing and truss. The free-body diagram for this system in shown in Figure 41.
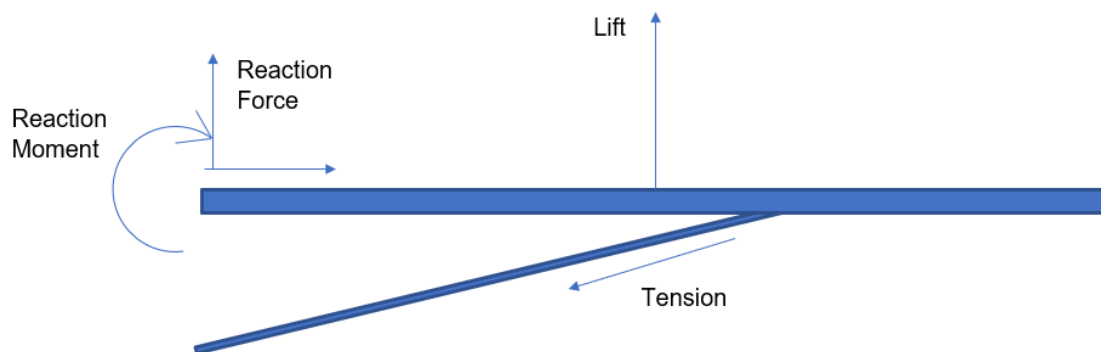
Fig. 41   Simplified Free-Body Diagram of Truss-Braced Wing

Using this process, the truss will need to be able to withstand 230,000 lbf of tensile force under the max load factor. Based on the tensile strength of Hexcel M21 specified in Table 42, the area of the truss spar cross-section was determined to be 2 inches squared. The truss spar will have a rectangular cross-section of two inches in height and one inch in width. The spanwise location for the connection of truss and wing was determined such that the overall weight of the wing-truss configuration can be minimized while also having clearance for the nacelle. This spanwise location was determined to be 38 ft away from the center of the fuselage. The truss will be connected to the main spar via a pin joint. With the consideration of ease of integration of the spar, the cap dimensions at the root along the web dimensions were designed as stated in Table 43. As the wing tapers, the geometry of the spars will change accordingly to accommodate.

With these dimensions, the truss-braced wing configuration was able to reduce the wing weight by 190 pounds compared to the conventional cantilever wing configuration assuming they both have the same skin thickness. Given the weight reduction, the team believes a truss-braced wing is preferable to a traditional wing to achieve the RFP requirements for block fuel reduction.

After designing the spars, the rib thickness of the wing was determined by analyzing the maximum shear flow that would act on the wing box. The ribs were calculated to be 0.57 inches thick. The rib and spar spacing is set according to the typical value as described in Roskam Part III [21]. Further refining of the rib spacing was done by analyzing areas with high stress. The areas under heavier load, such as the nacelle, will have a more dense rib arrangement. The rib that connects to the truss was also thickened to avoid large amounts of deformation. Through the sizing process, the structure of the wing with the current configuration is as shown in Figure 42.
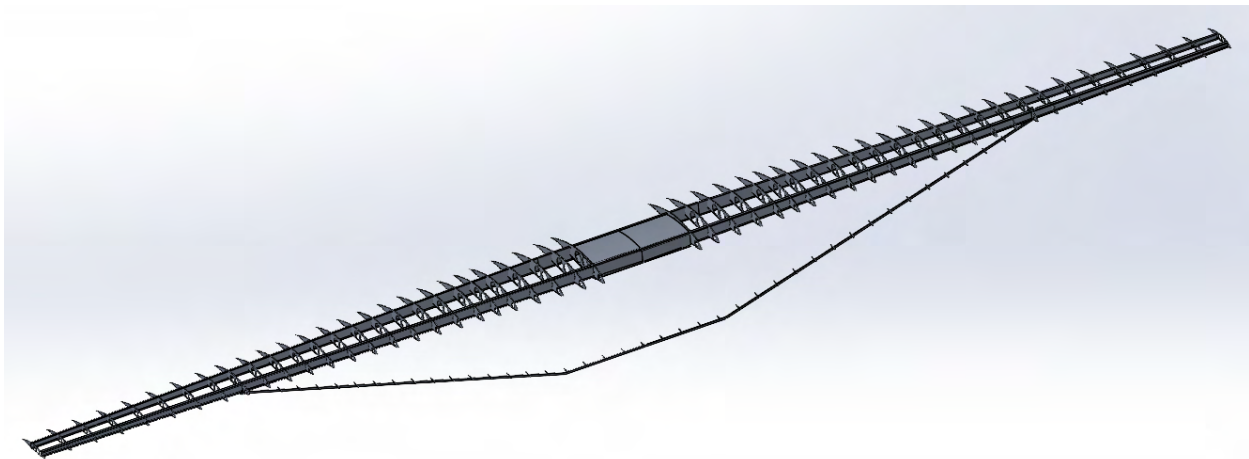
Fig. 42   CAD Model of Wing

With this configuration, finite element analysis was conducted on the half span of the CAD without the wing box through SOLIDWORKS [52]. The root of the spars and the horizontal part of the truss were fixed. A 2.5 g load with a safety margin of 1.5 was applied to the wing and truss with the inviscid lift distribution acquired from AVL.

The FEM in Figure 43 indicates the truss-braced wing configuration is effective and sizing done on the wing structure was adequate in maintaining the structural integrity of the aircraft in highest possible maneuver load. The FEM has indicated that strut and the main spar would be under the most stress which is anticipated. The skin of the wing was effective in preventing the wing twist induced by the aerodynamic loads and strut support.
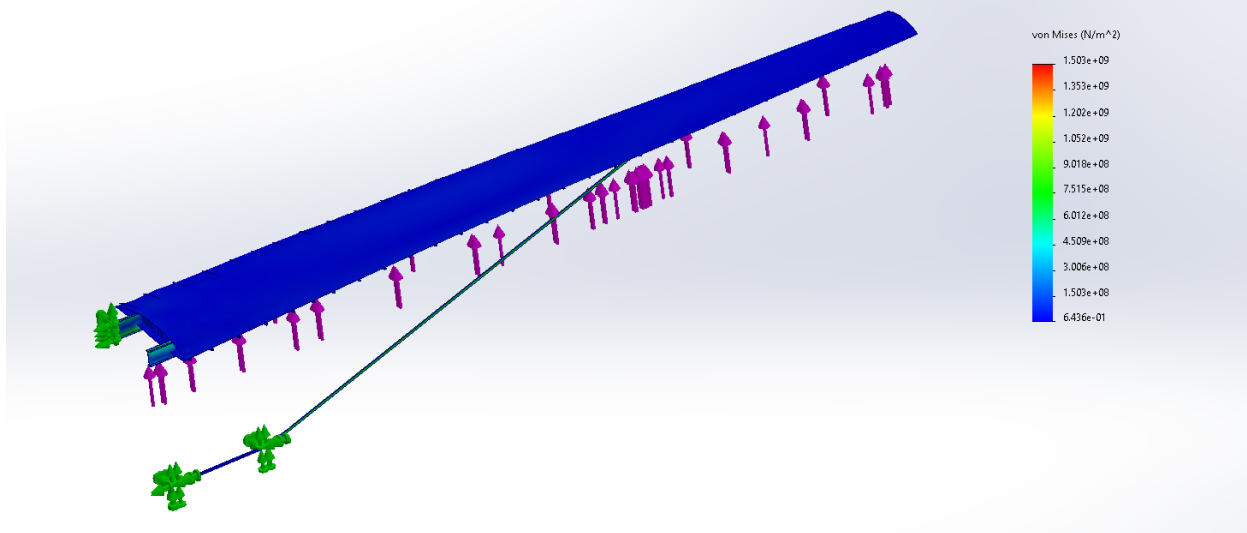
Fig. 43   Finite Element Method On Wing with Truss at 2.5 Load Factor and 1.5 Margin of Safety

The aircraft is designed to be pressurized to 8,000 ft altitude. While cruising at 28,000 ft, the pressure differential experienced by the fuselage would be 6.13 psi. Using this, the minimum thickness of the aluminum 2024-T4 fuselage skin was determined to be 0.05 inches. The bulkheads of the aircraft were sized based on Roskam Part III [21]. The thickness of the bulkheads was calculated to be 2.54 inches. The spacing of 20 inches between the bulkheads was also determined through Roskam Part III [21]. The longerons on the fuselage are hat-shaped with a spacing of 12 inches between them, which scales depending on the cross-section. Hat-shape longerons were chosen because they are easy to construct and efficient in weight. Z-shaped longerons were also considered but ultimately rejected because they will twist under loads, creating unnecessary complexities for structural analysis. Combining all these considerations, the full structure of Bounden was created as shown in Figure 44.
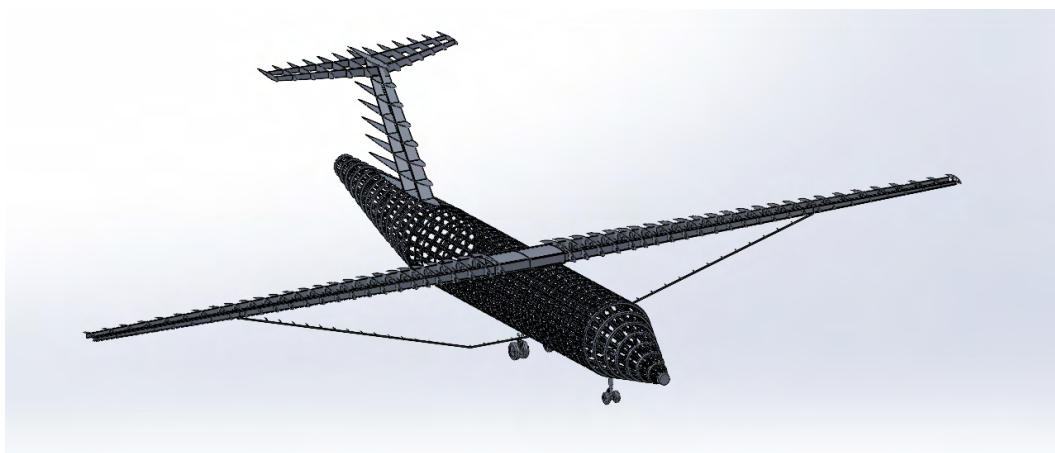
Fig. 44   Full CAD Drawing of Bounden

D. Load Paths

The aerodynamic forces during the flight will largely act on the wing at first. The spars will carry the load and transfer the load into the fuselage. For Bounden, about 80 percent of the lift will be carried by the front spar while the rest will go to the rear spar. The load path of lift is depicted in Figure 45.
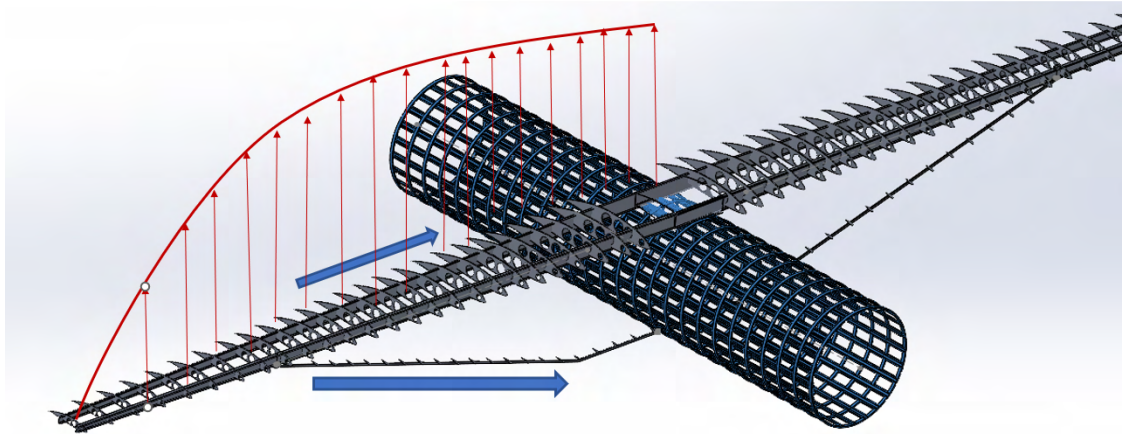
Fig. 45   The load path of lift on wing and truss

The load will travel down the wing spar and truss spar which will then be transferred into the bulkheads that are connected to the wing and truss. Then, the load will travel down the longerons until it reaches the center of gravity. A few parts of the bulkheads will sustain higher stress, specifically at the connection of the wingbox and the connection of the truss to the fuselage. Due to these reasons, these frames will be reinforced and thickened to prevent failures.

IX. Mass Properties

A. Weight Assessment

To start the process of computing key weights, a study was first conducted to determine which methodology offered the best estimation and would be used to produce a part-by-part build up for Bounden. This involved creating a component weight calculator using the weight equations provided by Raymer [4], Roskam [53], and Kroo [54] along with actual weights and weights obtained from the CAD model. The references to each equation used from each source are provided in Table 44, and the components in which the actual weights or the CAD model are used are also specified.

Table 44   Component Weight Estimation Equations References

Component	Raymer 6th Edition [4]	Roskam Part V [53]	Kroo Aircraft Design [54]
Wing, Struts, and Strut Box	15.25	5.70	Component Weights: 1
Horizontal Tail	15.26	5.19	Component Weights: 2
Vertical Tail	15.27	5.20	Component Weights: 3
Fuselage	15.28	5.27	Component Weights: 4
Nose and Main Landing Gears	CAD Model Used		
Propellers	Actual Weight Used		
Nacelle Group	15.31	5.33	-
Engines and Gearbox	Actual Weight Used		
Engine Controls	15.32	-	-
Propulsion System	-	6.39b	Components Weights: 7
Pneumatic System	15.33	Section 7.20	Component Weights: 10
Fuel System	15.34	6.24	-
Flight Controls	15.35	7.70	Component Weights: 6
APU	15.36	7.40	Component Weights: 8
Instruments	15.37	7.25	Component Weights: 9
Hydraulics System	15.38	Section 7.20	Component Weights: 10
Electrical System	15.39	7.17	Component Weights: 11
Electronics	-	7.25	Component Weights: 12
Avionics	15.40	7.25	-
Furnishings	15.41	7.45	Component Weights: 13
Air Conditioning System	15.42	7.31	Component Weights: 14
Anti-Ice System	15.43	7.31	Component Weights: 14
Oxygen System	-	7.37	-
Cargo Handling Gear	15.44	7.48	-
Flight Deck Seats, Passenger Seats, and Lavatory	Table 15.30	-	-
Operating Items	-	7.45	Component Weights: 15
Paint	-	7.51	-

The equations were used once the aircraft geometry was defined. It was determined that the part-by-part build up provided by Roskam Class II Torenbeek paired with the actual weights of the propellers, engines, and gearbox along with the CAD model for the nose and main landing gears was the most suitable for this analysis since this methodology was closely tailored to that of regional turboprop aircraft and specifically the team's design. The Raymer equations were closely tailored to cargo or transport aircraft, and the Kroo equations were more tailored to larger transport aircraft compared to a regional turboprop that the RFP is requesting. The equations also offered flexibility to account for varying configurations with factors that can be applied to the equations based on the type of variation being implemented.

This enables the weight estimate to be more representative of Bounden than using the weight equations from the other references, which were more general to transport aircraft. The specified methodology was also chosen since it provides explicit estimations for many components that Bounden requires such as the paint, propellers, engines, gearbox, and nose and main landing gears. The actual weight for the propellers were obtained from the EASA Type Certificate Data Sheet for the Dowty R408 propellers [55], and the engine weight was obtained from a civil turboshaft/tubroprop specification sheet [23]. Table 45 also shows the empty weight estimations for the Fokker 50 and Bombardier Dash 8-Q300 using each of the three methods specified. These were compared to the actual empty weights, and it can be seen that the Roskam Class II Torenbeek method offers the lowest percent difference, which proved to be another reason why this methodology was chosen.

Table 45   Empty Weight Comparison

Methodology	Fokker 50 [lb]	Dash 8-Q300 [lb]	Percent Difference From Actual [%]
Raymer 6th Edition	29,579	24,059	**Fokker 50:** 0.13 **Dash 8-Q300:** 7.70
Roskam Part V	29,538	26,705	**Fokker 50:** 0.01 **Dash 8-Q300:** 2.46
Kroo Aircraft Design	29,489	28,447	**Fokker 50:** 0.18 **Dash 8-Q300:** 9.14
Actual	29,542 [15]	26,065 [11]	-

In order to obtain component weights, several assumptions had to be made. First, to use the Raymer equations, the system electrical rating for the aircraft power was assumed to be 50 kW. Additionally, for all three methods, with assistance from the Avionics group, the uninstalled weight of avionics was found to be 1,600 lb based on the size of Bounden. The distance that the cables and pulleys need to travel was also assumed based on the length, span, and number of engines of Bounden. To account for the weight of the struts and strut box, the system was assumed to behave like a wing-body since the component consists of an airfoil-shaped skin, an I-beam spar, and multiple ribs; factors specified by all three methods were also implemented to the main wing to account for this component. To use the Kroo equations, the maximum fuselage pressure differential was assumed to be 1,238 lb/ft^2 or 8.60 psi. Furthermore, specific factors provided by all three methods were implemented to account for normal high lift devices, ailerons, and flaps. Finally, to account for the use of composite materials, the Structures group provided specific components that were to be made out of this material; these were the spars and ribs of the wing, struts, vertical tail, and horizontal tail, the wing and strut box, the tail cone of the fuselage, and the nacelle mounts. Factors obtained from Raymer with underestimations were applied since sub parts of components were to be made of composite materials [4]. Table 46 provides the factors that were applied to the relevant parts.

Table 46   Composite Factors

Component	Composite Factor
Wing	0.90
Struts and Strut box	0.93
Vertical Tail	0.87
Horizontal Tail	0.86
Fuselage	0.97
Nacelle	0.97

The maximum fuel weight was found by selecting fuel tanks that were capable of supporting the fuel weight required by Bounden for the specified design mission. Based on this requirement, Bounden will utilize two integral wing tanks, one in each outer wing, and two collector tanks located in each nacelle that can hold up to 9,180 lb of fuel [56]. The use of larger fuel tanks when compared to the mission fuel requirement enables Bounden to travel farther than other aircraft within the class making Bounden more marketable and desirable. Table 47 offers the weight breakdown from the three references along with the actual weights used for the propellers, engines, and gearbox, and the weights for the nose and main landing gear that were obtained from the CAD model that build up to the operating empty weight of Bounden. The chosen method is highlighted in blue.

To calculate the weight of the hybrid components, the specific powers of the electric motor, circuit breaker, converter, inverter, and controller were used to convert the power required for hybrid that was obtained from Section XI to weight. Additionally, the specific energy of the battery and the specific weight of the cables were used to find the weight estimate. Table 48 shows the specific powers, energies, and weights used. The specific energy of the battery was obtained from Section V and was used to compute the weight. Finally, the electrical wire weights used for the hybrid components were based on the required power of the hybrid system, which was obtained from Section XI. Since the hybrid system will be used throughout the climb and cruise phases, the cables will need to be rated for high-performance aerospace applications in addition to withstanding high temperatures since the hybrid power will be supplied for a prolonged period of time. The cable chosen that achieves this is the M22759/84-04 nickel-plated copper electrical wire. This cable supports the largest power requirement based on its voltage rating of 600 volts and amperage rating of 300 amps [57].

Table 47   Component Weight Estimation

Component	Raymer 6th Edition [lb] [4]	Roskam Part V [lb] [53]	Kroo Aircraft Design [lb] [54]
Wing	4,173	4,862	6,640
Struts and Strut Box	1,235	2,819	3,118
Horizontal Tail	567	547	1,144
Vertical Tail	437	589	698
Fuselage	4,855	5,201	5,552
Main Landing Gear	2,026	2,026	2,026
Nose Landing Gear	476	476	476
Propellers	1,810	1,810	1,810
Engines and Gearbox	3,161	3,161	3,161
Nacelle Group	1,458	1,208	1,745
Engine Controls	696	In Propulsion System	In Nacelle Group
Propulsion System	In Nacelle Group	1,084	In Nacelle Group
Pneumatic System	92	572	494
Fuel System	196	684	In Nacelle Group
Flight Controls	793	841	798
APU	440	540	371
Instruments	182	2,020	2,134
Hydraulics System	226	In Pneumatic System	In Pneumatic System
Electrical System	1,959	1,172	689
Electronics	-	In Instruments	900
Avionics	1,600	In Instruments	In Instruments
Furnishings	792	4,553	3,715
Air Conditioning System	993	854	795
Anti-Ice System	127	In Air Conditioning System	In Air Conditioning
Oxygen System	-	90	-
Cargo Handling Gear	57	57	57
Flight Deck Seats	180	In Furnishings	In Furnishings
Passenger Seats	1,600	In Furnishings	In Furnishings
Lavatory	61	In Furnishings	In Furnishings
Operating Items	-	In Furnishings	1,400
Paint	-	286	-
Crew	570	570	570
OEW Without Hybrid	30,762	**36,022**	38,293

Table 48   Specific Energies, Powers, and Weights of Hybrid Components [58]

Parameter	Value
Electric Motor Specific Power [kW/kg]	5
Cables Specific Weight [lb/1000ft]	661.4
Circuit Breaker Specific Power [kW/kg]	28
Converter Specific Power [kW/kg]	11
Inverter Specific Power [kW/kg]	11
Controller Specific Power [kW/kg]	11
Battery Specific Energy [Wh/kg]	250

Using the values from Table 48 along with the power required that was obtained from Section XI, the hybrid component weights are provided in Table 49. It should be noted that the PMDS weight includes the weights of the circuit breaker, converter, inverter, controller, and cables.

Table 49   Hybrid Component Weights

Parameter	Weight [lb]
Battery Weight (Both Modules)	9,600
PMDS Weight	1,447
Electric Motor Weight	176

Using the selected part-by-part method and weights for the hybrid components, the major weight parameters of Bounden are shown in Table 50. These include the operating empty weight, maximum takeoff weight, maximum landing weight, maximum zero fuel weight, maximum fuel weight, and maximum payload weight; it should be noted that these weight limits are in accordance with 14 CFR § 25.25. Additionally, the major weight parameters shown include the hybrid component weights.

Table 50   Major Weight Parameters

Parameter	Weight [lb]
OEW	47,245
MTOW	63,526
MLW	62,314
MZFW	58,028
Maximum Fuel Weight	9,180
Maximum Payload Weight	12,125

B. Center of Gravity Assessment

To compute the CG of the aircraft, as previously mentioned, the Roskam Class II Torenbeek method paired with the actual weights of the propellers, engines, and gearbox along with the CAD model for the nose and main landing gears was utilized. The Class II method of CG estimation was also used to conduct a part-by-part build-up. Once the component weights were found, the moment arms from the datum, which was set to be 100 in or 8.33 ft in front of the nose of the aircraft, to the centroid of the various components were found. The CG was then calculated as the distance from the datum in feet and also as a percent of the MAC, in which the MAC of the wing is 7.04 ft, and the leading edge of the MAC is positioned to be 41.08 ft from the datum.

The CG estimate also accounts for the placement of the hybrid components, which were positioned in a way where the CG of the aircraft would not shift drastically forward or aft when adding in the hybrid aspect. Table 51 outlines the component weights, CG location of each component, and overall CG location of the operating empty weight and maximum takeoff weight of the aircraft. A visual representation of the CG of the aircraft and components with respect to the datum is shown in Figure 46.

- Datum
- Struts and Jurys
- Vertical Tail
- Nacelles
- Propellers
- Propulsion System
- Nose Landing Gear
- Hydraulic and Pneumatic System
- Instruments, Avionics, and Electronics
- Oxygen and APU System
- Battery (Aft Module)
- Electric Motors

- Wing
- Horizontal Tail
- Fuselage
- Engines
- Fuel System
- Main Landing Gear
- Flight Controls
- Electrical System
- Air-Conditioning, Pressurization, and Anti and Deicing Systems
- Battery (Front Module)
- PMDS
- CG Aircraft Location

Fig. 46   Overall CG Locations From Datum

Table 51   Center of Gravity Breakdown

Component	Roskam Part V [lb] [53]	CG Location [ft from Datum]
Wing	4,862	41.50
Struts and Strut Box	2,819	39.41
Horizontal Tail	547	84.82
Vertical Tail	589	74.28
Fuselage	5,201	45.54
Main Landing Gear	2,026	43.83
Nose Landing Gear	476	14.89
Propellers	1,810	36.33
Engines and Gearbox	3,161	39.83
Nacelle Group	1,208	42.85
Propulsion System	1,084	23.09
Hydraulic and Pneumatic System	572	43.33
Fuel System	684	42.33
Flight Controls	841	48.79
APU	540	21.45
Instruments, Avionics, and Electronics	2,020	21.45
Electrical System	1,172	41.13
Furnishings	4,553	43.44
Air Conditioning, Pressurization, and Anti and Deicing System	854	39.49
Oxygen System	90	21.45
Cargo Handling Gear	57	42.52
Paint	286	53.16
Battery (Front Module)	4,800	34.13
Battery (Aft Module)	4,800	49.70
PMDS	1,447	43.59
Electric Motors	176	40.33
Crew	570	21.45
OEW	**47,245**	**41.02 (33.21% MAC)**
MTOW	**63,526**	**41.23 (36.25% MAC)**

1. CG During Loading, Mission Segment, and Unloading

In order to reach the CG location of the aircraft for maximum takeoff weight as shown in Figure 46, a loading path from loading the battery modules to the maximum takeoff weight was examined. Figure 47 shows how the CG shifts from loading the batteries, passengers, and baggage in both the forward to aft and aft to forward configurations, along with loading the fuel in the fuel tanks. Figure 47 also highlights the loading conditions that yield the extreme forward and aft limits, which will be discussed in the coming sections.
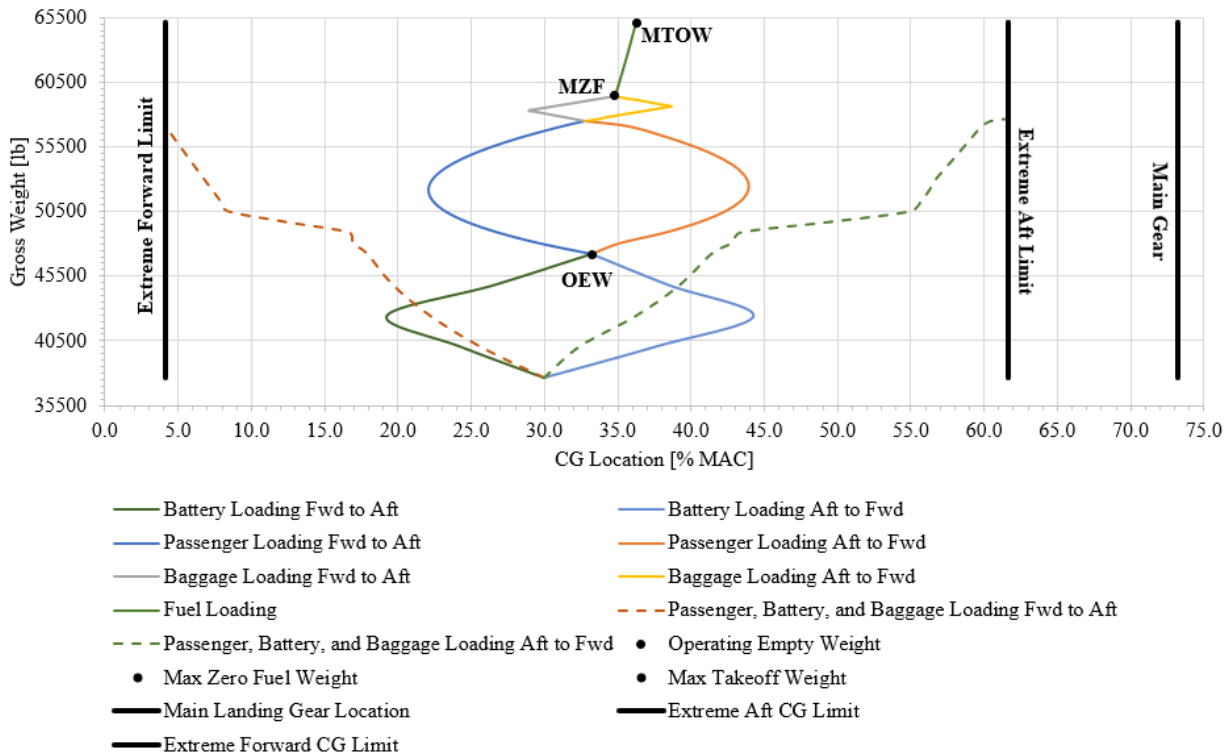
Fig. 47   CG Path During Loading

Once Bounden has been loaded and has taken off, the CG will shift during the various segments of flight. The path the CG takes as it flies through the various mission segments is shown in Figure 48. During this time, only the mission fuel will be burned, and when landing, the reserve fuel, passengers, baggage, and batteries will remain. It should be noted that the CG path shown in Figure 48 is during a 1,000 nmi mission.
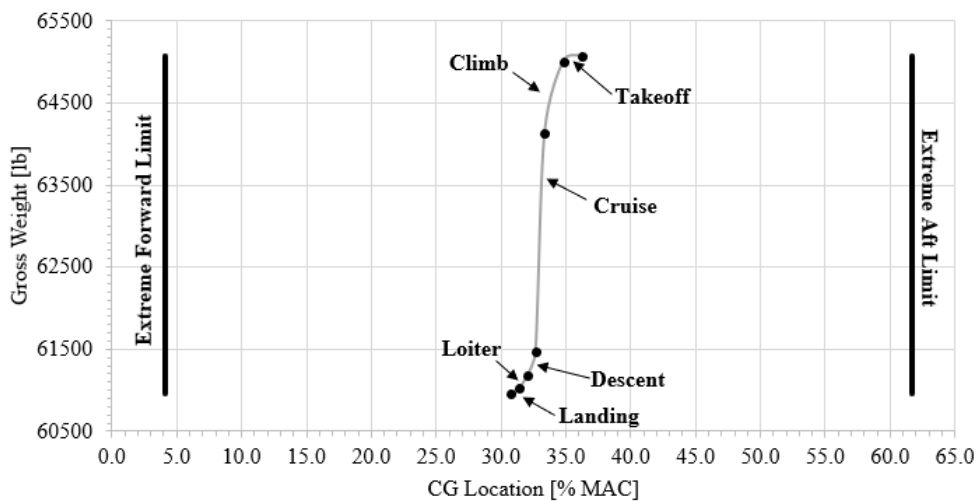
Fig. 48   CG Path During 1,000 nmi Mission

Finally, after the mission has concluded and Bounden has landed, the unloading of the aircraft can begin. This is shown in Figure 49 with first the unloading of the passengers and baggage followed by the battery modules in both the forward to aft and aft to forward configurations. This unloading path is done with the consideration in mind that the reserve fuel will remain in the fuel tanks.
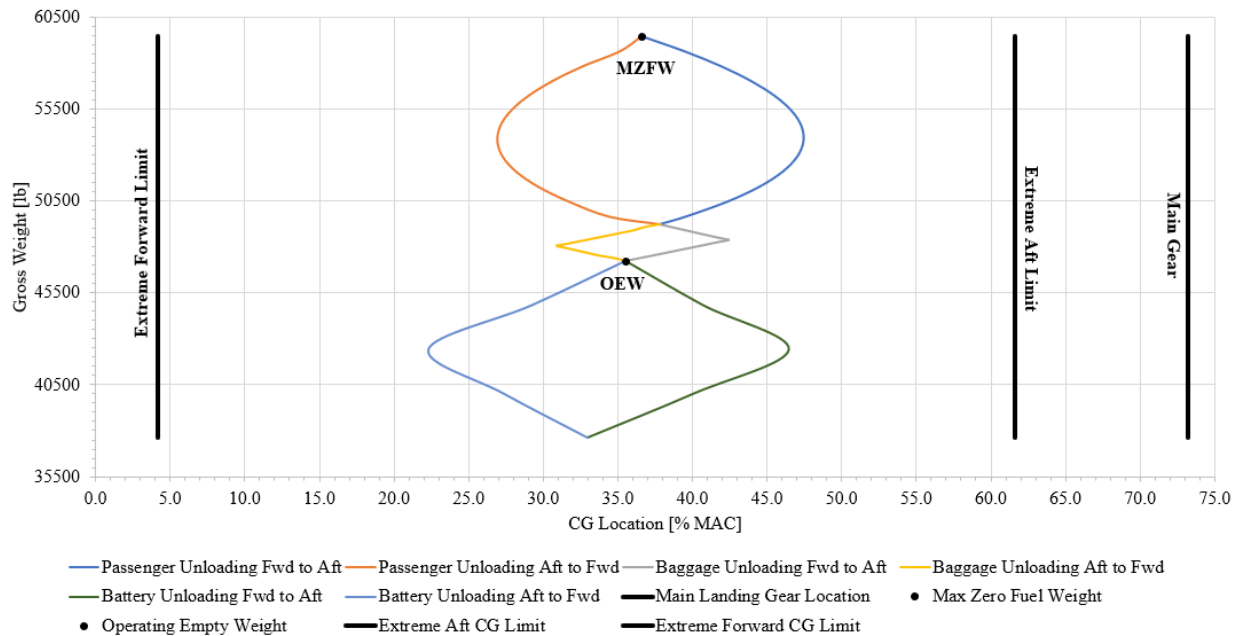
Fig. 49   CG Path During Unloading

Figures 47 and 49 indicate the forward and aft limits during the loading and unloading period, where the operational forward limit occurs during the battery module loading in the forward to aft configuration, and the operational aft limit occurs during the passenger unloading in the forward to aft configuration. It can be seen that the CG shifts forward to 19.26% MAC and the aft limit is 47.40% MAC. From the figures it can also be seen that the main landing gear is positioned to be at 73.19% MAC. This position leaves a large margin so that the safety of the aircraft will not tip backwards during any point whether it be under normal operating conditions or under extreme situations, which will be discussed next.

2. Operational CG Envelope and Procedures

Figure 50 specifies the CG limits of the aircraft. It shows the envelope of where the CG of the aircraft will ever be within during normal operating conditions. These normal operating conditions that should be followed during loading, unloading, and flight are the loading of the battery modules first, followed by passenger, baggage, and finally fuel loading. For unloading, normal operating conditions consists of passenger and baggage unloading followed by battery module unloading.
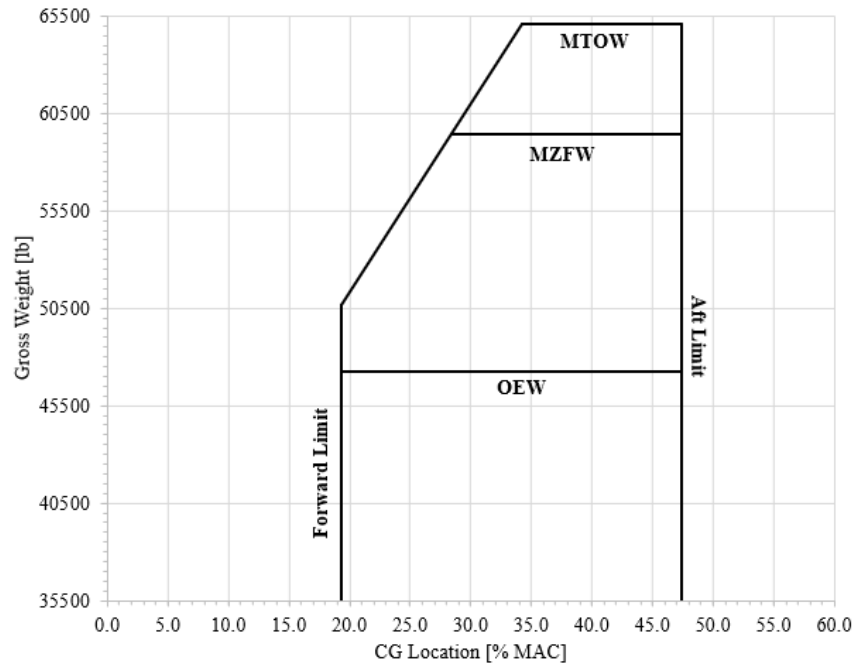
Fig. 50   Operational CG Envelope

Multiple other scenarios were examined, and the case that yields the extreme forward and aft limits are during passenger, battery module, and baggage loading simultaneously in the forward to aft and aft to forward configurations. These extreme forward and aft limits are 4.14% MAC and 61.65% MAC, respectively, and the path that the CG takes that yields these extreme limits are shown in Figure 47. It is not advised that the aircraft be operated in this manner during loading, unloading, or flight, and only the loading and unloading configurations specified during normal operating procedures be followed.

C. Trade Studies

A trade study was performed in conjunction with the Stability and Control group to size the horizontal tail. This was done by creating a scissor or notch diagram that is discussed in further detail in Section VII. Various horizontal tail areas were considered, and the shift in the aircraft CG location was observed to obtain a range of forward and aft CG limits as a function of horizontal tail area.

Finally, several locations for the two battery modules were considered. The placement of the front module was restricted by the strut box, which meant that the centroid of the front module could be placed as far forward as desired, but it could only be placed at a maximum aft location of 34.13 ft from the datum. Similarly, the centroid of the aft module could be placed as far aft as desired, but it could only be placed at a maximum forward location of 44.70 ft from the datum. Various positions of the modules were tested within this range, and the results are shown in Table 52.

Table 52   Battery Positions

Location of Front Battery Module [ft from Datum]	Location of Aft Battery Module [ft from Datum]	Forward CG Limit [% MAC]	Aft CG Limit [% MAC]	Aircraft CG Location [% MAC]
19.78	64.25	-3.81	67.68	36.46
34.13	49.70	19.26	44.29	36.25
26.96	44.70	7.73	36.25	23.50

Based on Table 52, it can be seen that placing the front module too far forward and the aft module too far backward yields a forward and aft limit that are outside of normal operating conditions. To go on, placing the front module at 26.96 ft from the datum and the aft module at its maximum forward location of 44.70 ft from the datum leads to an aircraft CG position that is too far forward. Finally, placing the front battery module at its aft most limit of 34.13 ft from the datum and the aft module at 49.70 ft from the datum provides CG limits that is within the operational range along with an aircraft CG that is at a reasonable 36.25% MAC.

X. Systems

A. Subsystems

1. Flight Controls

Bounden will utilize a fly-by-wire system for flight control. The system will read inputs from the yokes and deflect the elevators, rudder, ailerons, and leading and trailing edge flaps to control the aircraft. The layout for this systems is shown in Figure 51.
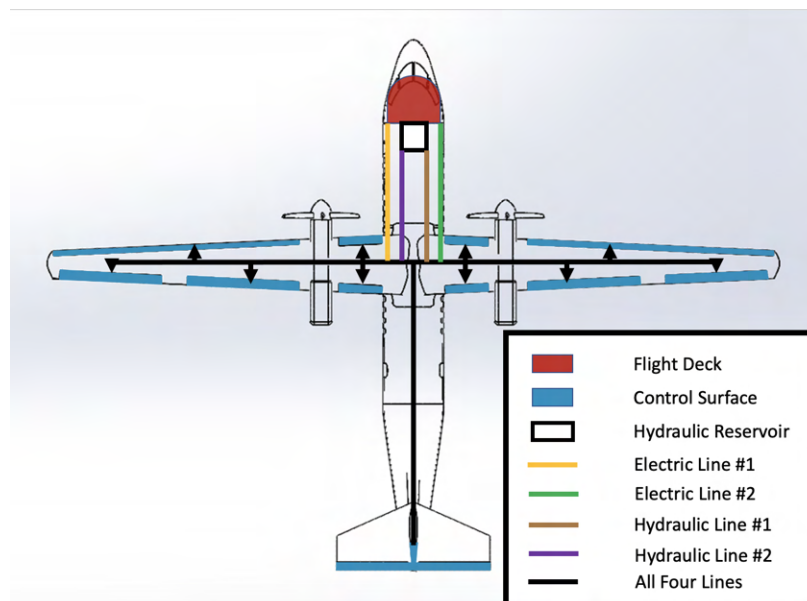

Fig. 51   Fly-By-Wire System Layout

The aircraft will have two primary hydraulic systems that travel the aircraft in accordance with CFR §25.1435. Each system will have its own pump and accumulator, and they will share a central reservoir. In addition, each hydraulic actuator will also have an electro-mechanical actuator with two sets of wires as a backup system, following the 2H2E architecture. The major control surfaces, including the ailerons, flaps, slats, elevator, and rudder will be controlled by continuously variable actuators to allow for precise control. The brakes, landing gear, and cargo doors will be controlled by two state actuators. Figure 52 shows the hydraulic system in more detail.
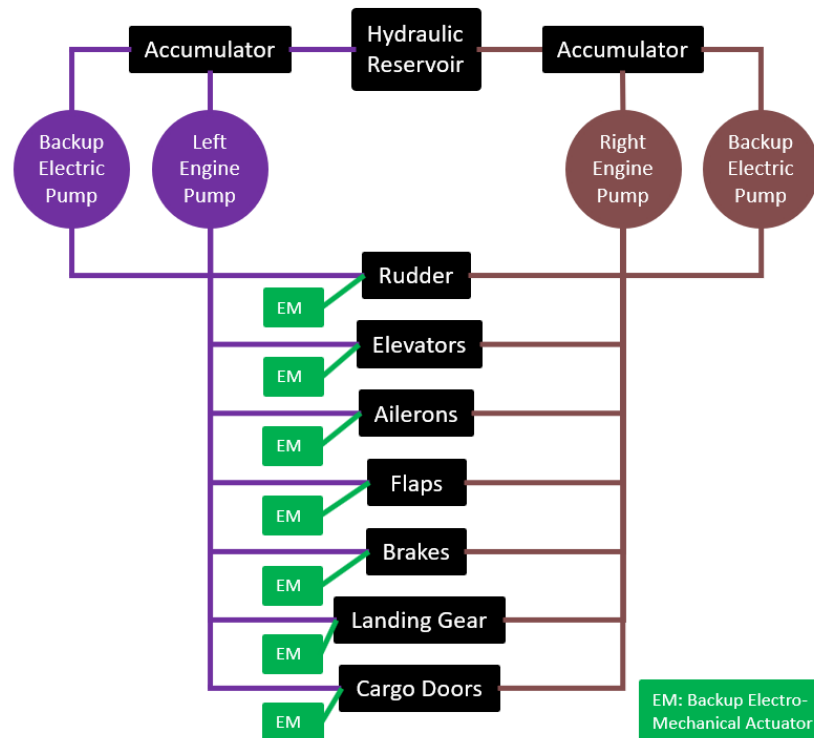
Fig. 52   Hydraulic System Connection Diagram

2. Propulsion System

Since Bounden is a hybrid aircraft, the propulsion system includes both the battery-motor system and the fuel-engine system. Both of these systems are included in Figure 53. Bounden will have two fuel tanks per side of the aircraft. Each engine will have a collector tank located in the wing next to the nacelle, along with a main tank further along the wing. The wing's skin, rib, and spar structure will be used to contain the fuel in order to save weight. The collector tank will connect to the engine through a gravity feed, as is typical on high-wing aircraft. The main fuel tank will utilize a transfer pump to send fuel to the collectors, with a transfer valve in the main tank that allows fuel to transfer to the collectors. In addition to the transfer valves, there are also refueling valves, fuel vent valves, and fuel dump valves for emergencies only. The fuel system is shown in more detail in Figure 54.
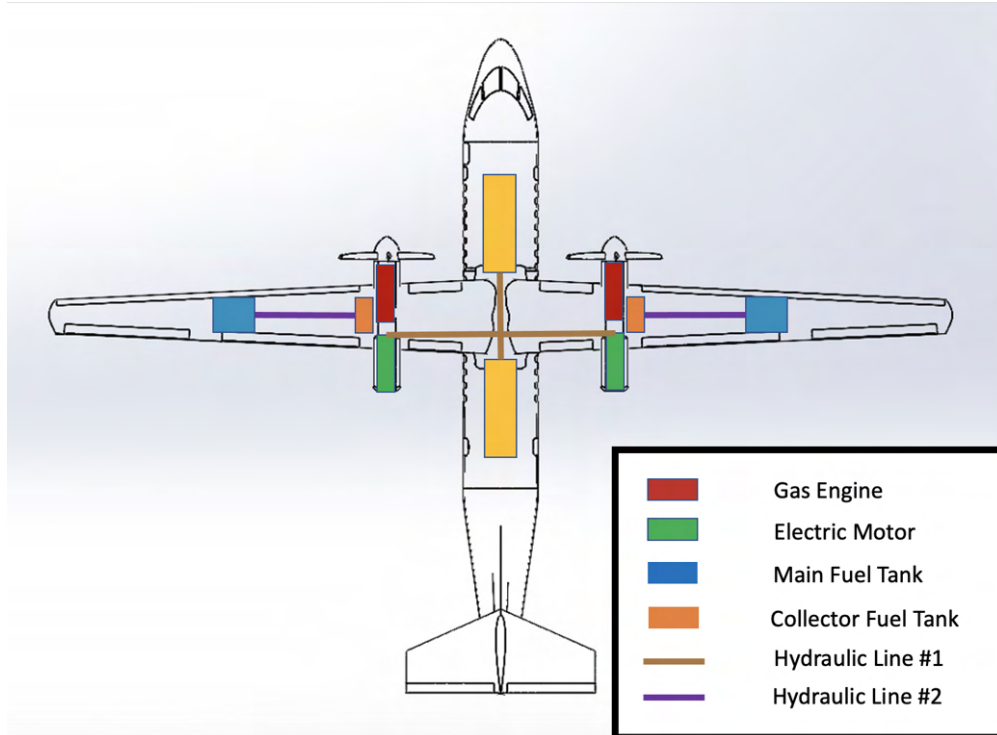
Fig. 53   Propulsion System Diagram
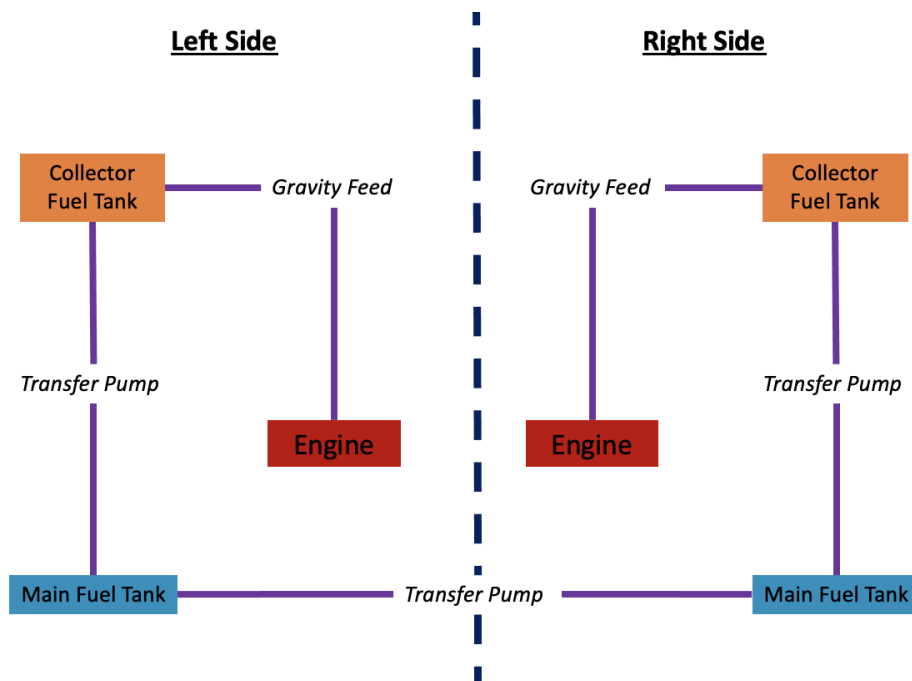
Fig. 54   Fuel System Connection Diagram

3. Engine Controls

The engines on the aircraft are managed by the Full Authority Digital Engine Control (FADEC) computer system. This computer will interpret data including throttle position, air data, and speed and will output fuel flow and other parameters to both engines. This will simplify the engine controls that the pilot has to input, along with improving engine efficiency and engine life. In accordance with CFR §25.1329, manual override is an option in the case of failure. The yoke design is covered in more detail in Section IV.B.

4. Anti-Icing

Bounden will utilize an electro-thermal blanket system to account for icing on the leading edge of the wing. Most turboprop aircraft have boot systems on the leading edge that de-ice the aircraft, but these systems interfere with aerodynamics and can be dangerous. Electro-thermal blankets do not have this issue as they are located on the inside of the wing. This technology is already in use in the Boeing 787, demonstrating its viability. Bleed air systems were also considered, but electro-thermal systems are significantly more efficient in terms of energy used. Drag is also decreased in an electro-thermal blanket system due to the lack of vents for the bleed air. The system will follow CFR §25.1419 requirements [59].

5. Electronic System

To provide electricity to the avionics and fly-by-wire system, the aircraft will feature an electronic system separate from the main battery used for propulsion. The electronic system is shown in detail in Figure 55.
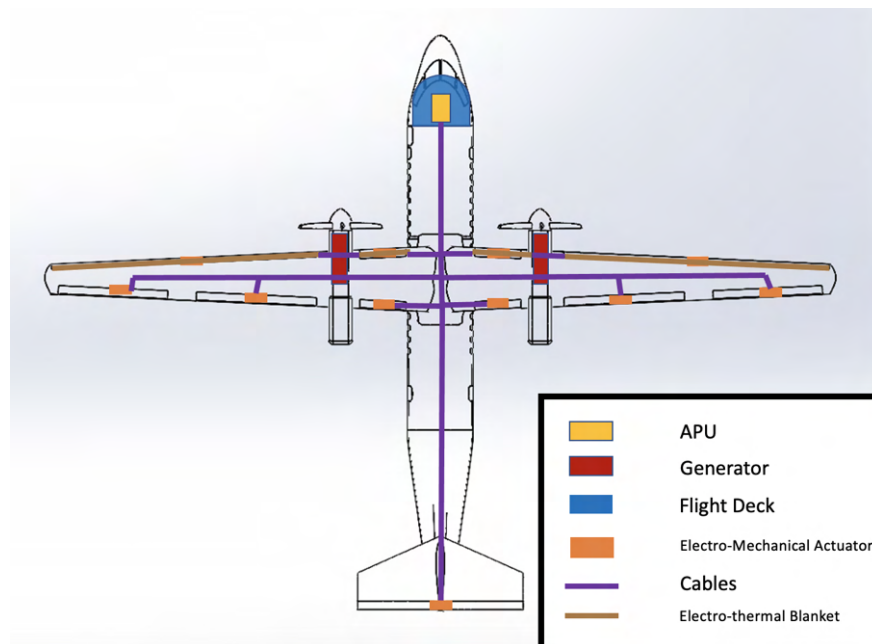
Fig. 55   Electronic System Schematic

Designed in accordance with CFR §25.1715, the system will feature an auxiliary power unit (APU) that is charged by generators in the nacelle. The APU will be located directly under the floor of the flight deck. Electricity will travel from the generator and APU to the flight deck, where the fly-by-wire system will take inputs from the yoke. These inputs will pass information to the hydraulic actuators through the electronic system. The APU will also power the avionics and the electro-thermal deicing blankets.

6. Environmental Control Systems

Using the bleed-air system, the entire cabin and flight deck will be pressurized. A climate control system with air conditioning and heating will ensure the safety and comfort of the cabin throughout the flight. The aircraft is pressurized using the bleed air from the pneumatic system. The air is regulated as it flows through a precooler, air filter, and air conditioning unit before entering the cabin. The system is shown in detail in Figure 56. [60]
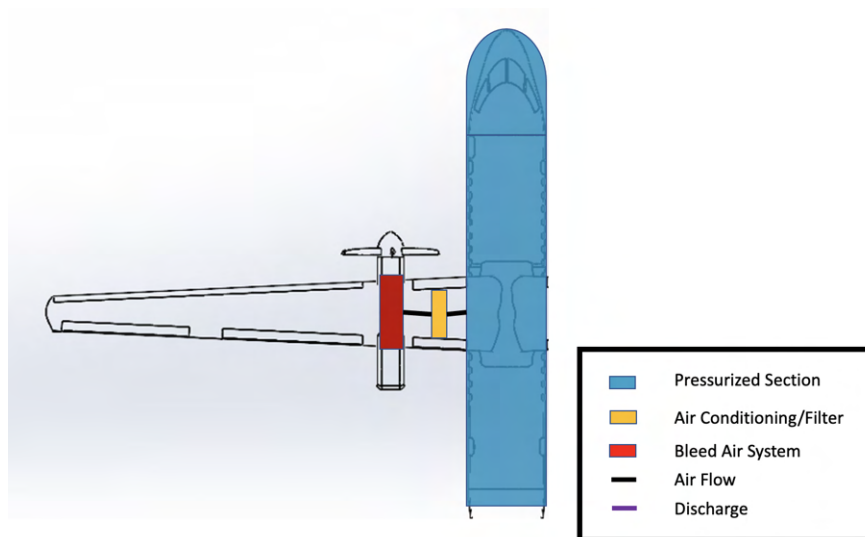
Fig. 56   Pneumatic-Environmental Control System

7. Emergency Systems

In the unlikely event of flight control failure, Bounden has a number of built-in emergency systems in accordance with CFRs §25.1713 and §25.810. The aircraft are backup electro-mechanical actuators built into the hydraulic system, along with a manual emergency release handle to lower the landing gear. There are a number of sensors built into systems that ensure the crew is properly notified in the case of emergencies and to supress these issues. In the event of a fire, there is a robust fire sensing and suppression system built in to the aircraft, especially around the main propulsion batteries. There are sensors in the fuel tanks to measure fuel level, and in the case of an emergency, the fuel dump valves are available to rapidly lose weight in the aircraft. In the event of pressurization failure, there are backup oxygen systems along with drop-down masks for all passengers and crew. [60]

B. Avionics

The avionics suite is designed to be in regulation with FAA regulations by conforming to the requirements for flight and navigation instruments presented by 14 CFR §25.1303. Additionally, the suite must be capable of VFR and IFR flight with an autopilot and capable of flight in known icing conditions. Improving upon the incumbent regional turboprops' flight decks, Bounden will have a glass cockpit with a dark cockpit philosophy and a centralized crew alerting system. The LCD displays will utilize synthetic vision systems (SVS) with the optional addition of heads-up displays (HUDs) in the flight deck to further improve awareness and aid pilots with navigation. Although this glass cockpit is more expensive than traditional avionics suites with steam gauges, almost all new aircraft are designed with this style of the flight deck and Bounden is staying competitive in its class with this design.

This decision for a glass cockpit is also made to support the future autonomous features that will likely be deployed to the next generation of aircraft. Bounden will not be designed to support fully autonomous operations due to the other driving requirements of the plane such as hybridization taking precedence in driving the design and cost. Although this aircraft is not designed to be fully autonomous, the latest technologies were chosen to accommodate features that will decrease pilot workload and potentially support reduced pilot operations, thus supporting partially autonomous operations. Table 53 outlines additional reasons that full autonomy will not be pursued given the aircraft mission.

Table 53   Autonomy Trade Study

Autonomy Requirements	Derived Requirements	Effects
Additional Sensors	Ability to Fit/Retrofit Sensors Additional Wiring Space for Large Sensors	Increase Cost Increase Weight Increase System Complexity
Turboprop Autothrottle	Complex System	Increase Operating/Training Costs Increase R&D Cost
2035 EIS for Technology	Autonomy Certification by 2035	Potential Certification Issues by Required EIS

Bounden will be fit with avionics packages in an a la carte style solution to reduce costs. Down-selection was guided by choosing the latest technology and ensuring the avionics would be compatible with new mandates, such as the 2020 ADS-B Out Mandate [61]. The specific avionics packages Bounden is equipped with are listed in Table 54. It should be noted that packages from suppliers like the Collins Multimode receiver include multiple required sensors from 14 CFR §25.1303 such as direction indicators, pitot tubes, and radio altimeters [62]. Similarly, the Honeywell Primus 1000 is an autopilot system capable of VFR and IFR flight as required, meeting RFP requirements and reducing complexity as an integrated avionics system [63].

Table 54   Selected Avionics Equipment

Category	System	Product
Communications	Antennas	Collins Aerospace DFA-901
Communications	Datalink	Collins Aerospace CMU 9000
Communications	SATCOM	Collins Aerospace IRT NX SATCOM System for Iridium
Communications	VHF	Collins Aerospace VHF-2200 Multi-channel Software-defined Radio
Communications	HF	Collins Aerospace HFS-900D/CPL-920D High Frequency Radio Set
Indicating Systems	Dual digital ADS	Collins Aerospace SmartProbe Air Data System
Indicating Systems	Angle of Attack Systems	Collins Aerospace Angle of Attack System
Indicating Systems	TAT Sensors	Collins Aerospace TAT Sensor
Indicating Systems	EFIS	L3Harris EFI-650
Navigation	Integrated Multi-Mode Receiver	Collins Aerospace GLU-2100 Multimode Receiver
Navigation	Digital Radio Altimeter	Collins Aerospace LRA-2100 Low Range Radio Altimeter
Navigation	Automatic Direction Finder Sensor	Collins Aerospace ADF-900
Navigation	Distance Measuring Equipment	Collins Aerospace DME-2100
Navigation	Heads Up Displays	Collins Aerospace Compact HUD
Flight Management	FMS	Honeywell Aerospace Next Generation Flight Management Systems (NGFMS)
Flight Management	Flight Recorders	Honeywell Aerospace Connected Recorder-25 (HCR-25)
Flight Management	Autopilot	Honeywell Aerospace Primus 1000
Flight Management	Flight Control Electronics	BAE Systems Integrated Flight Controls
Displays	LCD Displays	Honeywell Aerospace DU-875 LCD Display
Warning Systems	Surveillance	Collins Aerospace ISS-2100 Configurable Integrated Surveillance System

Special attention is given to the design of the throttle quadrant given the electric motors in addition to the turboprop engines. The turboprop engines are driven by a standard throttle for power and levers for propeller control, with all knob shapes and sizes designed in compliance with 14 CFR §25.781. The electric power will be controlled with a single electric throttle. The throttle can be disengaged, set to a scheduled electric power, or throttled given the lever position. The schedule option allows the electric power to go into a scheduled hold under climb conditions with a positive rate of climb, resulting in the turboprop engines scaling back power per the schedule and simplifying operations for pilots. For Bounden's mission profile, the pilot can set the throttle to the schedule function to follow the throttling schedule described in Section XI. The power quadrant design is illustrated in Figure 57.
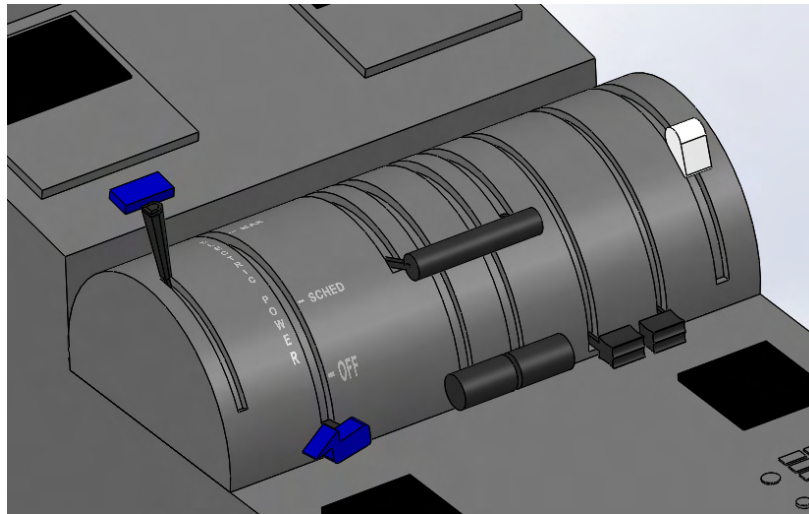
Fig. 57   Power Quadrant Design

XI. Performance

The aircraft was sized for a 1,000 nmi mission with cruise at 28,000 ft altitude and a cruise speed of 300 kts. This is much higher than most turboprops of similar ranges, so the use of hybrid-electric is necessary to reach the performance requirements and satisfying block fuel reduction. These conditions were chosen based on the RFP requirements of the aircraft to have initial cruise at a minimum of FL280 and a cruise speed above 275 kts, targeting 350 kts. The plot in Figure 58 shows how the speed and cruise point was chosen. At the chosen cruise altitude of 28,000 ft, Bounden went furthest per pound of fuel at 250 kts, but because this was below the required minimum cruise speed, the highest speed it could reasonably go at this altitude was chosen instead as shown in the constraint diagram and discussed in Section III.
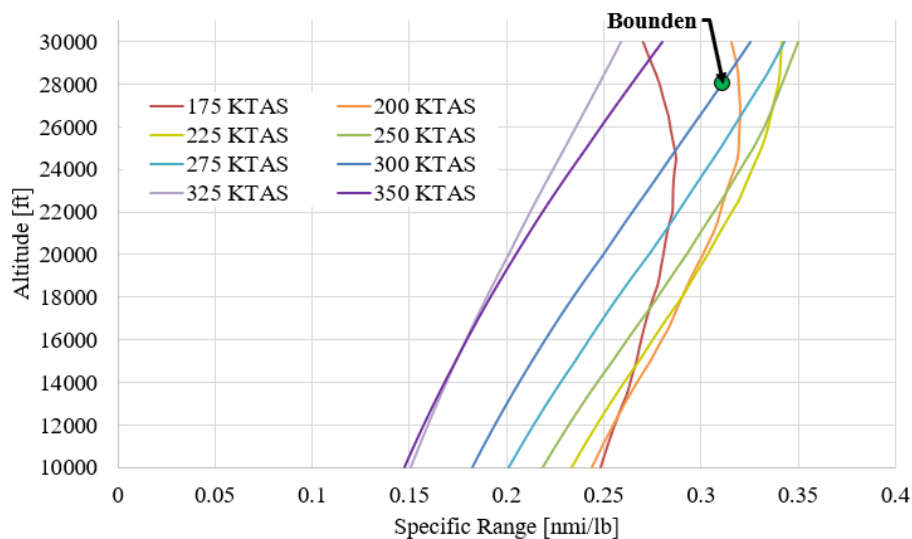
Fig. 58   Specific Range Diagram

A. Mission Analysis

The mission was broken down into each section mentioned in Table 6, and for each section of the mission profile, the distance, the fuel weight, and the energy required was calculated. A summary of Bounden's performance is shown in Table 55 for the designed 1,000 nmi mission following the mission profile described in Figure 3. The flight envelope is also shown in Figure 59 showing the limits of the aircraft and the designed flight path for Bounden. The flight envelope for Bounden is bounded by the stall speed, the structural ceiling, the maximum speed, and the maximum dynamic pressure allowed on the aircraft.

Table 55   Mission Summary by Section

| Mission Section	Distance	Time [min]	Fuel Burn [lb]	Battery Energy [kW-hr]	Power Split
Takeoff	2,555 ft	15	71.99	0	0%
Climb	143.6 nmi	38	875.6	496.2	15.9%
Cruise	712.2 nmi	142	2,661	517.8	6.47%
Descent	144.3 nmi	49	287.7	0	0%
Loiter	-	10	156.8	0	0%
Landing	3,693 ft	15	65.68	0	0%
Total	*1,000 nmi*	*270*	*4,119*	*1,014*	*1.53%*
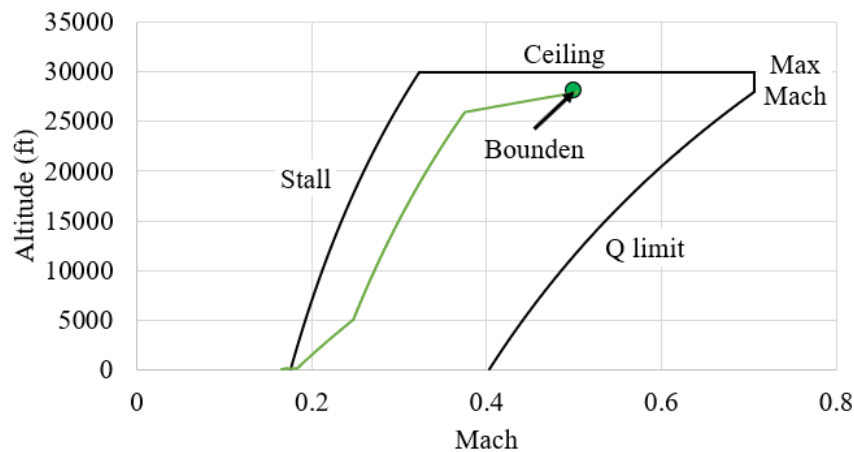
Fig. 59   Bounden Flight Envelope

B. Takeoff and Landing Performance

The aircraft must be able to takeoff and land within a 4,500 ft field length over a 50 ft obstacle on dry pavement at sea level and DISA 18°F [1] at sea level and 5,000 ft above sea level. Other certifications that drove performance require that the aircraft be able to takeoff in OEI conditions [64]. A summary of the performance can be seen in Table 56. Takeoff analysis was broken into three sections: ground roll, rotation, and transition as seen in Figure 60. In the ground roll analysis, performance was integrated over velocity using the averaged thrust for each segment of Raymer's

ground roll distance estimate [4]. The initial speed was set as 0 fps and the final velocity as $1.1V_{stall}$ (184 fps). This method assumed a quasi steady-state for each step at a constant velocity. Rotation period is assumed to be 3 times the takeoff velocity. Transition accelerated the aircraft speed to climb speed following a circular transition arc to clear a 50 ft obstacle over steps of altitude. It is with this analysis balanced field length was also analyzed. Looking at velocities below the rotation speed, it was found that the balance field length is 2,383 ft and 2,826 ft at sea level and at 5,000 ft above sea level respectively.
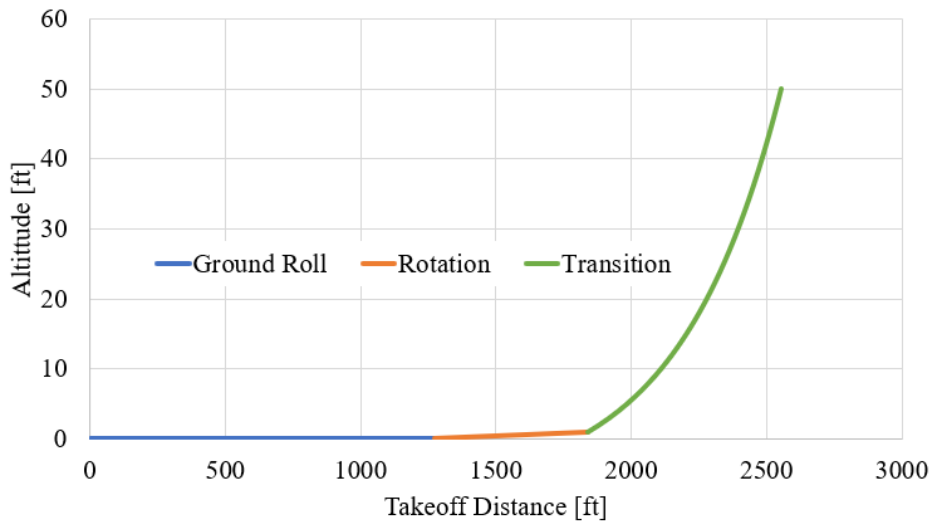
Fig. 60   Takeoff Distance

Landing analysis follows the same process as takeoff, but backwards. The landing segment starts with the transition period to pass the 50 ft obstacle, the rotation period is where the aircraft begins to flare, and it finishes with ground roll. During ground roll, Bounden will use reverse propellers, brakes, and spoilers.

Table 56   Takeoff and Landing Performance

Section	Climb/Approach (kts)	Rotation (kts)	Ground Roll (kts)	Field Length SL + DISA 18°F (ft)	5,000 ft Field Length + DISA 18°F (ft)
Takeoff	122	117	112	2,555	2,552
Landing	132	117	101	3,955	3,693

C. Climb and Cruise Performance

The RFP requirements limit the aircraft's climb range to less than 200 nmi and the minimum initial cruise altitude of 28,000 ft [1]. Looking at how excess power and specific energy change with altitude and speed shown in Figure 61, the fastest climb at a given altitude is given at the speed at which the excess power and specific energy are tangent. So, after an initial climb to 5,000 ft, climb is to be held at a constant KCAS of 150 kts until 26,000 ft altitude. From 26,000 ft

to 28,000 ft, KCAS constantly climbs until KTAS reaches 300 kts at FL280. Both throttles for gas and electric were also kept constant throughout the climb for ease of the pilot. As Bounden climbs, the power supplied by the engine lapses, but the power from the motor is constant at all altitudes. Because of this, the power split of Bounden increases as Bounden climbs until it completes its final section of climb as seen in Figure 62 and Figure 63.
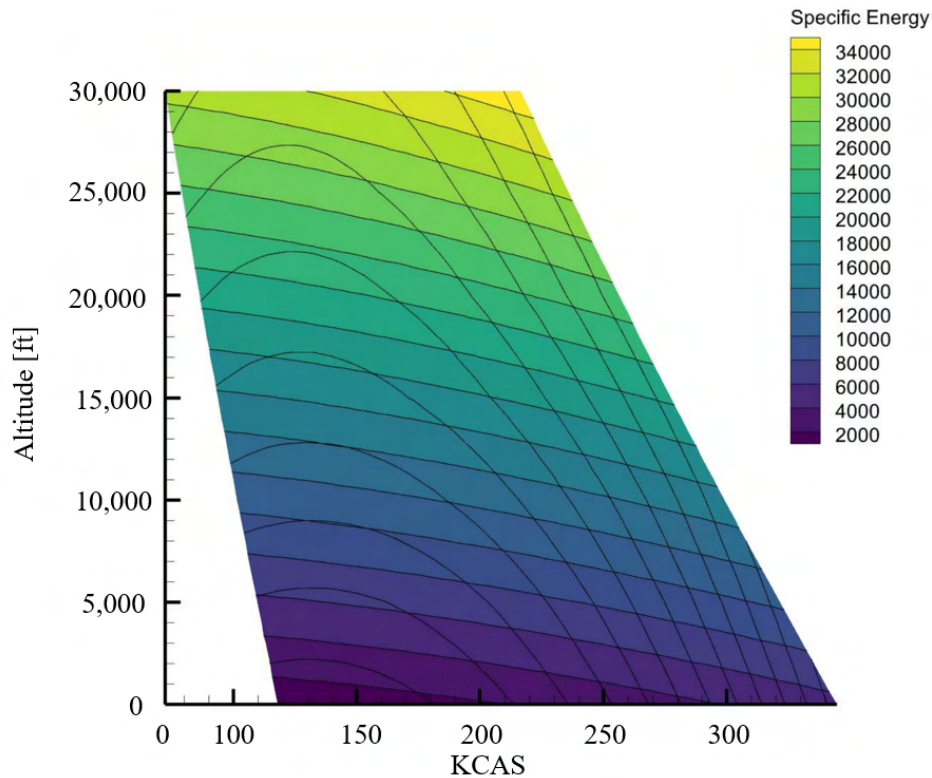
Fig. 61   Excess Power and Specific Energy Plot
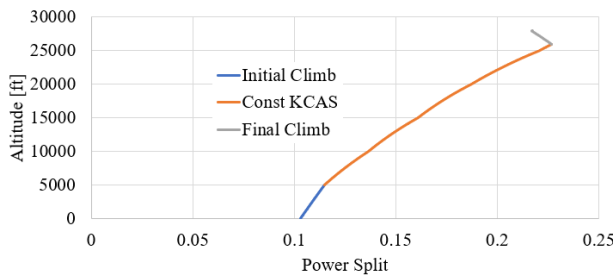
Fig. 62   Power Split Through Altitude
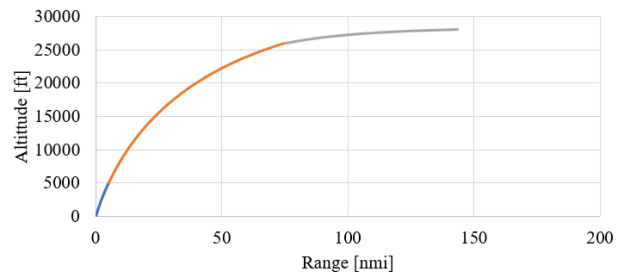
Fig. 63   Climb Trajectory

Climb angle was calculated in a spreadsheet using an iterative method of calculations from vertical velocity and VTAS until the angle for each step converged [65]. This climb analysis resulted in an initial rate of climb of 2,878 fpm at an angle of 11.3 degrees and a final rate of climb of 68 fpm at an angle of 0.13 degrees for a trajectory seen in Figure 63. A more in depth summary of climb performance is shown in Table 57.

Table 57   Climb Performance

Climb Speed	Initial ROC	TOC ROC	Initial Climb Angle	Average Climb Angle	Gas Throttle	Electric Throttle
150 KCAS	2,445 fpm	65 fpm	10.6°	4.07°	60%	35%

Similarly, the cruise stepped through quasi steady-states of constant weight through distance to ensure the mission reaches the design range of 1,000 nmi with a speed of 300 kts. Just as in climb, electric throttle is kept constant at 35% while the the pilot will adjust the throttle slightly throughout flight as shown with other cruise parameters in Table 58. This keeps L/D constant as weight is lost during the cruise.

Another alternative to changing throttle was to climb while cruising or to speed up instead. As seen by the coefficient plots in Figure 64, if the speed of Bounden increased, Bounden's coefficient of lift would decrease, decreasing its endurance and power. Likewise, Figure 25c shows how a given L/D can vary with CL, whether it changes from weights, dynamic pressure, or wing area. This was extremely helpful in choosing cruise conditions as the team saw which parameters needed to be in place for the highest L/D. It was ultimately decided to change throttle through cruise instead of altitude or speed because of requirements set by Air Traffic Control for pilots to cruise at a set altitude and speed.
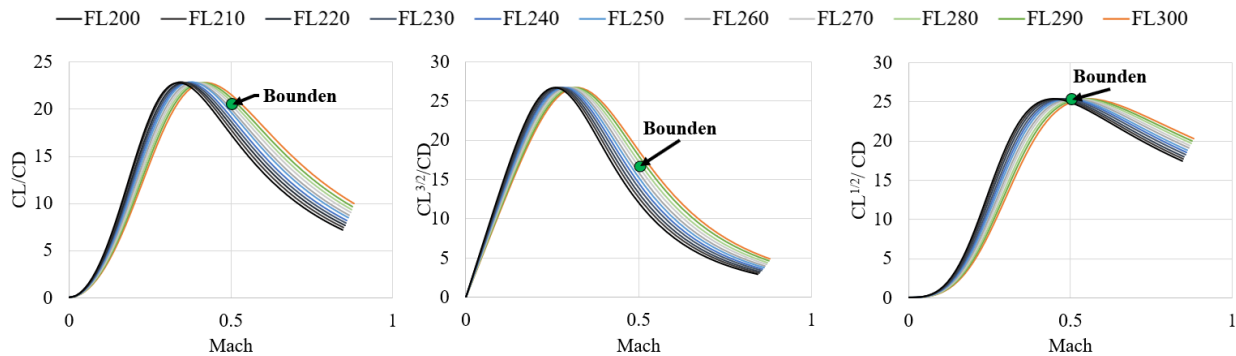
Fig. 64   Performance Coefficients

Table 58   Cruise Performance

Cruise Time	Cruise Range	Initial Gas Throttle	Final Gas Throttle	Electric Throttle	Average Power Split	L/D
142 min	712 nmi	55.9%	70.8%	35%	0.065	20.7

Due to the battery being used for both the climb and cruise portion of the mission, the battery can be depleted of its charge. The 1,000 nmi is designed to use up 80% of the battery, then use only gas for the rest of the mission. Whenever the battery runs out, the gas throttle will go from 55% to 70% as the electric throttle goes from 35% to 0%. Alternative electric throttle settings were looked at for cruise, and the results are shown in the visualization of the power split in

Figure 65. The battery avoids depletion only when using a throttle less than 10%, which causes a dramatic increase in fuel consumption as seen in Figure 66. By increasing the throttle from 10% to 50%, the block fuel reduces by only 20 lb. Thus, Bounden prioritizes pilot ease by using the same throttle setting for each section of the mission that uses a hybrid system. If the throttle for the electric portion were to change for climb as well as cruise, the battery size would need to increase significantly to at least 10,000 lb.
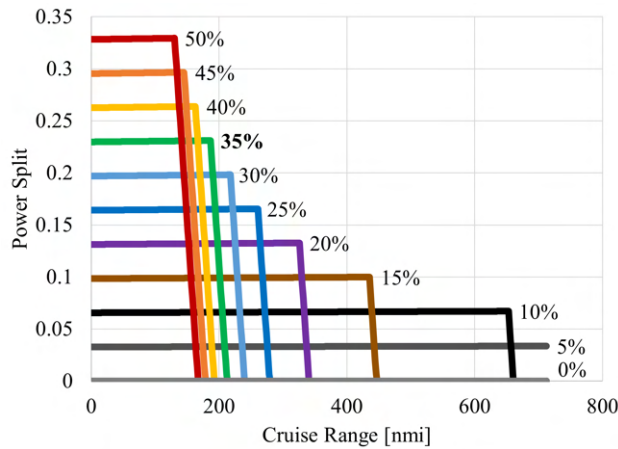
Fig. 65   Power Split for Cruise
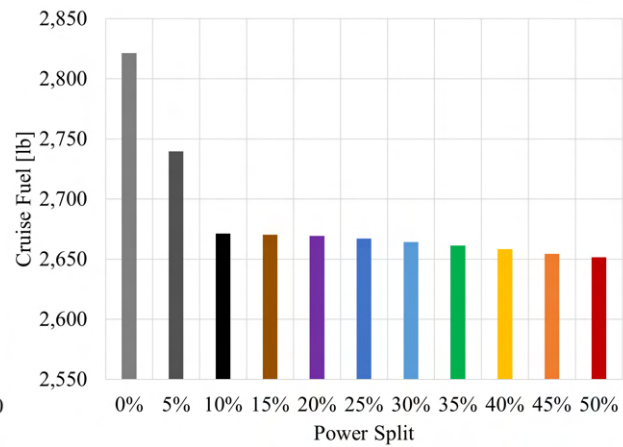
Fig. 66   Cruise Fuel Burn

D. Descent and Loiter

Similar to climb, the descent was stepped through altitude. The aircraft engine is as close to idle engine as possible for minimum fuel consumption through descent and no electric throttle. The aircraft is required to have an approach speed below 140 kts, and Bounden starts approach at 131 kts. For an accurate comparison of block fuel to other aircraft that will be discussed in Section XII, a loiter of 10 minutes was included. Using the maximum endurance speed at 10,000 ft, Bounden is designed to loiter at 142 kts. The summary of these sections are shown in Table 59. It was decided that while these sections are long, using hybridization during descent and loiter would not be helpful because of the already low throttle on the gas engine as the engine must be idle at minimum. A higher throttle would only decrease the distance traveled during descent, thus unnecessarily increasing the cruise duration.

Table 59   Descent and Loiter Performance

Section	Speed	Time	Range	Initial Angle	Average Angle	Gas Throttle
Descent	150 KCAS	49 min	144 nmi	-2.1°	-1.5°	5%
Loiter	142 KTAS	10 min	23 nmi	0	0	32%

E. Payload Analysis

A payload-range diagram is shown in the black lines of Figure 67 illustrating the trade-off between the payload and the range of Bounden as well as the fuel weights. The upper line (A-B) shows the maximum range of the aircraft at maximum payload, designed to be 1,000 nmi. The first sloped line (B-C) shows the trade-off between fuel and payload while the last sloped (C-D) line shows the trade-off between payload and range. While the maximum range is capable of going past 1,200 nmi with full tanks, the team will not allow for the tanks to take more fuel than is required for an empty flight as shown by the dashed line.
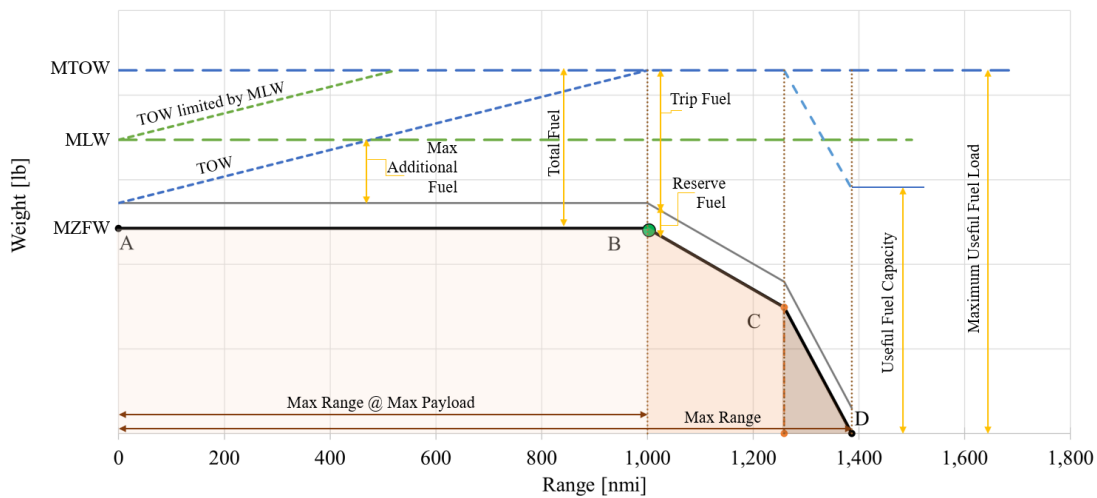
Fig. 67   Payload-Range Diagram

XII. Emissions

A. Block Fuel

Although Bounden was designed for a 1,000 nmi mission, block fuel and emissions will be compared at a 500 nmi mission per the RFP figure of merit [1]. The block fuel, battery use, and CO_2 for each section of the 500 nmi mission are shown below in Table 60.

Table 60   Emission Summary for 500 nmi Mission

Mission Section	Block Fuel [lb]	Battery Energy [kW-hr]	CO_2 Emissions [lb]
Taxi & Takeoff	72.0	0	227.5
Climb	877	496	2,767
Cruise	675	549	2,132
Descent	288	0	909.2
Loiter	157	0	495.6
Landing & Taxi	65.7	0	207.5
Total	2,132	1,045	6,739

Figure 68 shows the block fuel for the ATR 42-600, the ATR 72-600, and the Saab 2000 for a 500 nmi mission and the block fuel required for a 20% reduction to satisfy the RFP figure of merit. These aircraft were chosen for comparison due to their transparency in fuel consumption and CO_2 emissions and so Bounden could be compared to aircraft of similar passenger capacity and similar weight. ATR 42-600 carries a similar amount of passengers, but is much lighter than Bounden. Thus, by being comparable to one of the best in class, Bounden will be attractive to customers. The 500 nmi mission block fuel was estimated using the same performance analysis done for Bounden. For this estimate to match the given block fuel for the 200 nmi, 300 nmi, and 400 nmi missions, the analysis needed to include a 15 minute taxi before takeoff, a 15 minute taxi after landing, and a 10 minute loiter, so Bounden also includes block fuel for these sections. With this comparison, Bounden has an 21.2% reduction compared to the best in class.
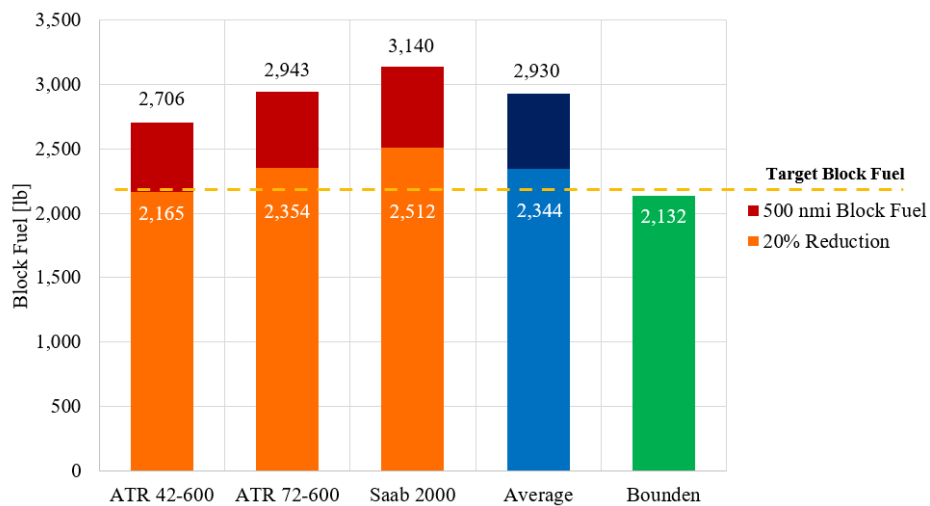
Fig. 68   Block Fuel Comparison

B. Aircraft Emissions

ICAO updated their performance standards in 2017 for new aircraft entering service after 2028 in order to improve fuel efficiency and reduce CO_2 emissions. The standard depends on the cruise fuel burn performance, aircraft size, and aircraft maximum takeoff weight [66]. While it mostly affects jets, it is important to note that ICAO is expecting no metric value reduction for smaller aircraft, 4% reduction for new aircraft, and 10% reduction for very large aircraft.

The RFP requires that the CO_2 emissions are reduced compared to similar aircraft, but in no measurement how. In order to compare the emissions of Bounden, the team's estimates were done by comparing the same method of calculation in the report given by the International Council for Clean Transportation [67]. In this report, The International Council on Clean Transportation details the CO_2 emissions of aircraft through three different years. Similar to the report, the total passenger weight is found with Eq. 2 and the fuel used per passenger is found with Eq. 3 as given from the report [67].

$$\text{Passenger Weight [lb]} = \text{Number of Passengers} \cdot (200 \text{ lb} + 40 \text{ lb}) \tag{2}$$

$$\text{Passenger Fuel Use [lb]} = \frac{\text{Total Passenger Weight}}{\text{Total Weight}} \cdot (\text{Total Fuel Weight}) \tag{3}$$

With this, the total CO_2 emissions are estimated using 3.16 ton of CO_2 emitted for every one ton of aviation fuel used as accepted by ICAO carbon emissions calculator [68]. Emissions for various aircraft are shown below in Table 61 with the team's calculations of aircraft with similar passenger capacity and weight as Bounden.

Table 61   Current Regional Aircraft CO_2 Emissions Adapted from [67]

Aircraft	Avg PAX	Total Weight [lb]	Fuel Weight [lb]	Range [nmi]	PAX CO_2 Emissions [lb/PAX/nmi]
Canadair CRJ200 [69]	50	51,000	17,800	550	7.62
ATR 42-600 [70]	48	41,000	9,900	730	3.83
De Havilland Dash 8-400 [71]	73	67,200	14,380	1,100	4.88
Fokker 50 [15]	56	44,000	9,090	920	2.70
Canadair CRJ700 [72]	68	73,000	19,600	1,680	2.61
Embraer E145 [73]	50	48,500	11,300	1,550	1.81
Bounden	*50*	*63,526*	*4,036*	*1,000*	*0.76*

Other emissions of concern are water vapor, nitrous oxide gases (NO_x), and particles including sulfates, soot, and hydrocarbons. All these emissions plus CO_2 contribute to the increase in greenhouse gases in the atmosphere that is worsening global warming. Bounden is designed to be a first-order effort to combat global climate change by reducing emissions and targeting a net zero-carbon world. Water vapor emissions contribute to the formation of contrails which can cause a greater impact on global warming than CO_2 emissions. While NO_x removes methane, a more impactful greenhouse gas, it has a net warming effect because it forms more ozone. Hydrocarbons, soot, and sulfates worsen the contrail impact by absorbing more heat. In short, by reducing these emissions on a small scale with Bounden, a large impact can be made to reduce aviation's contribution to global warming. Table 62 shows the emissions for the ATR 42-600, the ATR 72-600, and the Saab 2000 for their 500 nmi missions compared to Bounden with each emission index found from the Encyclopedia of Global Climate Change [74].

Table 62   Emissions Comparison for 500 nmi Mission

Aircraft	Block Fuel [lb]	CO_2 [lb]	H_2O [lb]	NO_x [lb]	Particles [lb]
Saab 2000	3,140	9,922	3,862	50.24	53.69
ATR 72-600	2,943	9,300	3,620	47.01	50.33
ATR 42-600	2,706	8,551	3,328	43.30	46.27
Bounden	*2,132*	*6,739*	*2,623*	*34.12*	*36.47*

C. Manufacturing Emissions

While all emission analysis was done with the control volume around the aircraft, it is important to keep in mind the CO_2 emissions that come from manufacturing the aircraft. The estimated emissions will vary depending on where the materials such as aluminum and the batteries are sourced from. Using the mass breakdown of Bounden from Table 47, Table 63 shows the high and low estimates of the CO_2 emissions for the manufacturing and the breakup for this estimate with the lowest estimate of 141 tons and the highest estimate of 572 tons of CO_2 emitted per aircraft.

Table 63   Emissions Comparison for 500 nmi Mission

Material	Emission Index	Aircraft Amount	$CO_2 Emission [ton]$
Composite [75]	24 kg CO_2/kg	3,910 lb	46.9
Aluminum (coal power) [76]	18 ton CO_2/ton	31,000 lb	281
Aluminum (hydropower) [76]	3 ton CO_2/ton	31,000 lb	46.9
Battery (low) [77]	3 ton CO_2/80kWh	1,210 kWh	45.3
Battery (high) [77]	16 ton CO_2/80kWh	1,210 kWh	241
Paint [78]	15 kg CO_2/kg	290 lb	2.14

To reduce the global carbon footprint from aircraft on a greater scale, cleaner methods for manufacturing should be accounted for and used. However, even without taking these into account, the reduced emissions shown above make a difference. Methods of manufacturing are already cleaner than the emissions produced by the aircraft without a battery in the long run. Even with coal power and the battery production, power plants that source the energy to create these are required to have scrubbers to reduce the pollutants they let out. With this, Bounden is the first step in more sustainable aviation in the long term future.

XIII. Acoustics

Unlike emissions, acoustics are not a driving factor in the design of the aircraft. The aircraft used as comparison to the team's design do not have any issues regarding 14 CFR Part 36 [64] and ICAO Annex 16 Stage 3 [79]. Furthermore, larger aircraft with heavy propellers are tabulated in the EASA Certification Noise Levels database [80]. The propeller Bounden is using is a Dowty R408 propeller on a PW150A engine, a combination used and recertified by Bombardier's Dash Q-400 on January 11, 2022 [80]. Because the aircraft is a heavy propeller driven aircraft, the certification metric is annoyance based, so certification is based on the effective perceived noise (EPNdB)[81]. This noise is measured by a microphone at a sideline reference point 450 m away from the microphone with full power, an approach reference point 2,000 m before the microphone, and a flyover reference point 6,500 m past the microphone. The noise values are difficult to calculate beforehand because calculations are done from microphone recordings during the certification test, so Bounden's acoustic certifications are estimated based on the Dash Q-400 certifications with the PW127B and the PW150A engines and the Dowty R408 Propeller shown in Figure 69.

(a) Sideline

(b) Approach

(c) Fly Over
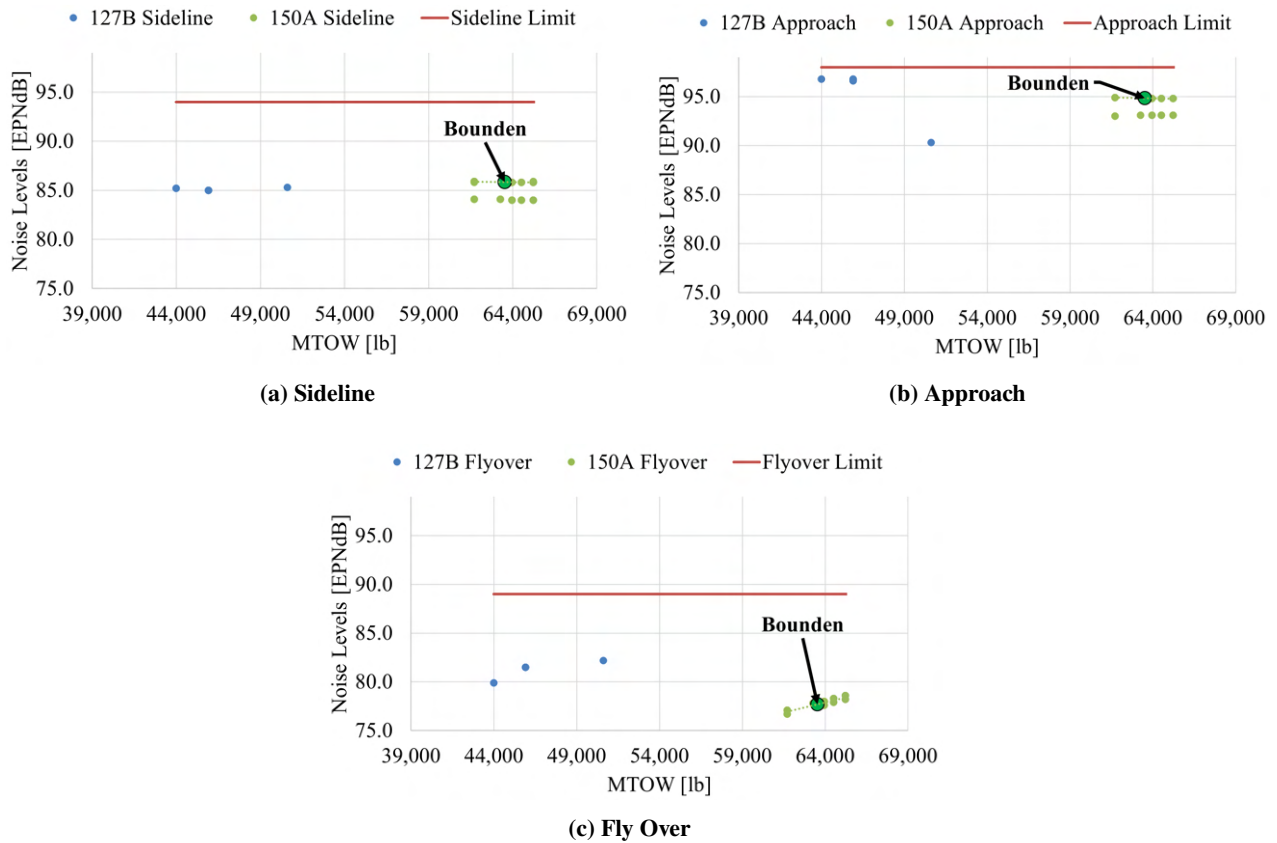
Fig. 69   Dash Q400 Noise Level Certification

Figure 69 illustrates the certified noise levels for each test of multiple Dash Q-400 aircraft as a function of their MTOW. Figure 69a and Figure 69b show that Bounden's certification in these categories is secured, for these tests as do not vary with MTOW. Figure 69c suggests that the noise levels for the flyover increases much more as a function of MTOW, but the estimated noise levels shown in Table 64 are well below the EASA limit. Bounden's propeller will also be operating at a lower rate per minute (850 RPM) than the Dash Q-400's maximum RPM (1,020 RPM), so it is expected that these noise levels will be much lower than was estimated.

Table 64   Bounden Acoustics Estimates and Limits

Certification	Estimated Noise [EPNdB]	Noise Limit [EPNdB]
Sideline	85.8	94
Approach	94.8	98
Fly Over	77.7	89

XIV. Repair and Maintenance

The repair and maintenance of Bounden will be similar to other turboprops such as ATR 42 and Fokker 50. It will have its line checks every day, an A check every six to eight weeks, a B check every six to eight months, and C and D checks as necessary. The main difference would be a comprehensive assessment of the electrical system related to the electric motor and batteries. Since lithium-ion batteries that were chosen have an estimated useful life of two years, the B check will serve as a good interval to conduct tests for battery health. Due to the fact that lithium-ion battery's degradation is hard to assess physically, a model of degradation for the battery can be to utilized to better gauge the health of the battery. More specifically, multivariate stacked bidirectional long short term memory can be utilized to create an effective battery management system as proposed by Andeshiri [82].

The batteries will be replaced between flights if more battery power is necessary to complete the next flight. The front battery modules will be extracted from a side hatch while the aft battery modules will be extracted from a rear hatch. The various connections will need to be manually extracted.

The Bounden has also adopted composites for many of its truss-braced wing and empennage internal structures. One of the common concerns of composite usage is the difficulty to repair. However, Boeing has developed methods to assess the integrity of composite structures and perform a permanent repair through a traditional bolted repair method [83]. Besides large area damage or severe damage, repairs of composite structures can be conducted in the field.

XV. Cost

A. Business Case Analysis

Per the RFP, the production run should be consistent with 2,000 units being produced over a 20 year span [1]. This means that the production run being analyzed will be based on 500 aircraft being produced in a 5 year period. This translates to roughly 2 aircraft being produced per week for the 20 year production period.

B. RDT&E, Flyaway, and Unit Cost

The Development and Procurement Cost of Aircraft (DAPCA-IV) model produced by the RAND Corporation, which can be found in Raymer, was used to estimate the RDT&E and flyaway costs [4]. The model estimates the time required for research, development, testing, and evaluation for the production run and utilizes wrap rates to convert hours into cost. It should be noted that the model was produced in 2012, and, as a result, an inflation factor has been implemented into the cost calculations to provide an estimate in 2023 dollars. The inflation factor, which is based on historical inflation and United States CPI data, has been estimated to be 2.90% each year from 2012 to 2023, which leads to a total inflation percentage of 31.88% and each cost obtained from the DAPCA-IV model to be multiplied by 1.3188 [84].

To estimate the battery production cost, a price of \$151.00 per kWh was utilized [85]. To compute the engine cost of the PW150A that will be used on Bounden, the actual engine cost was used, which is \$1.8 million in 2023 dollars [86]. Finally, upon working with the Structures group, it was decided which components of the aircraft would be made out of composites; to account for this added cost, a factor of 1.30 as specified by Raymer was used [4]. Additionally, since the DAPCA-IV model does not account for additional costs associated with hybrid implementation, a 25% increase was applied to relevant production costs that would require more time and resources to implement hybrid. These components are the engineering, tooling, manufacturing, quality control, development-support, flight test, and manufacturing materials costs. A 10% increase was applied to relevant operating costs such as maintenance that would require more labor, materials, parts, and supplies to implement hybrid. These factors were obtained by conducting a trade study in which the hybrid factors were varied from 1.00 to 1.50 and the resulting unit and operating costs were plotted. This chosen range was based on the fact that on the low end there would be no hybrid implemented, and on the high end there would be 50% added for complexities. A factor larger that 1.50 was not examined since many of the complexities associated with hybrid were computed separately. The results of this study are shown in Figure 70.
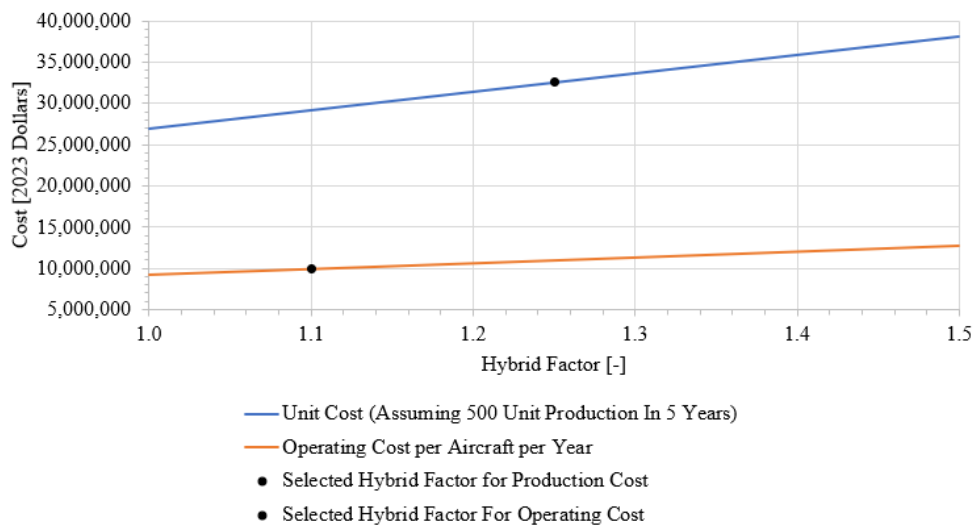
Fig. 70   Unit and Operating Cost Variation with Hybrid Factor

It can be seen from Figure 70 that the unit cost of the aircraft varies by a larger amount as the hybrid factor for production costs is changed. To not overestimate or underestimate the production cost of the aircraft, a factor that was in the middle of the lowest and highest unit cost was chosen. On the other hand, the operating costs vary minimally when varying the operating cost hybrid factor. A factor closer to the lower end was selected since this factor would only be applied to the maintenance costs as the charging and battery replacement costs were computed separately. Table 65 highlights the program cost for the production of 2,000 aircraft over a 20 year period. Additionally, Figure 71 shows a visual breakdown of the production cost for Bounden.

Table 65   DAPCA-IV Model Program Cost Breakdown in 2023 Dollars

Parameter	Value
Engineering Cost	$1.8 billion
Tooling Cost	$1.3 billion
Manufacturing Cost	$6.7 billion
Quality Control Cost	$1.3 billion
Development-Support Cost	$183.8 million
Flight-Test Cost	$69.3 million
Manufacturing Materials Cost	$2.7 billion
Battery Production Cost	$82.2 million
Engine Production Cost	$1.8 billion
Avionics Cost	$285 million
Interiors Cost	$56 million
RDT&E + Flyaway Costs for 500 Aircraft Over 5 Years	**$16.3 billion**
RDT&E + Flyaway Costs for 2,000 Aircraft Over 20 Years	**$65.1 billion**
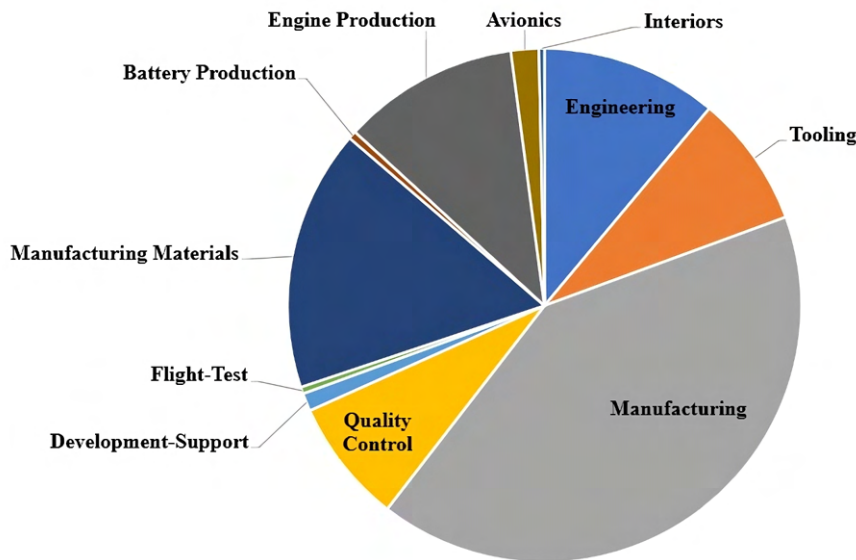
Fig. 71   Production Cost Breakdown

As shown in Table 65, the production cost for 500 aircraft over a 5 year timeline is $16.3 billion. This cost was multiplied by 4 to obtain the cost of 2,000 aircraft over a 20 year timeline. This total program cost is $65.1 billion. This means that the unit cost of each aircraft is $32.5 million. The RFP requires a 15% profit, making the list price of the aircraft to be $37.4 million. To compute the payback years, or the number of years that will be required to recover the initial production cost, the list price of the aircraft will be utilized. To recover the RDT&E and flyaway cost for 500 aircraft produced over 5 years, which is $16.3 billion, 435 aircraft would need to be sold at the list price of $37.4 million. This results in a payback period of 4.4 years after which any aircraft sold would result in profit.

C. Operating Cost

Using the model provided by Raymer, the total operations and maintenance cost includes the fuel, charging, battery replacement, crew salaries, maintenance, depreciation, landing, and insurance costs per aircraft per year [4]. It is assumed that the number of flight-test aircraft needed would be 4, the average yearly flight hours per aircraft is 4,000, and that the depreciation was spread over 13 years [4]. The landing fees were assumed to be $5.83 per 1,000 lb of MTOW [87]. The cost of A-1 jet fuel is $2.48 per gallon [88]. Furthermore, the United States average rate of electricity for the transportation sector is $0.1524 per kWh [89]. It was also assumed that the charge cycles for a lithium-ion battery is 2,000, which would require that the battery modules be replaced every 2.2 years [90].

The cost of this replacement is broken down into a yearly cost in Table 66. Finally, to calculate the crew salaries per aircraft per year, it was determined that three sets of crew, which include the captain, first officer, and flight attendant, would be required since 14 CFR § 135.267 requires that no crew member fly more than 1,400 flight hours in one calendar year [91]. The rates per flight hour per aircraft for the captain, first officer, and flight attendant are $90.45, $53.66, and $38.40, respectively, which includes a 20% increase for benefits [92]. Table 66 shows the operating cost breakdown for a 1,000 nmi mission in 2023 dollars. Figure 72 shows a visual breakdown of the operating cost for Bounden during a 1,000 nmi mission.

Table 66   Operating Cost for 1,000 nmi mission in 2023 Dollars

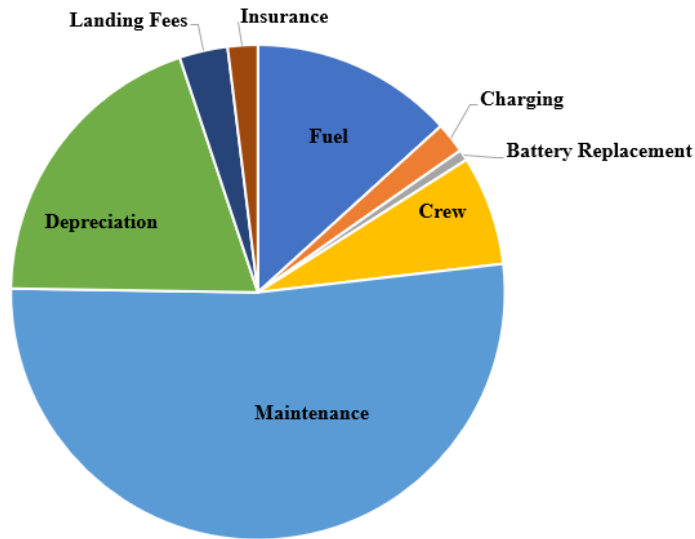| Parameter	Value (Per Year)	Value (Per Flight Hour)
Fuel	$1.4 million	$339
Charging	$205,000	$51
Battery Replacement	$73,000	$18
Crew Salaries	$730,000	$183
Maintenance	$5.3 million	$1,324
Depreciation	$2.0 million	$501
Landing Fees	$323,000	$81
Insurance	$200,000	$50
Total Operating Cost per Aircraft	**$10.2 million**	**$2,551**

Fig. 72   Operating Cost Breakdown for 1,000 nmi Mission

D. Cost Comparison

When compared to other aircraft, Bounden is at a marketable price point with operating costs similar to that of other regional turboprops within the class. Table 67 highlights the fuel cost per aircraft per year and per flight hour along with the operating cost per aircraft per year of the ATR 42-600, ATR 72-600, Saab 2000, and Bounden. It should be noted that these costs are based on data obtained for a 500 nmi mission and that Bounden's fuel cost accounts for both fuel and charging.

Table 67   Fuel and Operating Costs for 500 nmi mission in 2023 Dollars

Aircraft	Fuel Cost (Per Year)	Fuel Cost (Per Flight Hour)	Operating Cost (Per Year)
ATR 42-600	$1.9 million	$489	$8.9 million
ATR 72-600	$2.0 million	$511	$9.3 million
Saab 2000	$2.7 million	$670	$10.3 million
Bounden	**$1.6 million**	**$397**	**$10.6 million**

Based on Table 67, Bounden's fuel cost is lower than the ATR 42-600, ATR 72-600, and Saab 2000. This shows Bounden to be attractive within the market since the aircraft will offer lower emissions, newer technology, and lower combined fuel and charging costs at an operating cost and unit cost that is minimally larger than that of other aircraft within the class that have much higher emissions, older technology, and higher fuel costs.

E. Cost Saving Techniques

One of the three ways to decrease the aircraft cost would be to first increase the hybridization factor that is used. Currently, the aircraft uses an average hybridization factor of 16% for climb and 6% for cruise for the 1000 nmi mission profile. This reduces the cost of fuel when compared to a regular regional turboprop while ensuring the charging cost does not grow larger than the fuel cost, and the battery weight does not grow unreasonably large. By further increasing this factor while still remaining within design limits, the aircraft can become more efficient, which would reduce the fuel cost further. However, it should be noted that increasing the hybridization factor by a large amount could potentially drive the charging cost higher than the fuel cost, and it could also drive the battery weight to be unreasonably large, which would lead to minimal cost savings. To obtain this optimal hybridization factor, a more in-depth study would be required. Another way to reduce the cost would be to utilize less complex components and fewer moving parts, which would reduce costs further in terms of manufacturing and maintenance since less hours would be required to fix components. This can be done by selecting less complex control surfaces along with manufacturing parts in a way that can be blended to have fewer moving parts; the manufacturing process of composite materials would assist with this since many components can be blended together during a layup instead of connecting them with screws, rivets, or bolts. A final way to decrease the cost would be to produce more aircraft. As can be seen in Figure 73, the unit cost decreases as more aircraft are produced. The production number stated by the RFP is specified in the figure and is on the lower end of the chart, but by increasing the number of aircraft produced in 5 years to 550 or 600 will significantly reduce the unit cost.
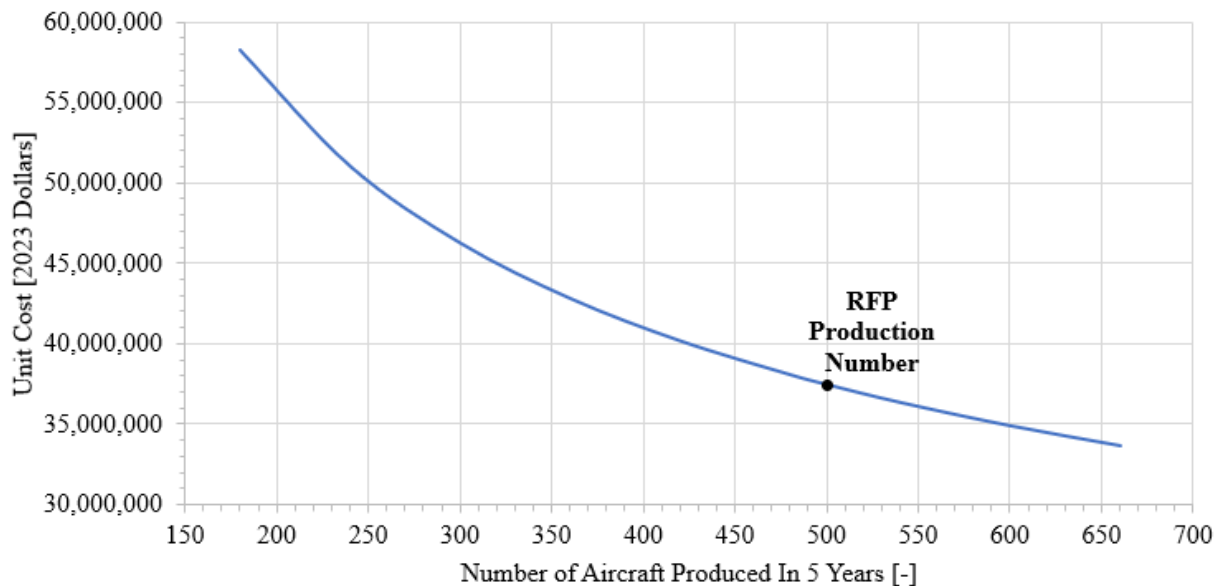

Fig. 73   Unit Cost Variation with Production Number

F. Model Uncertainties and Inaccuracies

The DAPCA-IV model used has a few uncertainties that can lead to an overestimation in cost. First, the model tends to overpredict the cost for transport aircraft, which may result in the overestimation of Bounden. Additionally, the model uses a factor to account for the aircraft being produced out of composites. However, this could lead to an overestimation if only subparts of certain components are produced out of composites instead of entire parts. Applying a factor generalizes the situation and does not take into account if only minor components are manufactured out of composite materials. Finally, the model does not predict the cost of hybrid components such as the battery, wires, and added maintenance, which is why a hybrid factor has been applied, but this is a factor derived from a trade study, which has assumptions that could overestimate or underestimate the cost.

XVI. Conclusion

As 50-seat regional turboprops and turbojets stay rooted in designs based in the 1980s while the US Domestic Scope Clause moves toward prioritizing fuel reduction, emissions reduction, and electrification, a new market segment is formed. Bounden stays competitive in the traditional regional aircraft market while fulfilling the new market demands by providing a newer and greener alternative to both regional jets and older turboprops by reducing emissions and block fuel with its hybridization. Through its truss-braced wing configuration and parallel-hybrid propulsion system, Bounden brings its innovation to the skies with modern technology that works to reduce the impacts of aviation on climate change. Reducing block fuel by over 21% and aircraft emissions compared to its competitors, Bounden is a clear choice for the future of regional aviation. In addition, Bounden provides a competitive price of $37.4 million while offering lower emissions, new technology, and lower fuel costs. The aircraft's battery replacement architecture allows for flexibility in ground operations given the length of the missions being flown to further increase the market size and reach of Bounden. While meeting all of the requirements outlined for the design, Bounden is also designed with consideration for cost, marketability, reliability, and maintainability. Through its strategic design objectives and features, Bounden is well-suited to replace the currently outdated regional aircraft fleet while reducing block fuel usage and taking the next step toward net-zero emissions in aviation.

References

[1] "Hybrid-electric Regional Turboprop RFP," `https://www.aiaa.org/docs/default-source/uploadedfiles/education-and-careers/university-students/design-competitions/2022_aiaa_hybrid_turboprop_rfp_06-08-2022-7.pdf?sfvrsn=f1134ec4_0`, 2022. Last accessed on 4 February 2023.

[2] Schonland, A., "The new reality for US Commercial Pilots and Scope Clause," *AirInsightGroup*, 2020. Last accessed on 9 February 2023.

[3] "Working to Build a Net-Zero Sustainable Aviation System by 2050," `https://www.faa.gov/sustainability`, 2023. Last accessed on 6 March 2023.

[4] Raymer, D. P., *Aircraft Design: A Conceptual Approach Sixth Edition*, American Institute of Aeronautics and Astronautics, Playa del Rey, California, 2018.

[5] "Who we are," `https://www.atr-aircraft.com/about/who-we-are/`, 2023. Last accessed on 6 March 2023.

[6] "Bombardier Q300 DHC-8 Dash 8," `https://www.aerospace-technology.com/projects/bombardier_q300/`, 2023. Last accessed on 18 April 2023.

[7] "Fokker F50," `https://www.aerospace-technology.com/projects/fokker_f50/`, 2023. Last accessed on 18 April 2023.

[8] Schonland, A., "Since there is no new regional jet that is Scope Clause complaint, let's talk about Turboprops," `https://airinsight.com/since-there-is-no-new-regional-jet-that-is-scope-clause-complaint-lets-talk-about-turboprops`, 2021. Last accessed on 9 February 2023.

[9] Schonland, A., "Turboprop market forecast," `https://www.atr-aircraft.com/our-aircraft/turboprop-market-forecast-2022-2041`, 2022. Last accessed on 9 February 2023.

[10] Megan S. Ryerson, X. G., "The role of turboprops in China's growing aviation system," *Journal of Transport Geography*, 2014. https://doi.org/10.1016, last accessed on 8 February 2023.

[11] *Airport Planning Manual*, 123 Garratt Blvd., Downsview, Ontario, 2001. Last accessed on 4 February 2023.

[12] "TYPE-CERTIFICATE DATA SHEET," https://www.easa.europa.eu/en/downloads/7257/en, 2021. Last accessed on 4 February 2023.

[13] "BOMBARDIER DASH 8 300/Q400," https://www.air-tecm.com/fleet/bombardier-dash-8-aircraft/, 2018. Last accessed on 4 February 2023.

[14] "De Havilland-Dash 8 Q300," https://www.flycemair.co.za/general_r/dehavilland_dash8-q300.php, 2018. Last accessed on 4 February 2023.

[15] *Fokker 50 Information Booklet*, 2022. Last accessed on 4 February 2023.

[16] "ATR 42-600," https://www.atr-aircraft.com/wp-content/uploads/2020/07/Factsheets_-_ATR_42-600.pdf, 2020. Last accessed on 23 April 2023.

[17] "ATR ATR 42-500," https://www.skybrary.aero/aircraft/at45, 2021. Last accessed on 23 April 2023.

[18] "Smoothed ATR airfoil coordinates," http://airfoiltools.com/airfoil/details?airfoil=atr72sm-il, 2023. Last accessed on 23 April 2023.

[19] Roskam, J., *Airplane Design Part I: Preliminary Sizing of Airplanes*, DARcorporation, Lawrence, Kansas, 2005.

[20] "Development of an efficient Mach=0.8 transonic truss-braced wing aircraft," https://www.aiaa.org/docs/default-source/default-document-library/publications/developmentofanefficientmach080transonictruss-bracedwingaircraft.pdf, 2020. Last accessed on 6 March 2023.

[21] Roskam, J., *Airplane Design Part III: Layout Design of Cockpit, Fuselage, Wing and Empennage: Cutaways and Inboard Profiles*, DARcorporation, Lawrence, Kansas, 1989.

[22] *Aircraft Landing Gear Design: Principles and Practices*, 1988. Last accessed on 28 April 2023.

[23] Nathan Meier, T. A., Andreas Parsch, "Civil Turboshaft/Turboprop Specifications," https://jet-engine.net/civtsspec.htm, 2021. Last accessed on 5 February 2023.

[24] "14 CFR 33 - Airworthiness Standards: Aircraft Engines," https://www.law.cornell.edu/cfr/text/14/part-33, 1964. Last accessed on March 6 2023.

[25] "Gasturb," https://www.gasturb.de/software/gasturb.html, 2023. Last accessed on 28 April 2023.

[26] "Bombardier Q400 Propeller - Dowty R408," https://www.flyradius.com/bombardier-q400/propeller-dowty-r408, 2015. Last accessed on 6 March 2023.

[27] Manuel A. Rendon, J. G. M. A. M. A., Carlos D. Sanchez R., *Aircraft Hybrid-Electric Propulsion: Development Trends, Challenges and Opportunities*, Journal of Control, Automation and Electrical Systems, 2021.

[28] Bright Appiah Adu-Gyamfi, C. G., "Electric aviation: A review of concepts and enabling technologies," *Transportation Engineering*, 2022. https://doi.org/10.1016, last accessed on 8 February 2023.

[29] "Volumetric Energy Density of Lithium-ion Batteries Increased by More than Eight Times Between 2008 and 2020," https://www.energy.gov/eere/vehicles/articles/fotw-1234-april-18-2022-volumetric-energy-density-lithium-ion-batteries, 2022. Last accessed on 4 February 2023.

[30] Alcock, C., "Collins and P&W Unveil Hybrid-Electric Propulsion Systems," https://www.ainonline.com/aviation-news/air-transport/2022-07-18/-and-pw-unveil-hybrid-electric-propulsion-systems, 2022. Last accessed on March 6 2023.

[31] "Electric Motor Demonstrator Sets Two World Records in Two Hours After Five Years of Work," https://car.osu.edu/news/2019/11/electric-motor-demonstrator-sets-two-world-records-two-hours-after-five-years-work, 2019. Last accessed on 6 March 2023.

[32] "Epicyclic Gearing," https://en.wikipedia.org/wiki/Epicyclic_gearing, 2023. Last accessed on 27 April 2023.

[33] "Planetary Gear Ratio Calculations," , 2023. Last accessed on 28 April 2023.

[34] "14 CFR 25 - Airworthiness Standards: Transport Category Airplanes," https://www.law.cornell.edu/cfr/text/14/part-25, 1964. Last accessed on March 6 2023.

[35] "Coulombic and Energy Efficiency with the Battery," https://batteryuniversity.com/article/bu-808c-coulombic-and-energy-efficiency-with-the-battery, 2021. Last accessed on 26 April 2023.

[36] "Roller Chains and Planetary Gearboxes Yield Accurate, Efficient Motion Control," https://www.machinedesign.com/mechanical-motion-systems/article/21837300/roller-chains-and-planetary-gearboxes-yield-accurate-efficient-motion-control, 2018. Last accessed on 27 April 2023.

[37] "AVL," https://web.mit.edu/drela/Public/web/avl/, 2023. Last accessed on 28 April 2023.

[38] "OpenVSP," https://openvsp.org, 2023. Last accessed on 28 April 2023.

[39] Erin Ting, N. N. J. T., Kevin Reynolds, "Aerodynamic Analysis of the Truss-Braced Wing Aircraft Using Vortex-Lattice Superposition Approach," , 2020. Last accessed on 6 March 2023.

[40] "XFLR5," http://www.xflr5.tech/xflr5.htm, 2023. Last accessed on 28 April 2023.

[41] "XFOIL," https://web.mit.edu/drela/Public/web/xfoil/, 2023. Last accessed on 28 April 2023.

[42] Ira H. Abbot, A. E. V. D., *Theory of Wing Sections*, Dover Publications, Inc., New York, New York, 1959. Last accessed on 9 February 2023.

[43] Tornbeek, E., "Synthesis of Subsonic Airplane Design," , 1976.

[44] Rudolph, P., "high-Lift Systems on Commercial Subsonic Airliners," https://ntrs.nasa.gov/api/citations/19960052267/downloads/19960052267.pdf, 2023. Last accessed on 28 April 2023.

[45] Shama Rao N., R. K. P., Simha T. G. A., and V, R. K. G. V., "CARBON COMPOSITES ARE BECOMING COMPETITIVE AND COST EFFECTIVE," https://www.infosys.com/engineering-services/white-papers/documents/carbon-composites-cost-effective.pdf, 2015. Last accessed on 6 February 2023.

[46] Dupen, B., "Applied Strength of Materials for Engineering Technology," Tech. rep., 2016. Last accessed on 4 February 2023.

[47] Mirdehghan, S. A., "Engineered Polymeric Fibrous Materials," https://doi.org/10.1016/B978-0-12-824381-7.00012-3, 2021. https://doi.org/10.1016, last accessed on 5 February 2023.

[48] https://www.hexcel.com/user_area/content_media/raw/HexPly_M21_global_DataSheet.pdf, 2020. Last accessed on 28 April 2023.

[49] "Python," https://www.python.org/downloads/, 2023. Last accessed on 28 April 2023.

[50] "Jupyter Notebook," https://jupyter.org/install, 2023. Last accessed on 28 April 2023.

[51] Eric Ting, N. N. J. T., Kevin Reynolds, "Effect of Flutter on the Multidisciplinary Design Optimization of Truss-Braced-Wing Aircraft," Tech. rep., NASA, 2015. Last accessed on 27 April 2023.

[52] "SOLIDWORKS," https://my.solidworks.com/try-solidworks, 2023. Last accessed on 28 April 2023.

[53] Roskam, J., *Airplane Design Part V: Component Weight Estimation*, DARcorporation, Lawrence, Kansas, 2003.

[54] Kroo, I., *Aircraft Design: Synthesis and Analysis*, Desktop Aeronautics Inc., 2001.

[55] "EASA TYPE CERTIFICATE DATA SHEET," , 2008. Last accessed on 27 April 2023.

[56] "Fokker 50 - Fuel System," https://www.smartcockpit.com/docs/Fokker_50-Fuel.pdf, 2009. Last accessed on 6 March 2023.

[57] "M22759 wire," https://www.carlisleit.com/wp-content/pdfs/prodinfo/M22759.pdf, 2013. Last accessed on 6 March 2023.

[58] Pornet, C., "Conceptual Design Methods for Sizing and Performance of Hybrid-Electric Transport Aircraft," Tech. rep., TECHNISCHE UNIVERSITAT MUNCHEN, 2017. Last accessed on 8 February 2023.

[59] https://www.boeing.com/commercial/aeromagazine/articles/qtr_4_07/article_02_4.html, 2008. Last accessed on 27 April 2023.

[60] I. Moir, A. S., "Aircraft Systems," , 2008.

[61] "Automatic Dependent Surveillance-Broadcast (ADS-B)," https://www.collinsaerospace.com/what-we-do/industries/commercial-aviation/flight-deck/adsb, 2023. Last accessed on 27 April 2023.

[62] "GLU-2100 Multi-Mode Receiver," https://www.collinsaerospace.com/what-we-do/industries/commercial-aviation/flight-deck/navigation-and-guidance/gps-devices/glu-2100, 2023. Last accessed on 27 April 2023.

[63] "Primus 1000 Integrated Avionics System," https://www.flyradius.com/bombardier-q400/avionics, 2023. Last accessed on 5 March 2023.

[64] "PART 36 - NOISE STANDARDS: AIRCRAFT TYPE AND AIRWORTHINESS CERTIFICATION," https://www.ecfr.gov/current/title-14/chapter-I/subchapter-C/part-36, 2023. Last accessed on 6 February 2023.

[65] "Excel," https://www.microsoft.com/en-us/microsoft-365/excel, 2023. Last accessed on 28 April 2023.

[66] "INTERNATIONAL CIVIL AVIATION ORGANIZATION'S CO2 STANDARD FOR NEW AIRCRAFT," Tech. rep., INTERNATIONAL COUNCIL ON CLEAN TRANSPORTATION, 2017. Last accessed on 6 February 2023.

[67] Graver B., R. D., and S., Z., "CO2 Emissions from Commercial Emissions," Tech. rep., The International Council on Clean Transportation, October 2022. Last accessed on 6 February 2023.

[68] "Carbon Emissions Calculator Methodology," https://www.icao.int/environmental-protection/CarbonOffset/Documents/Methodology%20ICAO%20Carbon%20Calculator_v11-2018.pdf, 2018. Last accessed on 6 February 2023.

[69] "TRANSMITTAL LETTER REVISION 8," https://customer.aero.bombardier.com/webd/BAG/CustSite/BRAD/RACSDocument.nsf/51aae8b2b3bfdf6685256c300045ff31/ec63f8639ff3ab9d85257c1500635bd8/\protect\T1\textdollarFILE/ATT1ES4H.pdf/CRJ200APMR8.pdf, Jan 2016. Last accessed on 8 February 2023.

[70] "ATR 42-600 The ideal local commuter," https://www.atr-aircraft.com/wp-content/uploads/2022/06/ATR_Fiche42-600-3.pdf, 2022. Last accessed on 8 February 2023.

[71] "Q Series," https://web.archive.org/web/20180416074022/https://commercialaircraft.bombardier.com/content/dam/Websites/bombardiercom/supporting-documents/BA/Bombardier_Q%20Series_Final.pdf, 2018. Last accessed on 8 February 2023.

[72] "TRANSMITTAL LETTER REVISION 15," https://customer.aero.bombardier.com/webd/BAG/CustSite/BRAD/RACSDocument.nsf/51aae8b2b3bfdf6685256c300045ff31/ec63f8639ff3ab9d85257c1500635bd8/\protect\T1\textdollarFILE/ATTE8Q23.pdf/CRJ700APMR15.pdf, Dec 2015. Last accessed on 8 February 2023.

[73] "ERJ145 in Detail," https://www.embraercommercialaviation.com/commercial-jets/erj145/, 2023. Last accessed on 8 February 2023.

[74] "Aircraft Emissions," https://www.dlr.de/pa/en/Portaldata/33/Resources/dokumente/mitarbeiter/Schumann_Encyclopedia_Aircraft_Emissions_c415-_o.pdf, 2002. Last accessed on 26 April 2023.

[75] Kawajiri, K., "Sustainable Materials and Technologies," https://www.sciencedirect.com/science/article/pii/S2214993721001202, 2022. Last accessed on 26 April 2023.

[76] de Berker, A., "Understand your aluminum emissions," https://www.carbonchain.com/blog/understand-your-aluminum-emissions, 2023. Last accessed on 26 April 2023.

[77] Crawford, I., "How much CO2 is emitted by manufacturing batteries?" https://meche.mit.edu/news-media/how-much-co2-emitted-manufacturing-batteries, 2022. Last accessed on 26 April 2023.

[78] Samia Saif, M. A. S. A. A. M., Anum Feroz, "Calculation and Estimation of the Carbon Footprint of Paint Industry," https://neptjournal.com/upload-images/NL-53-27-(25)D-250.pdf, 2015. Last accessed on 26 April 2023.

[79] "Reduction of Noise at Source," https://www.icao.int/environmental-protection/pages/reduction-of-noise-at-source.aspx, 2023. Last accessed on 6 February 2023.

[80] EASA, "EASA Certification Noise Levels," https://www.easa.europa.eu/en/domains/environment/easa-certification-noise-levels, 2022. Last accessed on 6 February 2023.

[81] "Noise Certification Workshop," https://www.icao.int/Meetings/EnvironmentalWorkshops/Documents/Noise-Certification-Workshop-2006/Depitre_4.pdf, 2006. Last accessed on 26 April 2023.

[82] Reza Rouhi Ardeshiri, C. M., Ming Liu, "Multivariate stacked bidirectional long short term memory for lithium-ion battery health management," https://www.sciencedirect.com/science/article/pii/S0951832022001430, 2022. Last accessed on 28 April 2023.

[83] "QTR04 14," *AERO*, 2014. Last accessed on 6 February 2023.

[84] "Inflation Calculator," https://www.inflationtool.com/, 2023. Last accessed on 25 April 2023.

[85] "Lithium-ion Battery Pack Prices Rise for First Time to an Average of $151/kWh," https://about.bnef.com/blog/lithium-ion-battery-pack-prices-rise-for-first-time-to-an-average-of-151-kwh/, 2022. Last accessed on 25 April 2023.

[86] "The Market for Aviation Turboprop Engines," , 2010. Last accessed on 25 April 2023.

[87] "Los Angeles World Airports," , 2022. Last accessed on 25 April 2023.

[88] "Daily Jet Fuel Spot Prices," https://www.airlines.org/impact/, 2023. Last accessed on 25 April 2023.

[89] "Electric Power Monthly," https://www.eia.gov/electricity/monthly/epm_table_grapher.php?t=epmt_5_6_a, 2023. Last accessed on 25 April 2023.

[90] "How Long Do Electric Car Batteries Last?" https://www.midtronics.com/blog/do-electric-car-ev-batteries-degrade-over-time/#:~:text=Most%20electric%20vehicle%20batteries%20have,last%20well%20over%20ten%20years, 2021. Last accessed on 25 April 2023.

[91] "14 CFR § 135.267 - Flight time limitations and rest requirements: Unscheduled one- and two-pilot crews." https://www.law.cornell.edu/cfr/text/14/135.267, 2023. Last accessed on 25 April 2023.

[92] "WHAT DO AIRLINE PILOTS EARN?" https://pea.com/airline-pilot-salary/, 2015. Last accessed on 25 April 2023.